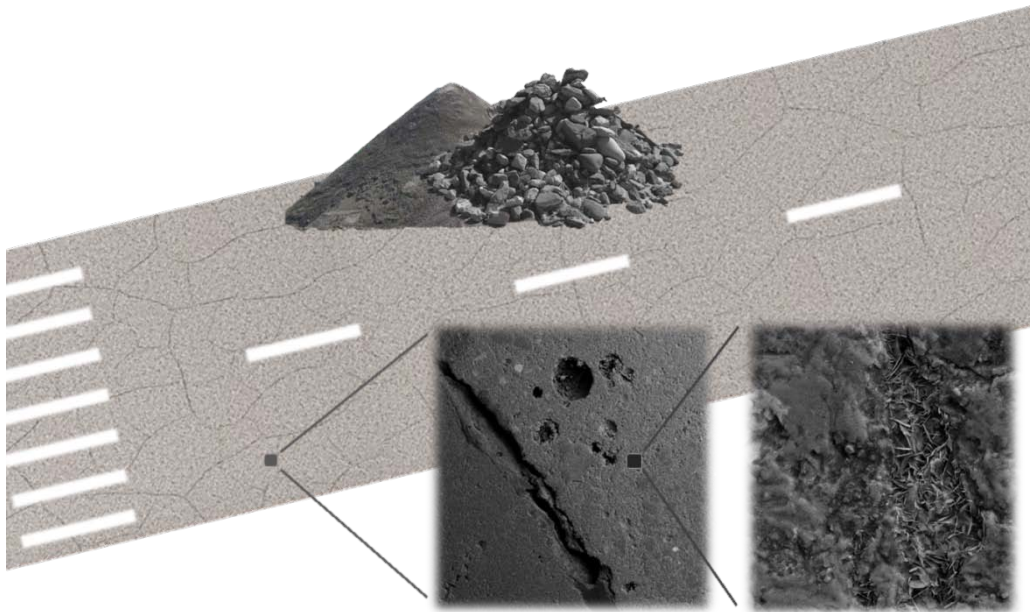An *IPRF* Research Report
Innovative Pavement Research Foundation
Airport Concrete Pavement Technology Program

Report IPRF-01-G-002-06-5

Role of Dirty Aggregates in the Performance of Concrete Exposed to Airfield Pavement Deicers

Programs Management Office
9450 Bryn Mawr Road
Rosemont, IL 60018   **July 2011**

An***IPRF*** Research Report

Innovative Pavement Research Foundation

Airport Concrete Pavement Technology Program

Report IPRF-01-G-002-06-5

Role of Dirty Aggregates in the Performance of Concrete Exposed to Airfield Pavement Deicers

Principal Investigators

Marc A. Anderson, Ph.D.
Steven M. Cramer, Ph.D., P.E.

Contributing Authors
Jessica M. Sanfilippo Silva
José F Muñoz
M. Isabel Tejedor

Table of Contents

LIST OF TABLES

LIST OF FIGURES

LIST OF APPENDICES

Appendix 1. Thermogravimetric and X-ray Diffraction Results from Task 4

Appendix 2. Air Void Analysis

Appendix 3. ASTM C1260 SEM Analysis

Appendix 4. Investigation of Potassium Acetate Penetration

Appendix 5. Micrographs and Thermodynamic Simulations of Potassium Sulfate Formation in Modified C1293

Appendix 6. Thermodynamic Simulations for the Formation of Solid Phases in the Modified C1293 Specimens

Appendix 7. Micrographs of Deterioration of the ITZ in Modified C1293 Specimens

Appendix 8. Deterioration of Microfines in Modified C1293 Specimens

Executive Summary

Overview

The objective of this research was to identify the roles that aggregate-based microfines may play in the durability of airport concrete exposed to potassium acetate-based deicers. Microfines in this study were defined as those particles below 75 microns ranging to smaller than 10 microns. Particular emphasis was placed on the potential for alkali silica reaction (ASR) and similar deleterious chemical reactions. In pursuit of this objective, a laboratory study was conducted that examined the nature and chemical reactivity of microfines associated with alluvial deposits of aggregates from select locations across the western half of the United States. Eight samples of microfines were initially obtained and characterized. A subset of five microfines was selected from the original set to cover a variety of locations and mineralogies. Microfines were selected and subsequently acquired from California, Colorado, Utah, Wisconsin and Wyoming. Two sets of fine and coarse aggregates were also obtained in quantities sufficient to prepare concrete specimens. One set of aggregates was obtained from Wisconsin with coarse aggregate being a dolomitic gravel and was established to be largely unreactive. At the other end of the activity spectrum, a granitic gravel was obtained from Utah that was known to be alkali-silica reactive.

Microfine Characterization and Reactivity

Microfines were characterized through a battery of tests that included the methylene blue test, California cleanness value, percent passing the No. 200 sieve, particle size distribution, alkali silica reactivity, X-ray diffraction, thermogravimetric analysis, and others. California and Colorado microfines contained significant quantities of 1:1 and 2:1 phyllosilicates. All sources contained significant quantities of silica in various forms and were categorized by their potential to cause deleterious reactions in concrete.

Microfines hold the potential for disrupting concrete hydration and microstructure formation through two mechanisms. One mechanism is the ability of 2:1 phyllosilicates to imbibe large amounts of water resulting in alterations to the workability of fresh concrete, the capture of water intended for cement hydration, and the potential for internal pressures from swelling microfine particles. A second mechanism is the release of ions and chemical alteration of the hydration products resulting in the potential degradation of expected compounds and the formation of new compounds that may or may not support the integrity of the cement paste microstructure.

Following initial characterization of the microfines, research centered on three tasks; 1) studying the reactivity of the microfine in alkaline solutions similar to what would occur in concrete; 2) evaluating the effect of microfines in concrete specimens subjected to a variety of durability and expansion tests; and 3) examining the microstructure of these specimens with respect to reaction products subject to various exposures.

Microfines from each source were introduced into each of three solutions at concentrations of 50 g/L and 76°C simulating conditions in concrete pore solutions in a controlled experiment and therefore providing an estimate of transformations that are likely to occur in concrete. Solids were extracted at 1 and 3 weeks and subjected to thermogravimetric analysis (TGA) and X-ray diffraction (XRD). The three solutions were; one saturated in $Ca(OH)_2$ and at0.8M NaOH; a second saturated in $Ca(OH)_2$, at 0.8M NaOH and containing 5M in KAc (potassium acetate) ; and a third saturated in $Ca(OH)_2$, containing 5M KAc but without NaOH. The results indicated that new products form depending on the Ca/Mg ratio and the pH of the solution. When the Ca/Mg ratio was less than 2, as one would anticipate in a concrete pore solution, the predominant phase at equilibrium was diopside $(CaMgSi_2O_6)$. In microfines having very small Ca/Mg ratios, the carbonates transformed into tremolite $(Ca_2Mg_5Si_8O_{22}(OH)_2)$.

Overall, this work showed that the microfines are highly reactive and are likely to impact the hydration process and the microstructure of the concrete.

Microfines and Potassium Acetate Effects on Concrete Specimens

Concrete specimens were prepared to assess the impact of the microfines in concrete exposed and unexposed to the potassium acetate commercial pavement deicer. Matched concrete specimens were prepared with each base aggregate, one from Wisconsin and one from Utah. Each condition consisted of the base aggregate washed clean of any microfines (control condition) and those with the individual addition of the microfines from the five different locations. Microfines were included in the concrete mixes by dip coating the aggregate where by approximately 1.5% by coarse aggregate weight was adhered directly on the coarse aggregate. Additional microfines were added with the cement such that a total of approximately 4.5% by total aggregate weight of microfines were introduced into the mix. All concrete specimens for a single condition (microfine type and aggregate type) were prepared from the same batch of concrete ensuring that slump, air content and other mixing parameters were the same for each specimen. The mix consisted of 0.45 w/c mix with a target air content of 6% and no additives other than an air entraining agent. There was considerable difficulty in achieving the target air content even with large additions of air entraining agent. Additions of some air entraining agents at levels an order of magnitude greater than recommended did not produce predictable or adequate levels of entrained air.

The primary mechanical evaluations of the concrete specimens consisted of two modified ASTM C1293 length-change protocols and a modified ASTM C666 freeze-thaw durability protocol. One modified C1293 protocol involved specimens prepared with no sodium hydroxide addition and subject to elevated temperature 100% humidity curing. The other modified C1293 protocol involved soaking similar specimens in potassium acetate deicer at elevated temperatures. Periodic length measurements were the primary measure of change in both protocols. The

modified ASTM C666 protocol included a 48 hour soak in deicer and 60 freeze-thaw cycles in water.   To examine the influence of sodium hydroxide additions, a series of ASTM C1260 tests was conducted on mortar bar specimens using each fine aggregate source and the microfines.

Microfines in quantities used in this research can cause slump loss and render air entrainment admixtures ineffective during concrete mixing. But assuming those problems can be overcome without compromising the mix, the hardened concrete performed satisfactorily in the absence of potassium acetate exposure. Potassium acetate does induce some expansion and paste degradation even in concrete specimens that do not contain microfines; however, these degradations are not to a level that identifies them as clearly harmful. When microfines are present in the concrete specimens and the specimens are exposed to potassium acetate, dramatic deterioration was observed in the form of expansions and reduced freeze-thaw durability. These deteriorations traced in consistent order of severity according to the source microfine present. Microfines with stronger phyllosilicate presence tended to cause the most severe deteriorations. Some microfines in the presence of potassium acetate cause expansions after one year that were 4 to 8 times larger than the control (no microfines present).   Expansions were larger with the reactive Utah aggregate as the base aggregate compared to the unreactive Wisconsin base aggregate. However, certain microfines in the presence of potassium acetate even in the Wisconsin aggregate specimens caused large expansions. In ASTM C1260 testing of mortar containing the two fine aggregate sources and the different microfines, the microfines actually decreased the expansions. The greatest reduction in expansion in the C1260 tests occurred with the microfines that caused the greatest expansions in the modified C1293 tests. The modified ASTM C666 test protocol with potassium acetate exposure proved to be considerably more severe than the standard C666 test procedure in water. Again, the presence of microfines caused deteriorations whereby relative elastic moduli were 2 to 4 times lower and relative weight losses were 2 to 4 times higher in specimens containing certain microfines as compared to controls (no microfines). Deterioration levels correlated with reduced air contents so it was not immediately evident whether or not these deteriorations were caused by the reduced air contents in those specimens or a more direct degradation from the combined potassium acetate-microfine presence or both. Considering of all the test data and an examination of the specimens, one concludes that both mechanisms likely contributed to the freeze-thaw deterioration.

Microstructural Investigations

A series of microstructural investigations were undertaken on the concrete specimens to determine if any chemical and/or microstructural changes could be associated with the deteriorations observed. Scanning Electron Microscope (SEM) analyses were conducted on concrete specimens that were exposed to the modified ASTM C1293 environments. By using SEM, the fate of the microfines introduced as coarse aggregate coatings in cured concrete were examined to determine their distribution between the interfacial transition zone (ITZ)

surrounding aggregate particles and bulk cement matrix. In addition, this technique allowed us to examine how the microfines reacted with the cement paste. By using SEM back scattering we could image the cement aggregate interface and by employing Energy-dispersive X-ray spectroscopy (EDS) we could determine the mineralogical makeup of the microstructure. Thermodynamic simulations were used to complement these results. Infrared Spectrometry (IR) analysis was used to establish the penetration levels of the potassium acetate.

The IR spectra analyses revealed that the potassium acetate had penetrated to the core in distressed concrete specimens. From this we conclude that distress was associated with the direct presence of the potassium acetate, derivative forms of potassium complexes, and chemical/physical transformations of the microfines.

Based on the microstructure analysis, it was concluded that the potassium acetate causes the structure of the paste to transform and increases the pH by freeing vast quantities of hydroxide. This effect has some similarities to the chemical effect of saturating concrete systems with sodium hydroxide. The potassium appears to transform over the exposure period from potassium acetate to calcium-potassium compounds and finally to potassium sulfate. Large areas of potassium sulfate crystals were observed in the interfacial transition zone (ITZ) in regions where one would expect to see ettringite crystals or monosulfate. The sulfate found in the new potassium sulfate complex is drawn from monosulfate and/or ettringite. The increased pH prompts a transformation of silica in the matrix into new species. These changes result in a degradation of the cement paste and the formation of less dense and larger volume products that appear to be responsible for degradation and expansion. These reactions are not what is traditionally viewed as an alkali silica reaction (ASR) and they occurred both in specimens containing the unreactive Wisconsin aggregates and in specimens containing the reactive Utah aggregate. Evidence of reaction rims around aggregates was not present, and behaviors observed in C1260 specimens were significantly different than those observed from the modified C1293 test. Examination of the C1260 specimens revealed the presence of ASR gel. ASR gel was also found in the modified C1293 specimens but not in significant amounts. Other by-products were observed in the modified C1293 specimens.   However, there appears to be similarities to the ASR reaction in that the potassium acetate promotes the occurrence of highly alkaline solutions that react with the silica and other elements in the microfines. These reactions are not confined to the reactions around the aggregates but occur both around the aggregates where some microfines were concentrated and in dispersed areas throughout the cement matrix where additional quantities of microfines were dispersed. Expansions in the modified C1293 tests were somewhat larger in the specimens containing the reactive Utah aggregate.

Discussion and Summary of Major Findings

The testing and analysis performed under this study has demonstrated that specific combinations of naturally-occurring aggregate microfines and potassium acetate deicer are deleterious to the

durability of portland cement concrete systems. The degree of distress depended on the mineralogical and chemical nature of the microfines, their quantity, and the degree of penetration of the potassium acetate into the concrete material matrix. The laboratory tests conducted in this research that form these conclusions are likely worst case scenarios that may not frequently occur in the field. None-the-less, combinations of these materials induce chemical and physical changes that even in field concretes under less severe conditions are likely to take a toll over time. The microfines often included 1:1 and 2:1 phyllosilicates, which in some cases can have positive and negative pozzolanic attributes, and are highly reactive. In addition, it was observed that microfines containing 1:1 and 2:1 phyllosilicates are not easily removed from coarse aggregates during washing. While some microfines are more reactive than others, none examined in this study was considered inert. Microfines fall on a differential scale of likely impact on concrete systems and with some microfines inducing impacts that can be many times greater than that of other microfines present in similar concretes at similar levels.

Major findings are:

- Even in the absence of potassium acetate, the presence of microfines at levels approaching, but below, five percent of the total aggregate weight had significant impacts on concrete mixing.
  - Slump reductions with some microfines were significant and would prompt water additions or create placement difficulties in the field in the absence of the use of water reducers or other mitigation strategies, particularly in slip-form paving operations.
  - Specific microfines matched with specific air entraining admixtures (AEA) tended to largely neutralize the function of the AEA making it impossible to achieve freeze-thaw resistant air contents regardless of the AEA dosage level.

- Combinations of microfines at the levels indicated and potassium acetate exposure caused significant deterioration of concrete that may be mistaken for ASR cracking and expansion. However, our analyses suggest it was not ASR, at least as traditionally diagnosed through the presence of ASR gel and reaction rims around aggregates. In addition, this degradation combined with the reduction in entrained air content led to dramatic loss of freeze-thaw durability. These degradations were associated with specific mineralogical profiles of microfines and these profiles consistently were associated with corresponding levels of degradation.

- The potassium acetate transformed in the concrete pore solutions to form potassium sulfate and calcium-bearing potassium sulfate compounds.

  - Both potassium and microfines were present in all cases where distress levels were the largest.

o During the transformation of the potassium acetate the level of hydroxide increases dramatically in the pore solution and can lead to reformation of silica species released by the microfines and the aggregates. While these reactions do not appear to be the classical alkali silica reaction, they may exhibit some similarity and create an environment where expansion internally within concrete leads to deterioration.

1. INTRODUCTION

In June 2007, the IPRF contracted with the University of Wisconsin-Madison to undertake the study entitled "Role of Dirty Aggregates in the Performance of Concrete Exposed to Airfield Pavement Deicer". The principal objective of this research is to elucidate the role that microfines from coarse and fine aggregates play in the development of the Alkali Silica Reaction (ASR) related distress observed in airport pavements subject to anti-icing agents. As a secondary objective, it was proposed to identify other potential impacts of microfines and deicers on concrete durability. Specific questions we sought to answer included:

- Do microfines accelerate and/or generate ASR?
- Does the combination of microfines and deicers (potassium acetate, KAc) accelerate ASR?
- Are the microfines involved in other harmful delayed chemical reactions, similar to ASR?
- Do microfines cause distress by themselves?
- Does potassium acetate cause damage to the cement paste microstructure?

2. RESEARCH PROJECT BACKGROUND

This study consisted of the 9 major tasks shown in table 1. Task 3 on aggregate screening and characterization occurred in two phases whereby a broader sample of aggregates was first received in smaller quantities leading to the selection of aggregates for subsequent tasks.

Table 1. Tasks for IPRF Project 01-G-002-06-5

Task
Task 1: Literature Review
Task 2: Develop Research Plan 　　　20% On-board review
Task 3: Aggregate Screening and Characterization
Task 4: Microfine Reactivity Tests 　　　TGA and XRD analysis 　　　40% On-board review
Task 5: Measurement of Concrete Durability 　　　Modified C1293 Testing 　　　Modified C666 Testing 　　　Microstructure Analysis 　　　Other related tests
Task 6: Reactivity of Microfines in Cement Paste
Task 7: Data Analysis
Task 8: Summary Reporting 　　　60% On-board review
Task 9: Final Report 　　　80% On-board review 　　　90% Desktop review 　　　Submit final report

Previous studies have reported on the effects that microfines, often in the context of a replacement of aggregate, have on concrete. Based on these references, table 2 was created with the variables classified by degree of impact that are believed to control the effect of microfines on the performance of concrete.

Table 2. Matrix of variables that control effect of microfines on concrete

Variable	Definition	Degree of Impact	References
Mineralogy	Type of the microfines	High	AbouZeid and Fakhry. 2003 Moukwa 1993 Bonavetti and Irassar 1994 Tasong *et al*. 1998 Caliskan *et al*. 2002 Kroyer *et al*. 2003
Amount	Quantity of microfines	High	Gullerud and Cramer 2003 Muñoz et al. 2007
Curing Conditions	Sudden loss of water in concrete during the first hours of hydration could induce significant microstructural damage and could be exacerbated by the presence of microfines	High	Nassif et al. TRR 1834 Muñoz et al. 2007
Dispersability	Agglomerations of ASR active microfines could provoke ASR damage	High	Rangaraju and Olek 2000
Dispersion	Distribution of microfines in the concrete	High-Moderate	Muñoz et al. 2007
Pozzolanic Activity	Microfine with significant pozzolanic activity can affect autogenous shrinkage	Moderate	Nassif et al. TRR 1834
ASR Activity	ASR active microfines may provoke damage in concrete and be nucleation sites for wider scale ASR	Undetermined	--

3. AGGREGATE SOURCES AND MICROFINE CHARACTERIZATION

Initial efforts focused on identifying potential sources of aggregates containing microfines. Based on previous studies, a set of tests was selected to determine the properties of the aggregates with the anticipation that most samples received would be ungraded pit-run material. Pit-run material was separated into fine and coarse aggregate fractions with each fraction containing its own amount of microfines. To determine the physical properties, both fractions were characterized following the testing protocols described in ASTM C136, ASTM C117, the California Test 227, the AASHTO TP 57 procedure, and a chemical method to determine alkali-silica reactivity. Additionally, the mineralogical composition and relevant properties of the microfines present in both fractions were examined by thermogravimetric analysis, X-ray diffraction, scanning electron microscopy, leaching and cation exchange capacity studies, and a

conductivity test. A summary of the methodology to initially characterize microfines is shown in table 3.

Table 3. Methodology used to characterize each aggregate sample

Test	Standard	Information
Sieve Analysis	ASTM C136	Size Distribution
Material finer than No. 200 sieve	ASTM C117	P200 Percentage
Evaluation of Alkali-Silica Reactivity	Chatterji, 2005	Potential for ASR Development
Thermogravimetric Analysis	UW-Madison	Microfine Mineralogy
X-ray Diffraction	UW-Madison	Microfine Mineralogy
Leaching and Cation Exchange Capacity Analysis	UW-Madison	Identification of Soluble Compound and Exchangeable Cation
Methylene Blue Test	AASHTO TP 57	Methylene Blue Value (MBV)
California Cleanness Test	California Test 227	Cleanness Value (CV)
Scanning Electron Microscope Analysis and Energy Dispersive Spectroscopy	UW-Madison	Size and Morphology
Conductivity Test	Luxán et al, 1989	Pozzolanic Activity

Seven aggregate sources were selected for initial characterization from aggregate producers across the western half of the United States to provide a spectrum of mineralogies. All sources are referred to using standard state abbreviations; Arizona (AZ), California (CA), Colorado (CO), Utah (UT), Wisconsin (WI), and Wyoming (WY). Some of these materials were chosen because of their known or suspected reactivity with respect to ASR. A comparison sample of an alluvial deposit from Wisconsin was also chosen adding an eighth source, since geology found in the state does not generally provoke ASR. The shipping information and contents received are shown in table 4.

Table 4. Aggregate source initial sampling

Sample	General Location
CA	South-Central California
CO-I	North-Central Colorado
UT	Northern Utah
CO-II	Northwest Colorado
CO-III	North-Central Colorado
WY	Wyoming
AZ	Southern Arizona
WI	Northern Wisconsin

The potential for alkali-silica reaction in microfines were measured using the test by Chatterji (2005). The summary of test results from ASR testing is shown in table 5. The overall analysis

of these microfines resulted in characterizing the microfines as shown in table 6 and eventually grouping them in table 7. Note that in table 6 high values tend to be harmful if in red and beneficial if in green.

Table 5. Δ[OH⁻] in the aqueous suspension of aggregates compared to ASTM C1260

Sample	Microfines	Coarse	Fine	ASTM C1260 expansion (%) at 14 days (fine aggregate only)
		Δ OH⁻		
Control Sand		--	45	
CA	290	114	128	
CO-I	190	34	249	
UT	276	270	295	0.26%
CO-II	276	--	208	
CO-III	192	40	47	
WY	292	151	210	
AZ	215	286	206	
WI	167	192	160	0.08%

Table 6. Summary of results for microfines

Sample	Methylene Blue	CA Clean Test	Pozzolanic Activity	ASR
CA	Low	High	Low	High
CO-I	Very High	Very Low	Mod	Low
UT	High	Low	Mod	High
CO-II	Mod High		Mod	High
CO-III	Mod High	High	Low-Mod	Low
WY	Very High	Low	High	High
AZ	Very High	Limit	Mod	Mod
WI	Mod High	High	Low-Mod	Low

Based on these analyses, five aggregates were selected for more extensive analysis and concrete sample preparation. Larger volumes of aggregate were then obtained from the sources associated with:

- CA
- CO-I (here after referred to as CO)
- UT
- WY
- WI

Table 7. Grouping of samples (aggregates and microfines) by potential to contribute to ASR

Sample	Classification	Group	Anticipated Impact
CA	G2 Low Alkali	G1	Inducers of physical changes for ASR development and promoters of ASR by increased alkali content and ASR active material
CO-I	G2 Low Alkali		
UT	G1 Mod Alkali	G2	Potential inducers of favorable physical changes for ASR development (at high P200) and promoters of ASR by increased alkali content and ASR active material
CO-II	G2 Mod Alkali		
CO-III	G3 Mod Alkali		
WY	G2 High Alkali		
AZ	G2 Mod Alkali	G3	Little or no effects on physical properties and potential source of ASR
WI	G3		

Coarse and fine aggregates were obtained for the UT and WI sources with UT representing ASR granitic gravel and Wisconsin representing unreactive dolomitic gravel. Coarse, fine, and pit-run materials were loaded in 55-gallon barrels and shipped to the University of Wisconsin-Madison. Barrels of pit-run materials were obtained from the remaining three sources to allow extraction of the microfines associated with each source. Each microfine source was further characterized and by combining results from various methods, the following characterization was made.

Thermogravimetric Analysis (DTG/TG)
The thermorgravimetric methodology involved heating the microfines in two atmospheres to differentiate dehydroxilation reactions from decomposition of carbonates, and collecting additional information about the nature of the carbonates. Weight losses on the TG curves recorded in air and carbon dioxide provides information on the carbonate and clay content present. The clay content describes the amount of either 2:1 clay or 1:1 clay based on the hydroxide content found in the TG analysis. A 1:1 clay is structured with a tetrahedral sheet layered with one octahedral sheet (e.g., kaolinite) where a 2:1 clay consists of an octahedral sheet between two tetrahedral layers (e.g., illite). The 1:1 clay type has nearly twice the OH^- content of the 2:1 type. The magnitude and temperature of the weight loss in the TG curves of microfines provide information on the type and quantity of clay. However, OH^-'s associated with metal hydroxyls are also released in the same range of temperatures that clay OH^-'s are, in addition, the crystallinity of the clay and impurities can also influence its temperature of dehydroxilation. Thus, data from the TG analysis should be used in conjunction with XRD to get a more exact interpretation on the microfine composition. It is important to note that some 2:1 type clays can

cause swelling when in contact with water and potentially redirect water from the cement hydration process.

X-Ray Diffraction Studies (XRD)
These studies were performed using a High Star 2-D X-ray diffractometer. The diffractograms were registered in a single run and in step mode. Unknown crystalline phases present in the sample were identified by matching the diffraction pattern to the patterns stored in the Powder Diffraction Files (PDF). The XRD can help identify certain crystallography of the minerals.

Scanning Electron Microscopy/Energy Dispersive Spectroscopy (SEM/EDS)
SEM and EDS analyses were conducted on gold coated samples of microfines using a JEOL 6100 Scanning Electron Microscope. The samples were observed and analyzed under 15 kV accelerating voltage. Each original image was 800 x 640 pixels with a resolution of 1,860 pixels/mm (47,058 pixels/inch) for a magnification of 2,500 x. By the atomic percentage of the elements the EDS, we can determine the mineralogy of different particles in the microfines.

By combining the SEM/EDS results, in table 9, with the ones from TG and XRD analysis, given in table 8, we can described more precisely the mineralogical composition of the microfines. For example, SEM/EDS provides information on the different mineralogical phases of the microfines through the chemical composition of different particles but may loss some minor phases because it is a microscopy technique. XRD, on another hand, provides an average analysis of a large sample size and identifies the different crystal structures present in the microfines; however, it may underestimate or not show at all poorly crystalline materials. Thus, by coordinating results from both techniques the different mineral phases composing the microfines are more accurately established.

Table 8. Microfine analysis from XRD and TG

Microfine Samples	Carbonates Content (% w)	Carbonate Species	Clay Type
CA	<<	-	1:1 and 2:1
CO	2	-	1:1 and 2:1
UT	21-23	Dolomite + Calcite + Proto-Dolomite	1:1 and 2:1
WI	27-41	Dolomite + Proto-Dolomite	-
WY	17-30	Calcite + Proto-Dolomite	2:1

Table 9. Description of microfines

Microfine Particle Mineraology

Chemical Composition of the major constituents from EDS

Source	General description	Some phases seen
CA	Contains primarily Si, Al, and Fe with small areas of Ca, K, and Mg.	Si4.5Al2.1Fe Mg0.5 (major phase) $Si_{5.6}$ Al $_{2.5}$ Fe Mg $_{0.3}Ca_{0.3;}$(from chemical analysis both are within the range of montmorillonite)
CO	Contains primarily Si, Al, and Fe with small areas including Na and K.	$Si_{18}Al_9Fe_3K_1Mg_1$ (montmorillonite) $Si_3Al_1Na_1$(Albite) $Si_3Al_1K_1$(Microcline) Quartz
UT	Contains a combination of Mg, Al, Si, K, Ca, and Fe.	quartz, calcite, dolomite $Si_3Al_1K_1$(Microcline) $Si_2Al_{1.5}Mg_1Ca_1$ (vermiculite) Si_2Al_1 (possibly illite)
WI	Contains primarily Si, Mg, and Ca.	dolomite, calcite, and areas of silica likely as quartz Si_1Mg_1 (talc) $Si_{16}Al_6Na_3Ca_1$ (feldspar) $Si_3Mg_1Ca_1Fe_1$ (pyroxenesilicates) $Si_3Al_1K_1$ (microcline)
WY	Composed of silica aluminum microfines mixed with varying levels of Ca or large aggregations of K.	calcite $Si_5Al_4K_1$ (possibly muscovite) $Si_5Al_3Ca_1Na_1$ (aggregate of albite and anorthite)

By considering all the data collected together from the thermogravimetric analyses, the X-ray diffraction, scanning electron microscopy/energy dispersive spectroscopy and reviewing basic mineralogy of minerals, we determined the constituents of the microfines. This information was used to determine how and why microfines perform differently in the different tests.

CA – XRD and TG show the presence of 1:1 and 2:1 phyllosilicates, quartz, and low contents of carbonate species. In addition, from SEM/EDS analysis we found that quartz is present as very small particles and aggregate with other mineral phases. The major constituents are 2:1 phyllosilicates more closely resembled montmorillonite than vermiculite based on the chemical composition. From the dehydroxylation loss in the TG curve and given that the major constituents are 2:1 type clays we can predict a high content of these minerals ($\cong$ 67 %). To account for the total constituents of the microfines, carbonates made about 2%, some humidity water accounts in general for less that 3% of the microfines weight, thus the rest should be due to the contribution of microclinic and quartz (seen only by XRD).

CO – From the XRD and TG we see 1:1 and 2:1 phyllosilicates, low contents of carbonates similar to the CA, and also some kaolinite, microcline, albite, and quartz. The three later minerals were also identified by SEM/EDS as individual particles. In addition, we found particles of montmorillonite (rather than vermiculate) as one of the major constituents. Since most of the hydroxylated silicates belong to the 2:1 type clays, the content of these minerals could be close to 52%.

UT – From XRD and TG analysis it was established that these microfines have between 21% to 23% dolomite and calcite. These techniques also showed the presence of quartz, non-hydroxylated silicates as microcline, and clays (1:1 and 2:1). Information extracted from SEM/EDS analysis reaffirmed these findings and identified most of the clays as illite and vermiculate. We were unable to locate particles of kaolinite (phase shown by XRD) because these particles were likely small and forming aggregates with other mineral phases.

WI – TG analysis showed that 35 % of the microfines are composed of dolomite. XRD showed quartz as the other major constituent. However, SEM/EDS data showed the presence of feldspar, pyroxenes, microcline, and talc as minor but independent phases.

WY – TG analysis and XRD showed the microfine was rich in calcite and dolomite, with some indication of the presence of 2:1 phylosilicates (montmorillonite or vermiculite). SEM/EDS analysis showed mainly particles of calcite and aggregates of albite and anorthite as major constituents. Particles with the chemical composition of muscovite (clay) were also identified.

Particle size distributions for the microfines are shown in figure 1. The microfines ranged in size from 0.1 microns to 100 microns with the microfines from Utah presenting the finest distribution. The percentages passing 45 microns (as one indicator of the different in fineness) for each set of microfines were as follows: CA : 68%, CO : 77%, UT : 95%, WI : 65%, WY : 85%.
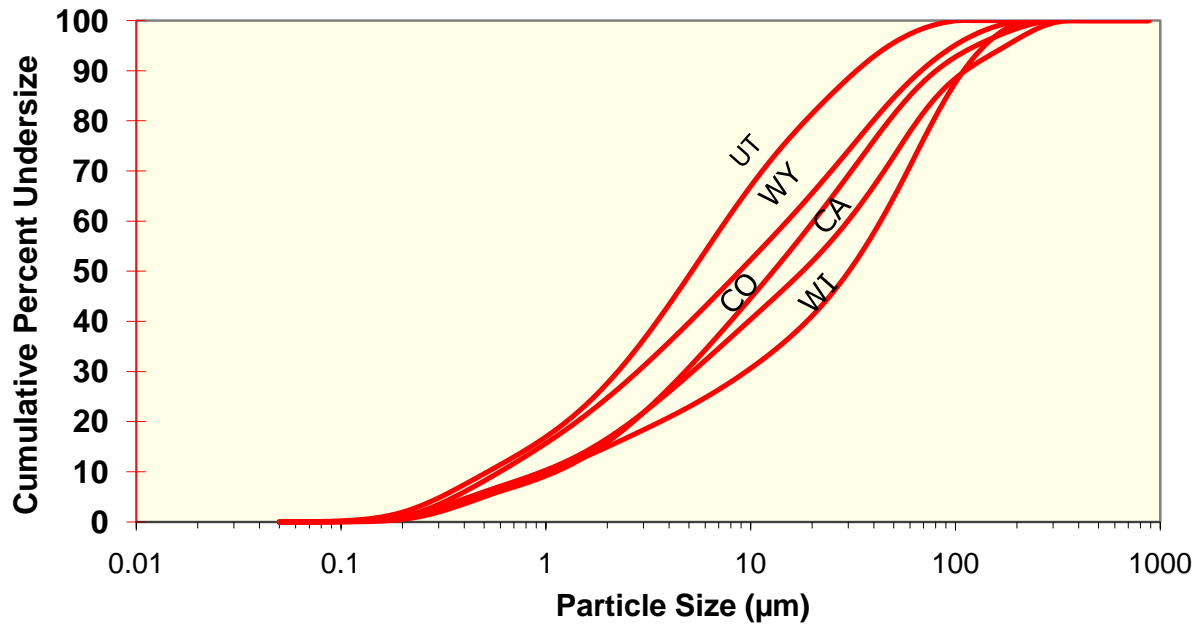
Figure 1. Particle size distributions for the microfines

4. RESEARCH WORK PLAN OVERVIEW

Following initial characterization of the microfines, the work plan for the research was formulated in three tasks embodied as tasks 4, 5 and 6 in table 1.Task 4 was targeted to identify reaction products from microfines in a controlled solution simulating concrete pore solutions. Task 5 was designed to evaluate the durability of concrete containing microfines subject to deicer and freeze/thaw exposure. Task 6 involved investigating the reactivity of microfine coatings on aggregates in a cement matrix. It was envisioned that the results of the three tasks would be interrelated to provide a description that relates the reactivity of the microfines to the observed macroscale durability of the concrete.

4.1 Task 4. Identification of Reaction Products of Microfines under Highly Alkaline Conditions in the Presence and Absence of Deicers

Objective: The objective was to identify the chemical transformation of microfines when they are exposed to a controlled highly alkaline (concrete-like) media in the presence and absence of deicers (potassium acetate).

Samples: Microfine samples as obtained from the aggregate sources were evaluated in this task. The microfines were immersed in solutions of 1) saturated $Ca(OH)_2$ in 0.8 M NaOH, 2) saturated $Ca(OH)_2$ in 0.8 M NaOH and 5 M KAc, 3) Saturated in $Ca(OH)_2$, and 5M KAc. See table 10.

Measurement technique: Scanning Electron Microscope/Energy Dispersive X-ray Spectroscopy (SEM/EDS).

Table 10. Matrix of samples to be tested in Task A

	Untreated		**Solution 1** (saturated $Ca(OH)_2$ in 0.8 M NaOH)		**Solution2** (saturated $Ca(OH)_2$ in 0.8 M NaOH and 5 M potassium acetate	
Microfine	Washed	Dry Sieve	Washed	Dry Sieve	Washed	Dry Sieve
California	X	X	X	X	X	X
Utah	X	X	X	X	X	X
Colorado	X	X	X	X	X	X
Wyoming	X	X	X	X	X	X
Wisconsin	X	X	X	X	X	X

4.2 Task 5. Effect of Microfines on the Durability of Concrete Exposed to Deicers.

Objective: The objective was to determine if the microfines combined with deicer instigate ASR or other durability related distress in concrete specimens.

Samples: Samples were prepared according to the specifications of modified ASTM C1293 and modified ASTM C666. The concrete mix design is summarized in table 11 and each condition was prepared in one batch of 2.3 cubic feet.

Table 11. Concrete specimen mix design for ASTM C1293 and C666

Mix Design Item	Quantity
Cement	658 lbs/yd^3 Type I Cement
Water/Cement	0.45
Coarse Aggregate	1715 lbs/yd^3 (60%)
Fine Aggregate	1044lbs/yd^3 (40%)
Target air content	6% ± 1%

For each test, three specimens were prepared to ensure repeatability and an additional sample was prepared to perform microstructure analysis. The tests and curing conditions are shown in table 12. The test specimen matrix is shown in table 13.

Measurement technique: Extensometer, Dynamic Modulus by Sonic Vibration, Weight loss, Scanning Electron Microscope/Energy Dispersive X-ray Spectroscopy (SEM/EDS).

Table 12. Summary of concrete specimen curing conditions

Test	Curing Conditions
Modified ASTM C1293-Humid	High relative humidity at 38 ºC for 12 months (no addition of NaOH)
Modified ASTM C1293-Deicer	Immerse specimens in a KAc-based deicer solution at 38 ºC for 12 months
Modified ASTM 666 Procedure A in presence of KAc	Initial 28 days of wet curing conditions ▪ Air dry at 23 ºC 50% RH for 24 hours ▪ KAc soak at 38 ºC for 48 hours ▪ Air dry at 23 ºC 50% RH for 24 hours ▪ Freeze-thaw cycles for 60 cycles ▪ Repeat

Table 13. Test matrix for Task 5 concrete evaluation
This matrix was completed for two aggregate sources, Utah aggregate and Wisconsin aggregate.

Sample	Modified ASTM C1293-Humid	Modified ASTM C1293-Deicer	Modified ASTM C666
California	X	X	X
Colorado	X	X	X
Control (No coatings)	X	X	X
Utah	X	X	X
Wisconsin	X	X	X
Wyoming	X	X	X

4.3 Task 6. Reactivity of Microfines as Coarse Aggregate Coatings in the Presence and Absence of Deicers

Objective: The objective was to determine if the reaction products identified in the Task 4 were also found when the microfines act as aggregate coatings and nucleation sites in a mortar matrix. The research team sought to detect alternative reaction products and associate them with ASR or other reactions. The team also sought to identify damage in the concrete microstructure as a consequence of the presence of both microfines and deicers such as: depletion of $Ca(OH)_2$ concrete reservoirs and/or dissolution of ettringite. This final exploratory phase of the research was designed to identify harmful reaction products under a wider variety of conditions than possible in Task 5.

Samples: The samples consisted of 2x2x2-inch mortar cubes with two ¾-in. microfine-coated stones embedded. The clean stones were dip-coated with microfines to provide a coating that was approximately 1.5% of the weight of the stone. Three of the microfine sources underwent testing (see matrix of samples below) with two types of aggregates; in one cube two non-reactive (Wisconsin) stones and in a second cube two ASR reactive stones (Utah), coated with the microfines, as depicted in figure 2. The three

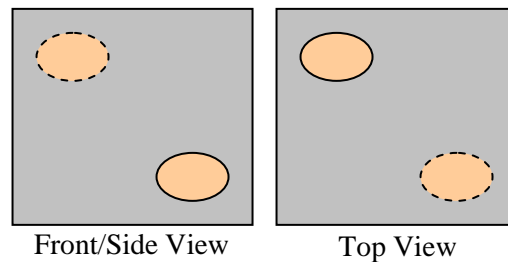microfines were selected from the five based on their unique morphology. The test matrix is shown in table 14.

Front/Side View   Top View

Figure 2. **Schematic view of the 2x2x2 in. mortar cubes with embedded aggregates**

The mortar was prepared with a w/c = 0.45.   The cubes were cured under wet burlap for 24 hours, submersed in the three solutions and brought to temperatures of 38ºC and 80ºC. The solutions are 1) water, 2) solution of saturated $Ca(OH)_2$ in 0.8M of NaOH and 5M potassium acetate, and 3) 5M potassium acetate. The microstructure of the stone-cement paste interface were analyzed at 3 days and 56 days after casting using two cubes of each set. The third cube will be held in reserve should further analysis be desired.

Analytical technique: Scanning Electron Microscope/Energy Dispersive X-ray Spectroscopy (SEM/EDS).

Table 14. Test matrix for Task 6

Microfine Samples	Solution A	Solution B	Solution C
Control (No coatings)	X	X	X
California	Not tested	Not tested	Not tested
Utah	X	X	X
Colorado	X	X	X
Wyoming	Not tested	Not tested	Not tested
Wisconsin	X	X	X

4.4 SEM Analysis

Scanning Electron Microscope (SEM) analyses were conducted on cylinder specimens that were formed at the same time and exposed to the same environment as those specimens prepared for modified ASTM C1293 and modified ASTM C666.

The following procedure was used to prepare the SEM specimens. At 3, 6, and 9 months, a ½-inch thick sample slice was cut from the specimen. The slice was taken after a ½-inch top layer was removed by wet saw. An aggregate and paste area was selected less than one inch from the outer edge of the cylinder where possible. This area was selected because a previous study found the average deicer penetration to be approximately ¾ to 1 inch in airport pavements

(Balachandran 2009). The SEM samples were processed in a similar manner to that of Muñoz et al. (2010) and Balachandran. The samples to be examined in back scattering electron (BSE) mode were cut and placed in acetone for 5 minutes then dried. The samples were then vacuum-impregnated with Buehler two-part epoxy. The impregnated specimens were cut using a Buehler lapidary saw with propylene glycol. Afterwards, they were lapped and polished on a Buehler Ecomet 4 Polisher using a series of lapping paper at 330, 400, 600, and 1000 grit, and finishing with 0.05µm micropolish. At this point, each specimen was coated with a thin layer of gold for 80 seconds at 20mV using a Denton Vacuum Desk II sputter coater/etch unit. Figure 3 shows an example of a specimen ready to be examined. Each of the samples was examined using a LEO 1530 Scanning Electron Microscope (SEM) in the back scattering electron (BSE) mode using an acceleration voltage of 15 kV.

In order to isolate the impact of microfines in the concrete, this research progressed from examination of the simplest to the most complex case. Uncoated aggregate and the microfines were individually examined under SEM and EDS using back scattering images. In addition, specimens from the modified ASTM C1293 tests were analyzed in sequence. This allowed for comparison of observations from one situation to the next. Reaction products similar to those found in the earlier microfine studies of this project will be targeted for identification. By using the BSE images and the molar ratios components of the matrix were identified.

Figure 3. SEM sample prepared for BSE mode and EDS analysis

4.5 SEM Background

In these studies, microfines were placed on the aggregate surface as a coating which concentrated microfines in the ITZ. In this research, the distance from the ITZ starts from the rock surface and moves outward towards the cement bulk. Typically the ITZ is referred to as a distance approximately 40µm to 50µm from the rock surface (Zampini 1998).

When analyzing the interfacial transition zone of concrete containing microfines, the microstructure of standard concrete was used as the baseline for comparison. As portland cement hydrates it produces various products including calcium silica hydrate (C-S-H), calcium

hydroxide (CH), ettringite, monosulfate, AFm and ADT phases, and hydrogarnet in small amounts. Each of these minerals can be identified by EDS using the molar ratios of the elements in the analysis. For example, C-S-H, is associated with a Si/Ca ratio ranging from 0.45 to 0.5 while alite has a Ca:Si ratio approximately between 2.5:1 and 3:1. Molar ratios expected for the different mineral phases in cement are reported in table 15 and table 16which were adopted from Muñoz et al. (2010).

Table 15. Principle characteristics followed to classify unhydrated cement particles

Compound	Formula	BSE Image Appearance	Major Elements	Ca/Si	Ca/Al	Additional Elements
Tricalcium Silicate (alite)	3CaO SiO2	Bright & delimitated	Si, Ca	2.6 - 3.0		None
Dicalcium Silicate (belite)	2CaO SiO2	Bright & delimitated	Si, Ca	0.7 - 2.5		None
Tricalcium Aluminate	3CaO Al2O3	Bright & delimitated	Al, Ca		1.3 - 2.1	None
Tetracalcium Aluminoferrite	4CaO Al2O3 Fe2O3	Bright & delimitated	Al, Ca		1.5 - 2.6	Fe

Table 16. Principle characteristics followed to classify hydrated cement particles

Compound	Formula	BSE Image Appearance	Major Elements	Ca/Si	Ca/Al	Additional Elements
C-S-H		No discernible	Si, Ca			None
Calcium Hydroxide	Ca(OH)2	No discernible	Ca			
Ettringite	3CaO Al2O3 3CaSO4 32H2O	No discernible	Ca, Al	3.1 - 2.2	2.0 - 20.0	S
Monosulfate	3CaO Al2O3 CaSO4 12H2O					

The analysis of the microfine-enfused concrete included examination for hydrated alkali silica gel. As previously presented in this research, the microfines can act as the vehicle for the introduction of these finer materials of diverse mineralogy into concrete. Microfines were a potential source of silica and also alkaline metals, the most important components in the ASR-type reactions. However, when studying the influence of aggregates and microfines on the durability of concrete, consideration was given to the formation of alkali silicates and the appearance of new solid phases that develop with time after the concrete sets. For example, the formation of silicates of the amphibolite family (e.g. tremolite: $Ca_2Mg_5Si_8O_{22}(OH)_2.2H_2O$) by transformation of sediments rich in dolomite and quartz has been widely reported (Woolast et al. 1968). Although, these silicates are not exactly hydrated alkali silicates (ASR products), the slow transformation of well crystalline phases, quartz and dolomite, into a single phase of different density and morphology could well be a very disruptive phenomenon in the microstructure of set concrete.

5. RESEARCH MEASUREMENTS AND OBSERVATIONS

5.1 Task 4

The objective of Task 4 was to identify the reaction compounds formed when microfines are in controlled alkaline solutions to provide predictions of what may also occur in concrete environment. To achieve this purpose, microfines from each source in powder form were introduced into each of three solutions at 50 g/L and 76°C. Solids were extracted at 1 and 3 weeks and subject to TGA and XRD. The three solutions were:

- Sol 1: Saturated in $Ca(OH)_2$, 0.8M NaOH; pH = 13.4
- Sol 2: Saturated in $Ca(OH)_2$, 0.8M NaOH and 5M KAc; pH = 13.6
- Sol 3: Saturated in $Ca(OH)_2$, 5M KAc; pH = 12.6

Thermogravimetric analysis revealed that the outcomes associated with solution 1 were approximately the same as those associated with solution 2. The major differences between the TG curves of treated and untreated microfines were associated with the evolution of Ca and Mg carbonates. Carbonate content was smaller in microfines treated with solutions 1 and 2.Carbonates consisting of Mg-poor dolomite (UT and WY) transformed in the solutions much faster than highly crystallized dolomite (WI).

Results from XRD analysis confirmed the thermogravimetric analysis findings. In addition, these results suggest the presence of diopside ($CaMgSi_2O_6$) and the partial dissolution of quartz (smaller particles upon treatment). Above pH 13, Mg Ca carbonates in microfines rich in SiO_2 evolved towards $Ca_2Mg_5Si_8O_{22}(OH)_2$, $CaMgSi_2O_6$, $CaCO_3$ or a mixture of these minerals, depending on the Ca/Mg ratio. When the Ca/Mg ratio was greater than 2, the predominant phase at equilibrium was $CaCO_3$. When Ca/Mg ratio was less than 2, the predominant phase at

equilibrium was $CaMgSi_2O_6$. In microfines having very small Ca/Mg ratios, the carbonates transformed into $Ca_2Mg_5Si_8O_{22}(OH)_2$.

Thermodynamic predictions and equilibrium diagrams were used to calculate the solid phases formed in the pore water of concrete in the presence of Mg and KAc. Assuming that the pore water is very rich in Ca and silicates, has a Mg concentration of 130 mM, and a pH above 13, 60% of the Ca could potentially be in the form of $CaSiO_3$, 30% as $CaCO_3$, and the rest as $CaMgSi_2O_6$; 100% of Mg should be $CaMgSi_2O_6$.

From these tests and analysis, given enough time, the presence of Mg Ca double carbonate microfines in aggregates should change the mineralogy of the ITZ and therefore affect some properties of concrete. The magnitudes and timing of these impacts cannot be determined from Task 4 findings alone. See appendix 1. Thermogravimetric and X-ray Diffraction Results from Task 4 for TG and XRD figures showing these results.

5. 2 Task 5

5.2.1 Task 5 – Concrete Specimens

The objective of Task 5 was to prepare concrete specimens containing microfines and evaluate their macroscale performance under a variety of durability tests. Microstructure evaluation of the concrete followed to link macrostructural observations to findings in Task 4 (chemical transformations in controlled alkaline solutions). The aggregate was prepared by dipping washed, dry aggregate in aqueous slurries of microfines. The slurry was made of a mixture of microfines that were extracted from the various sources of aggregate in either a washing manner or from dry sieving. The microfines were recombined in a ratio that mimicked the original extracted ratio and table 17 lists the ratio of dry to wet microfines for each source.

Table 17. Microfine recovery from aggregate sources

Microfine Percentage Combinations		
Microfine Source	Microfines recovered from dry sieving [%]	Microfines recovered from washing [%]
California	34	66
Colorado	28	72
Utah	9	91
Wisconsin	61	39
Wyoming	27	73

The microfines were weighed dry and then added to water making the slurry. By weighing the dry coarse aggregate before and after dipping, the percent of microfines that adhered to the

aggregate was determined. The microfines were coated onto both unreactive WI aggregate and reactive Utah aggregate separately with an effective adhesion of approximately 1.5% ±0.1% by coarse aggregate weight. An additional 3.5% (based on total aggregate weight) of dry mixed microfines was added to the fine aggregate portion. In addition, the Wisconsin fine aggregate contained 0.8% microfines by weight and 1.7% for the Utah fine aggregate. These microfines were not removed for practical reasons to preparing materials for mixing. ASTM C1293 calls for the addition of sodium hydroxide to raise the NaO equivalent to 1.25% based on the mass of cement. This addition was not made for two reasons. First, there was concern that such an addition would mask the alkali contribution of the microfines. Secondly, such an addition would have necessitated separate batching of the modified C1293 specimens.

During mixing, the microfines appeared to neutralize the initial selection of air entraining admixture. As indicated in figure 4,with Wyoming microfines, the research team was unable to achieve target air levels independent of the amount of air entraining agent used. The air entraining agent used was a common agent provided by a national distributor. An alternative and less commonly used air entraining agent was ultimately selected for use in mixing. As shown in figure 5, this AEA proved more effective though dosage rates far exceeded normal field levels. Figure5 shows the air contents achieved with the second AEA in trial batches. Ultimately, AEA #2 produced air contents as shown in figures 6 and 7 with the dosage rates shown. These figures show that microfine-containing mixes require significantly larger dosages of AEA. The target air content was not achieved in all cases because of the unpredictability of the process.
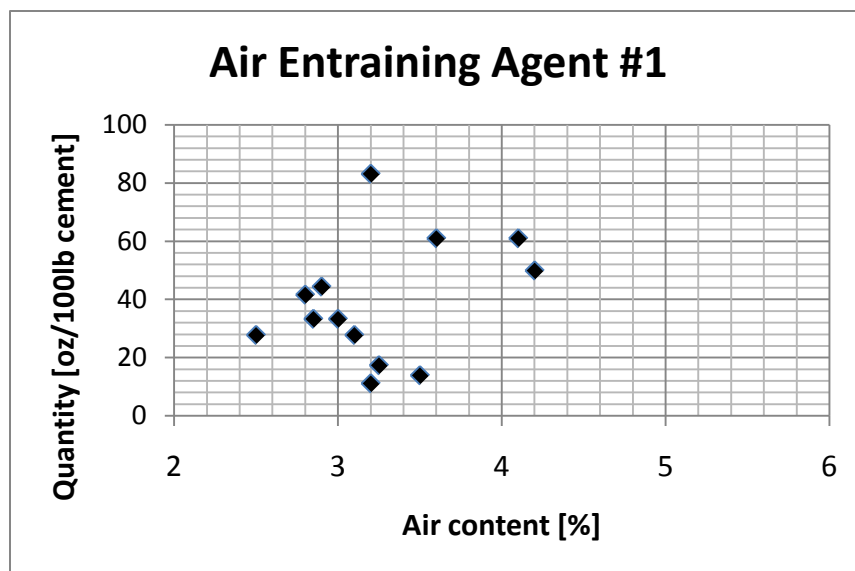
Figure 4. Air content achieved in concrete batches containing WY microfines with different dosages of air entraining agent No. 1. The manufacturer's recommended typical field dosage falls between 1 and 3 fl. oz. per 100 lbs of cement.

Air Entraining Agent #2
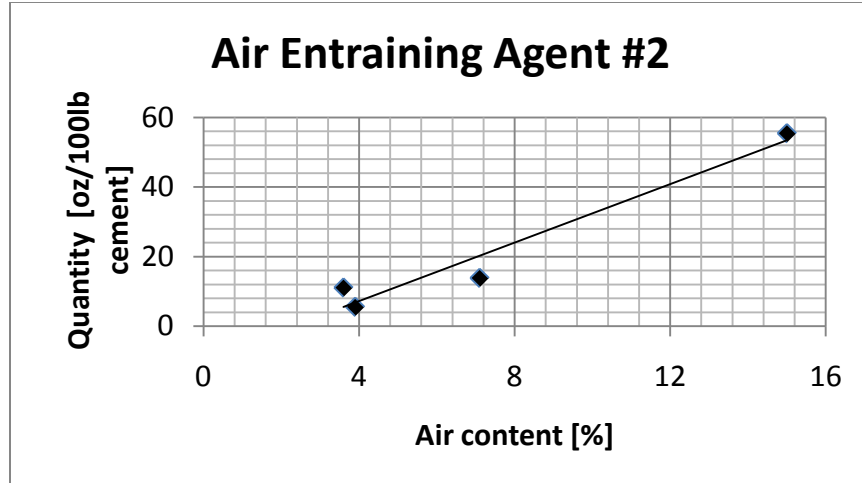
Figure 5. Air content achieved in concrete batches containing WY microfines with different dosages of air entraining agent No. 2. The manufacturer's recommended typical field dosage falls between 0.15 and 3 fl. oz. per 100 lbs of cement.

Wisconsin Specimen Air Content
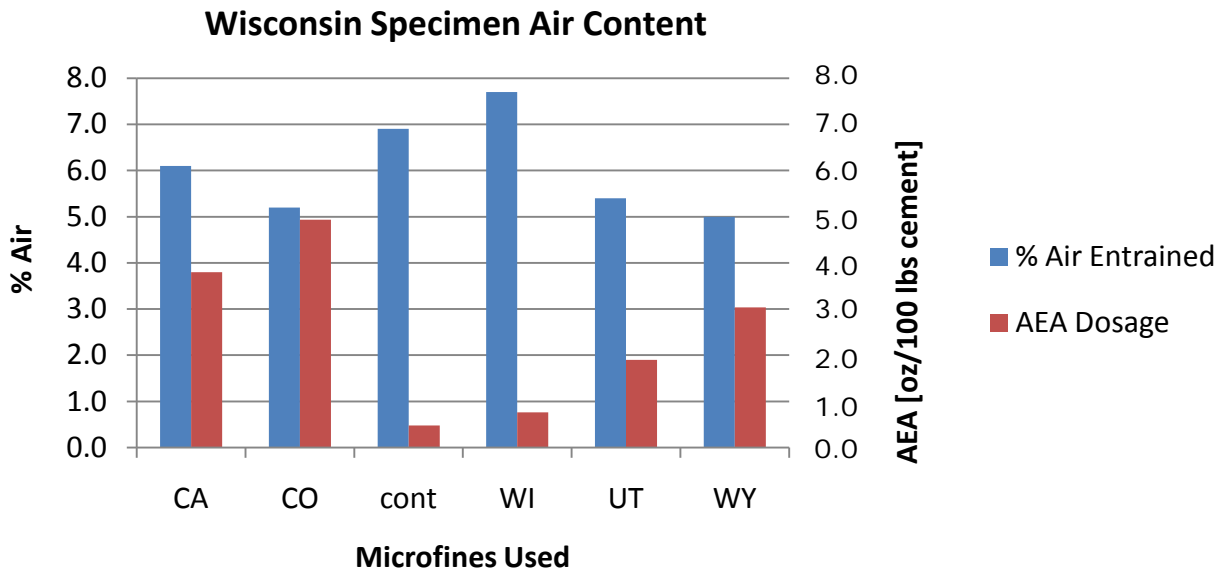
Figure 6. Air content and air entraining agent dosages for concrete batches using Wisconsin aggregate.

Utah Specimen Air Content
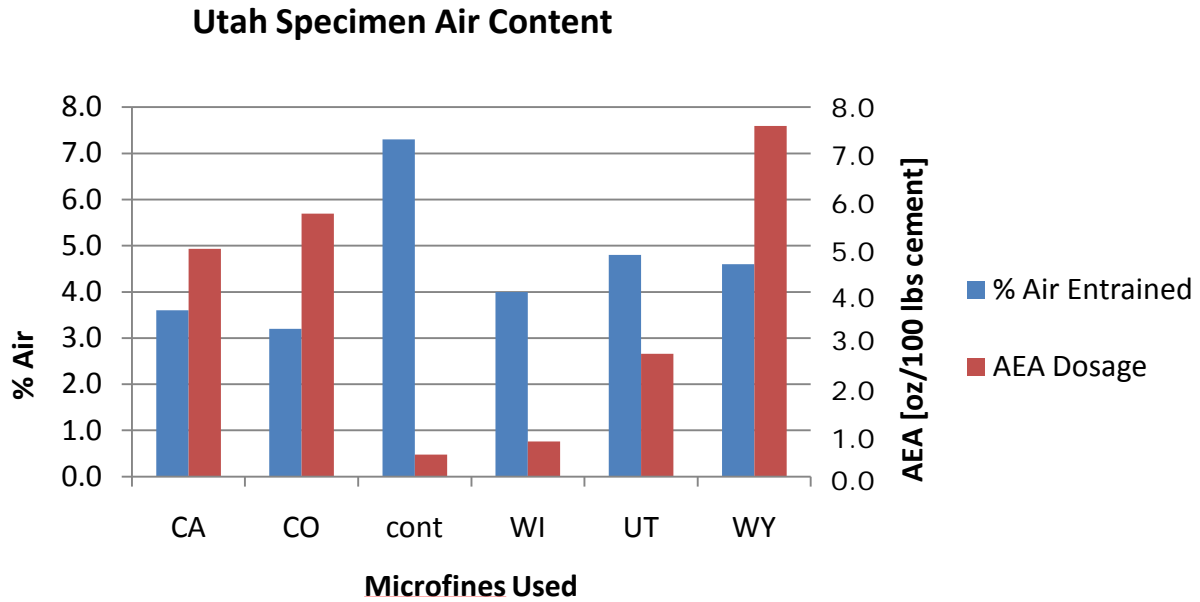
Figure 7. Air content and air entraining agent dosages for concrete batches using Utah aggregate.

The outcome of the concrete batch and specimen fabrication process is shown in table 18. These data highlight the large variation in slump and the challenge in managing air content with microfine additions that contain 1:1 and 2:1 phyllosilicates.

Table 18. Mix parameters associated with concrete specimen preparation

Mix	Adhered Fines [%CA wt]	Total Added Microfines [% total aggregate wt]	Total Added Microfines [% FA wt]	Slump [in.]	Fresh Air Content [%]	ounces of AEA / 100lbs cement
CA on WI	1.6	4.5	11.9	0.75	6.1	3.80
CO on WI	1.5	4.4	11.7	0.375	5.2	4.93
cont WI	0.0	0.0	0.0	9.5	6.9	0.47
WI on WI	1.3	4.3	11.4	2	7.7	0.76
UT on WI	1.4	4.4	11.6	4.5	5.4	1.90
WY on WI	1.5	4.4	11.7	0.75	5.0	3.04
CA on UT	1.4	4.4	11.6	0.25	3.6	4.93
CO on UT	1.4	4.3	11.6	0	3.2	5.69
cont UT	0.0	0.0	0.0	6.25	7.3	0.47
WI on UT	1.3	4.3	11.4	1.25	4.0	0.76
UT on UT	1.5	4.4	11.7	3	4.8	2.66
WY on UT	1.3	4.3	11.4	0.25	4.6	7.59

A subset of specimens was analyzed according to ASTM C457 to determine hardened concrete air content. The linear transverse model was used to determine the spacing factor of the air void system. Table19 allows comparisons of the fresh air content to the hardened air content and corresponding spacing factors. The expectation was that the air content values would be within two percent of each other and as shown in table 19 they were (Whiting 1998). It is noted that the largest discrepancies occurred in the lowest air contents with spacing factors that were larger than what one might expect from the corresponding air contents. Air bubbles varied in size and spacing with the WI microfines on WI aggregate specimens showing the most regular size and distribution of both entrained and entrapped air. See appendix 2 for more information about the air voids within the modified C1293 specimens.

Table 19. Hardened air content and spacing factor of C1293 Humid specimens

Specimen Name	Fresh Air Content [%]	Hardened Air Content	Spacing Factor [in.]
Typically Recommended	5.0 - 7.0	5.0 - 7.0	0.004 to 0.008
CA on WI	6.1	6.8	0.007
WI on WI	7.7	7.2	0.006
CA on UT	3.6	5.5	0.021
CO on UT	3.2	4.5	0.023

Alkalinity

Increased alkalinity translates to free hydroxide (OH^-) ions that can react and deteriorate siliceous aggregates. Often increased alkalinity comes in the form of KOH or NaOH. The ions from these hydroxyls, K^+, Na^+, and OH^- are available to form secondary reaction products such as gels including ASR gel. When the concentration of alkaline ions is large they associate with other anions available such as sulfates by taking them from other products such as ettringite. In order to determine the total alkali content of the mix, the cement was analyzed with the results shown in table 20. These results were combined with the microfine Na_2O to determine a total percentage as seen in table 21. The microfine alkali content as included in table 21 accounts for only the exchangeable alkali cations of the clay minerals. The method used did not account for the total amount of alkali cations liberated due to dissolution under cement pore solution as might occur for mineralogical phases such as certain feldspars.

Table 20. Cement analysis

XRF FB, Vicat, Blaine, Soundness (Autoclave)

FUSED BEAD (Loss Free)

SiO2	20.05	%
Al2O3	4.64	%
Fe2O3	2.68	%
CaO	63.31	%
MgO	2.39	%
SO3	2.516	%
K2O	0.429	%
Na2O	0.228	%
TiO2	0.22	%
P2O5	0.128	%
Mn2O3	0.124	%
SrO	0.059	%
Total	99.48	%
Alkalis Eq.	0.51	%
C3S	60	
C3A	7.8	
C2S	12.3	
C4AF	8.2	
Loss On Ignition	2.71	%
Blaine	4340	sg.cm./gm.

Vicat Setting Time

Initial	125	minutes
Final	240	minutes

Autoclave Expansion   0.013   %

Table 21. Alkali content of the cement and microfines

Mix	Total Added Microfines [% total]	Weight of fines added [lbs]	Alkali Content Added from microfines	Total NA_2O [%cement wt]
CA on WI	4.5	10.58	0.064	0.34
CO on WI	4.4	10.34	0.807	1.67
WI cont	0	0	0	0.23
UT on WI	4.4	10.34	0.259	0.69
WI on WI	4.3	10.11	0.005	0.24
WY on WI	4.4	10.34	2.637	4.93
CA on UT	4.4	10.34	0.062	0.34
CO on UT	4.3	10.11	0.788	1.63
UT cont	0	0	0	0.23
UT on UT	4.4	10.34	0.259	0.69
WI on UT	4.3	10.11	0.005	0.24
WY on UT	4.3	10.11	2.577	4.82

5.2.2 Task 5 – Concrete Length Change in Various Environments

After an initial 24 hours of curing, samples were subject to the modified ASTM C1293 (less the NaOH additive and using AEA) and modified ASTM C 1293 (KAc deicer and using AEA) protocols. (These specimens will be referred to as C1293-Humid to indicate the humid environment and C1293-Deicer to indicate the deicer soak.) Environmental chambers were constructed for these tests consisting of galvanized steel tanks wired to a heating system. The tanks were insulated around the sides with fiberglass insulation and the top and bottom with foam board insulation to prevent heat loss and to maintain the specimens under stable environment. The heating system was composed of the following parts from Ash Equipment and assembled by an electrician: 1 heater, 2 temperature sensors, and two regulators along with various circuitry components. Measurements were taken at 7days, 14 days, 28 days, monthly from 2 until 12 months.

Expansion data for C1293-Humid testing are shown in figures 10 and 11. Expansions from specimens associated with each of the aggregate sources have been negligible. Since these specimens lacked the artificial alkali addition of NaOH, this result is perhaps not surprising. As such, it does not appear that any significance can be attached to the small differences in these values.
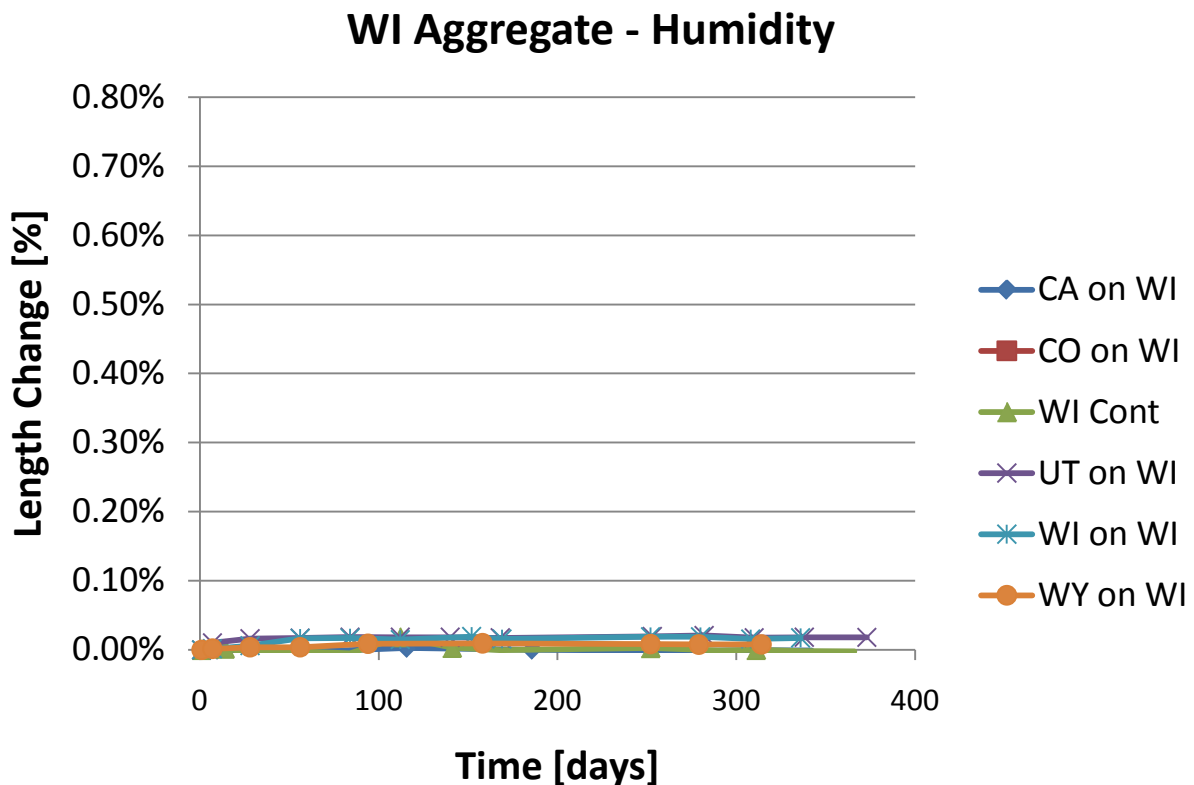
Figure 10. Length change for C1293 Humid specimens based on Wisconsin aggregate
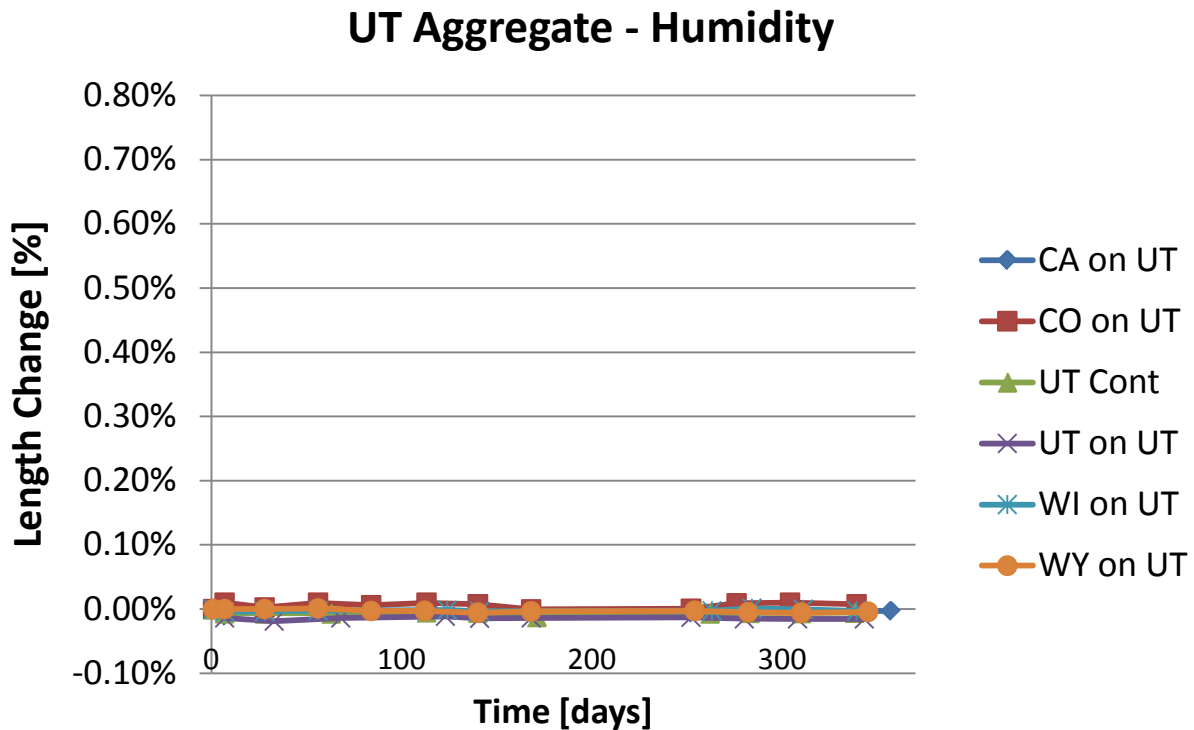
Figure 11. Length change for C1293 Humid specimens based on Utah aggregate

Expansion data measured from C1293-Deicer testing are shown in figures 12 and 13. In the presence of deicer, the expansions become large for those specimens with the more reactive microfines. Specimens containing CA, CO, or WY microfines tended to show the largest expansions with both the Wisconsin aggregate and the Utah aggregate. Expansions of specimens with the Utah aggregate tended to be higher than those with the Wisconsin aggregate.

As mentioned all modified C1293 test results shown in figures 10-13 excluded the addition of NaOH typically included in the ASTM C1293 procedure. To gain insight into the possible influence of this intentional omission, the research team added a series of ASTM C1260 tests. This test used gradations for fine aggregate as specified in the standard with additional microfines added at a dosage level of 11.6% of fine aggregate. This dosage rate is equal on average to the dosage rate (as a percentage of fine aggregate) as was used in the C1293 tests. The results of these tests are shown in figure 14 for the Wisconsin fine aggregate and figure 15 for the Utah fine aggregate.

The C1260 results were primarily distinguished by the base aggregate source such that the Utah aggregate specimens showed much larger expansions than those associated with the Wisconsin aggregate. Within a base aggregate set, the largest expansions occurred with the washed control specimens while the microfines appeared to mitigate the expansions. The influence of the

microfines was different between the C1293-Deicer expansions and those of the C1260 tests. In fact, the microfines that provoked the most severe expansions in the C1293-Deicer testing caused the least expansions in the C1260 testing. The ability of the microfines to mitigate expansions associated with ASR suggests that highly reactive silica in the microfines (particularly CO and WY) were creating a pessimum effect. As reported by Ichikawa, homogeneous mixing of a sufficient amount of very fine siliceous materials in concrete inhibits the ASR by absorbing Ca^{2+} ions for the rim formation (2009). At the conclusion of the ASTM C1260 tests, specimens were cut from the center of the bar for SEM analyses of the specimens. It was found that specimens containing the reactive Utah fine aggregate showed signs of ASR. Unlike the samples from ASTM C1293-Deicer, a gel composed of Si, Na, and Ca was found despite the source of microfines. Images are shown in appendix 3.
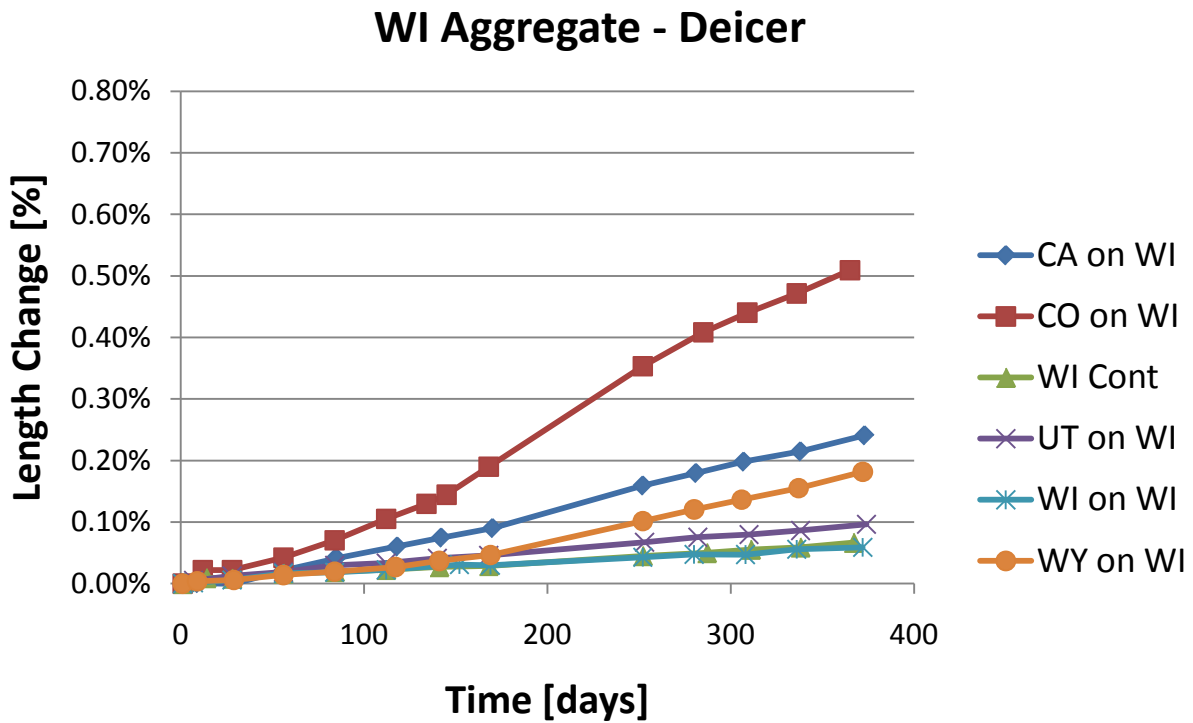
Figure 12. Length change for C1293-Deicer specimens based on Wisconsin aggregate
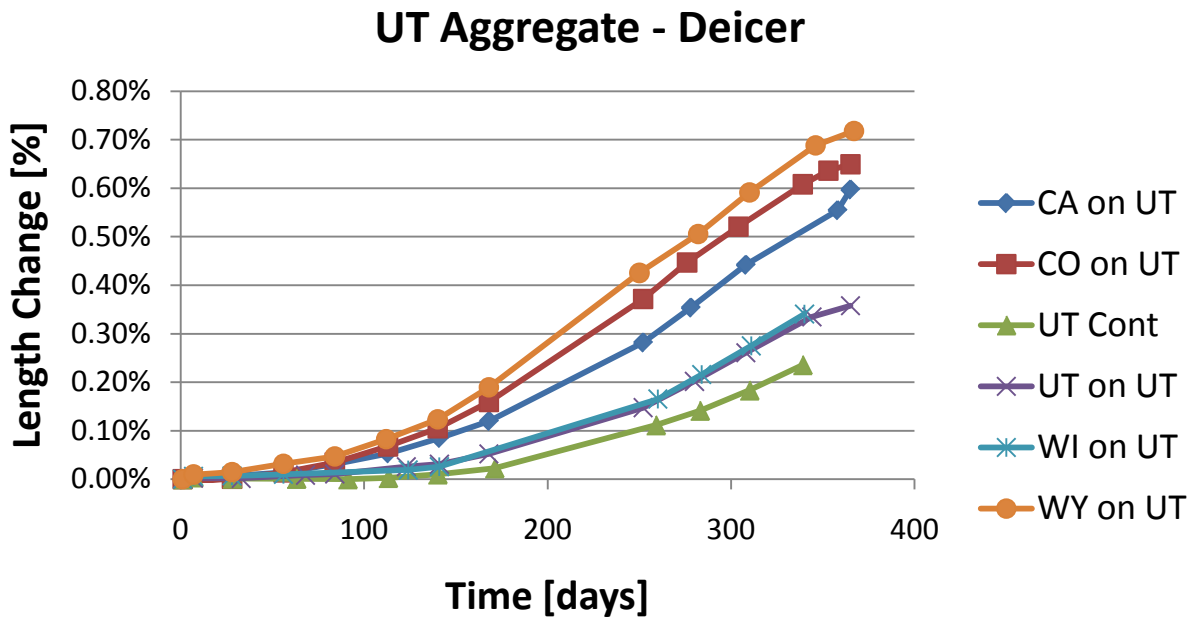
Figure 13. Length change for C1293-Deicer specimens based on Utah aggregate
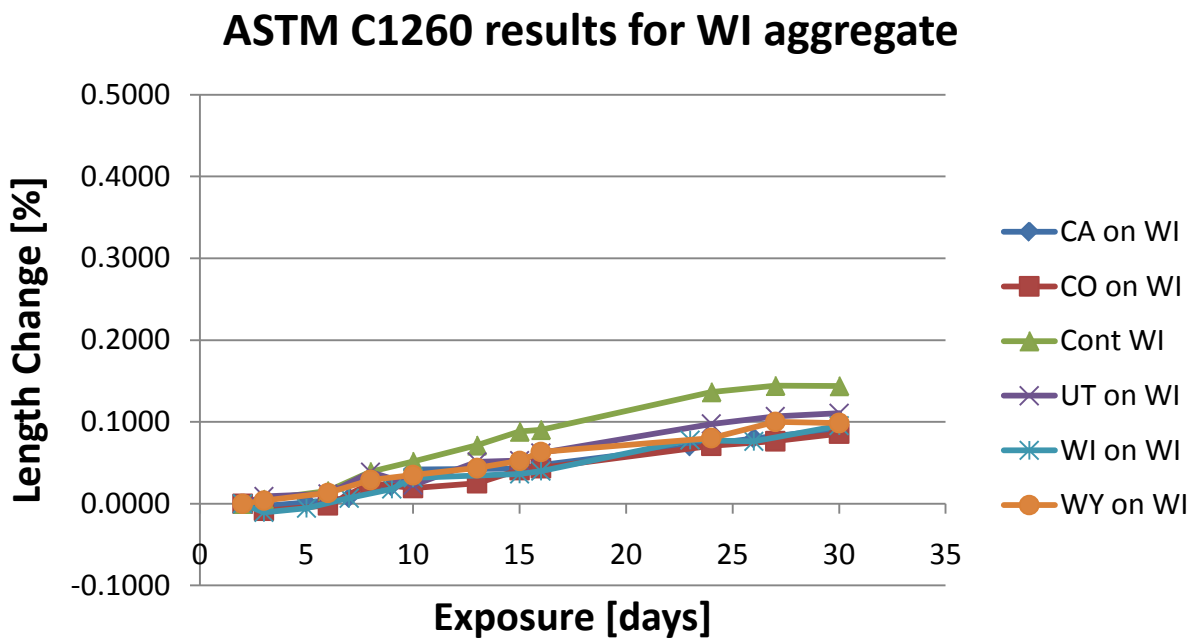
Figure 14. ASTM C1260 expansion for specimens containing Wisconsin fine aggregate different sources of microfines

ASTM C1260 results for UT aggregate
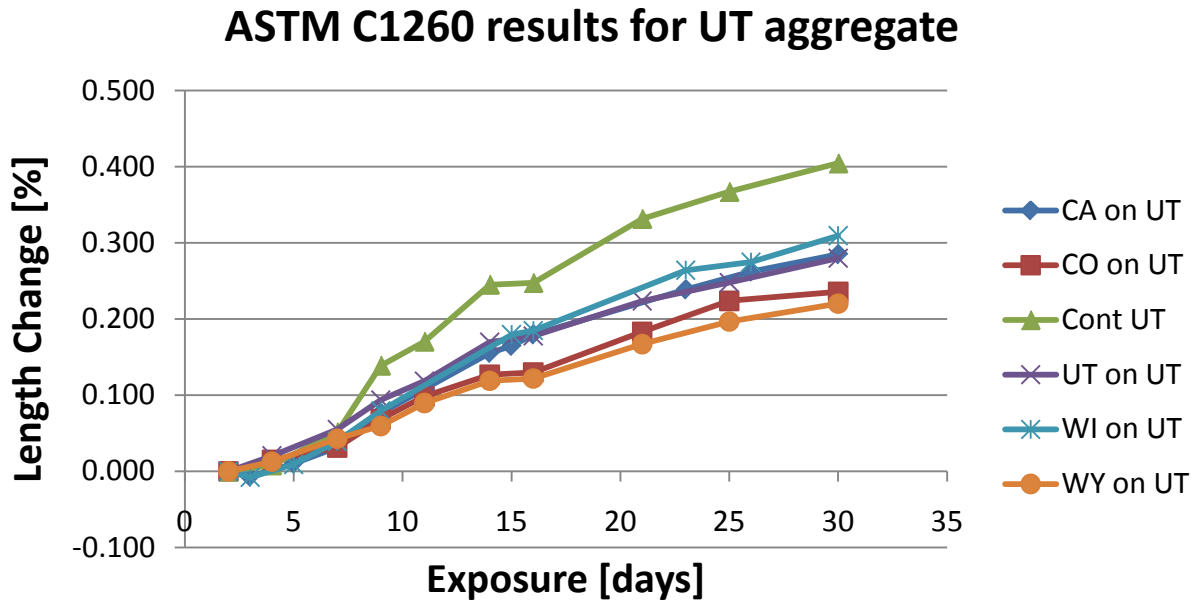
Figure 15. ASTM C1260 expansions for specimens containing Utah fine aggregate and different sources of microfines

5.2.3 Task 5 –Freeze-Thaw Durability

Modified ASTM C666 was performed in an identical manner to the format used by Clemson University in IPRF Project01-G-002-05-7. For this test, specimens were poured from the same batch as those for the modified ASTM C1293procedures. The specimens were demolded after 24 hours of standard curing and then placed into the humidity room. After 28 days, the specimens were removed and the dimensions, weight, and transverse frequency was measured and then the specimens were frozen until all specimens reached the same maturity. The specimens were dried and thawed for 24 hours in an environmental chamber held at 50% RH and 25°C and then put into a standard freeze thaw cabinet and cycled 60 times between the temperatures of 10°F to 50°F. At this point, the specimens were removed from the chamber and detached particles were wiped from the surface, and subsequently placed into the environmental chamber for 24 hours. Specimens were then submersed in deicer at a temperature of 38°C for 48 hours. The deicer bath was identical to that used in the C1293-Deicer test above. Specimens were then returned to the environmental chamber for 24 hours. Before returning the specimens to the freeze thaw cabinets, the specimens were measured.

The dynamic elastic moduli for the specimens were computed from the weights and transverse fundamental frequencies every 60 cycles. The relative elastic moduli at 300 cycles are shown in figures 16 and 17 for the Wisconsin and Utah aggregates respectively versus the air content of the corresponding concrete batches. Because of an error made in measuring the initial transverse frequencies, a correction was made to the data such that the relative elastic moduli at 300 cycles

are accurate to ± 5%. This correction does not impact the main findings of these tests. As shown in figures 18 and 19, the degradations at 300 cycles tend to correlate strongly to the level of air content. As indicated earlier, the resulting air content was greatly impacted by the type and amount of microfines in the mix.

The order of the specimen degrade from the largest to the smallest degrade is comparable in the two sets of specimens. The no-microfines controls and the specimens with the Wisconsin microfines degrade the slowest while Colorado-microfine specimens are degrading the fastest followed by the California-microfine specimens. It is interesting to note that the order of freeze-thaw degrade while consistent amongst the two data sets is not identical to the order of C1293-Deicer expansions. The overall consistency in the C666 data and the C1293-Deicer data suggests that microfines (at these levels) may have a greater influence in durability than the aggregate type.
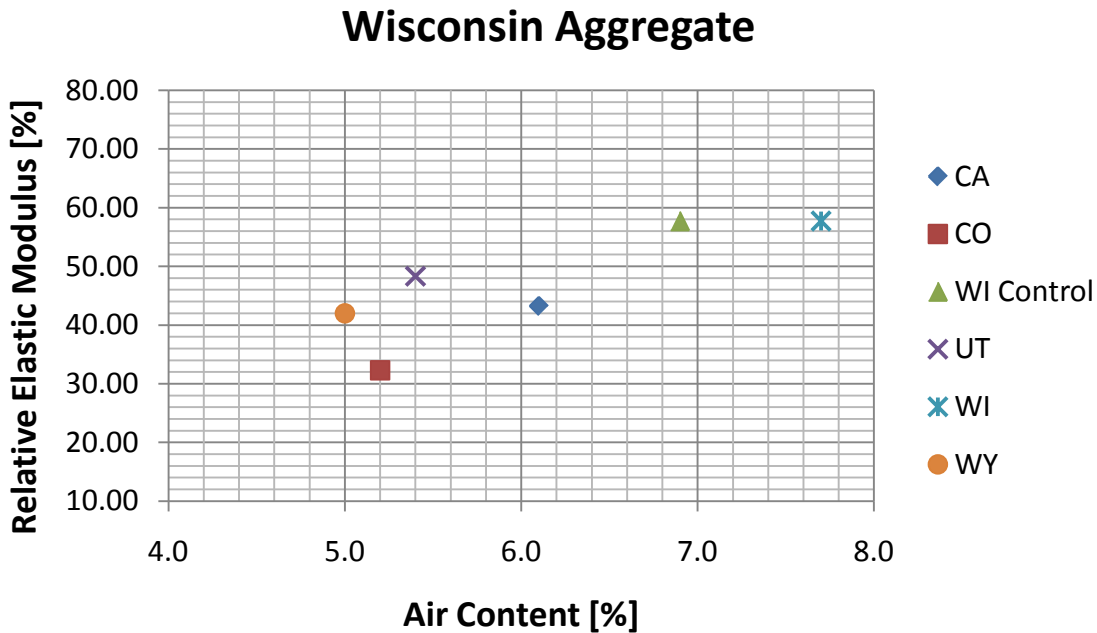
Figure 16. Relative dynamic modulus for specimens containing Wisconsin aggregate and subject to the modified ASTM C666 protocol versus the corresponding air content
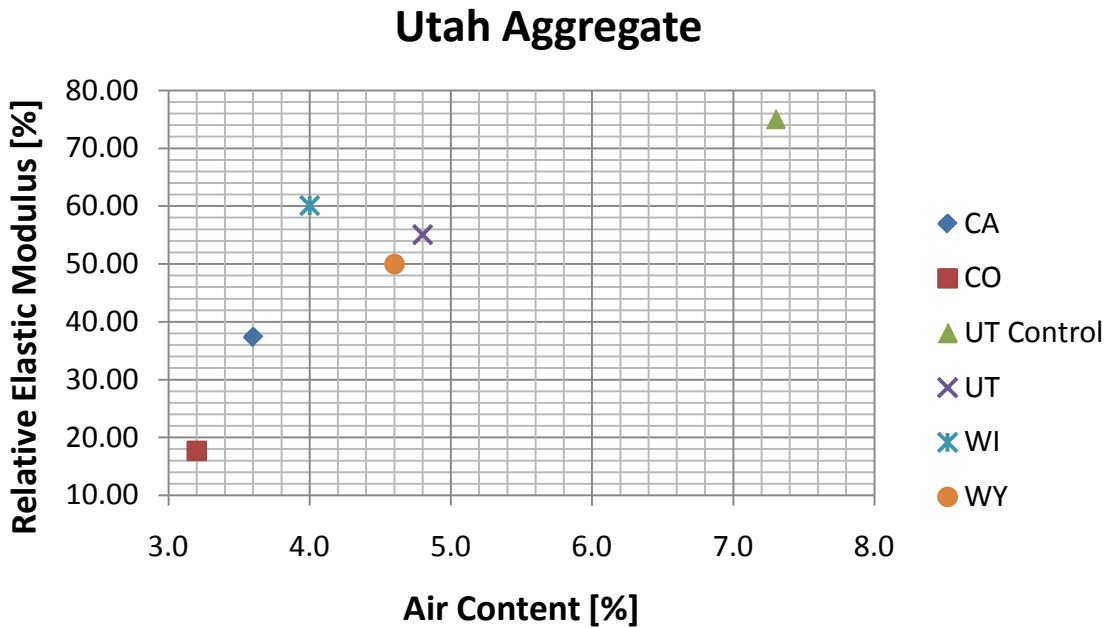
Utah Aggregate

Figure 17. Relative dynamic modulus for specimens containing Utah aggregate and subject to the modified ASTM C666 protocol versus the corresponding air content

Weight loss data for increasing freeze-thaw exposure is shown in figures 17 and 18. The trends are similar to those with the relative elastic modulus data.

WI Aggregate - Weight Loss
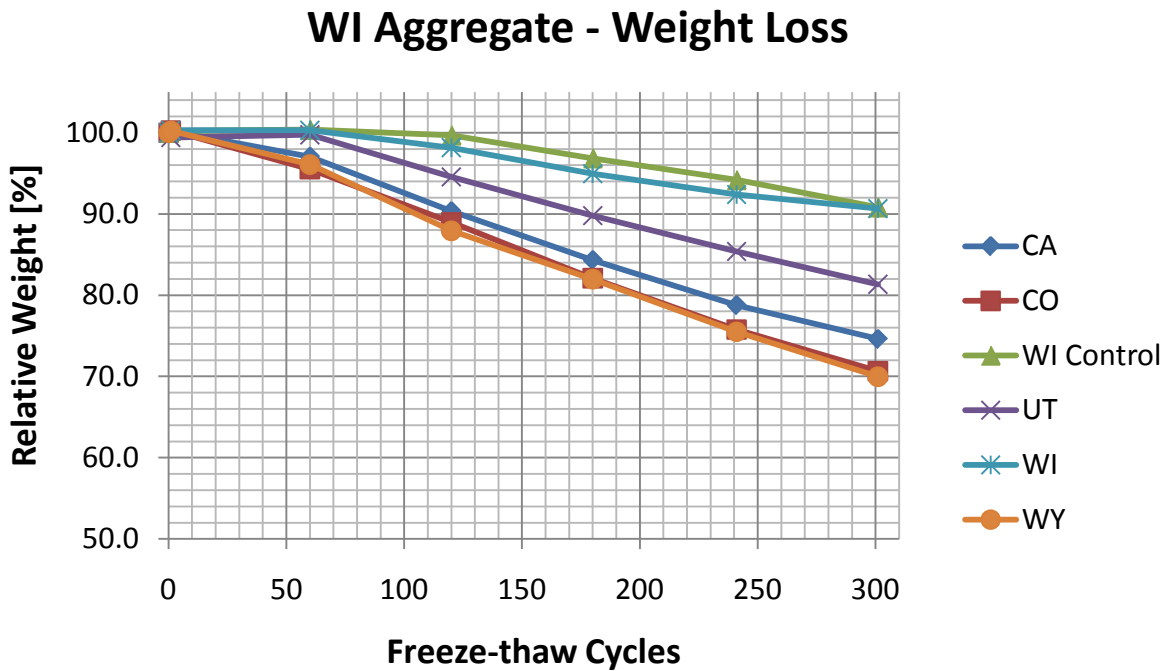
Figure 18. Relative weight loss of Wisconsin aggregate specimens with freeze-thaw cycles

UT Aggregate - Weight Loss
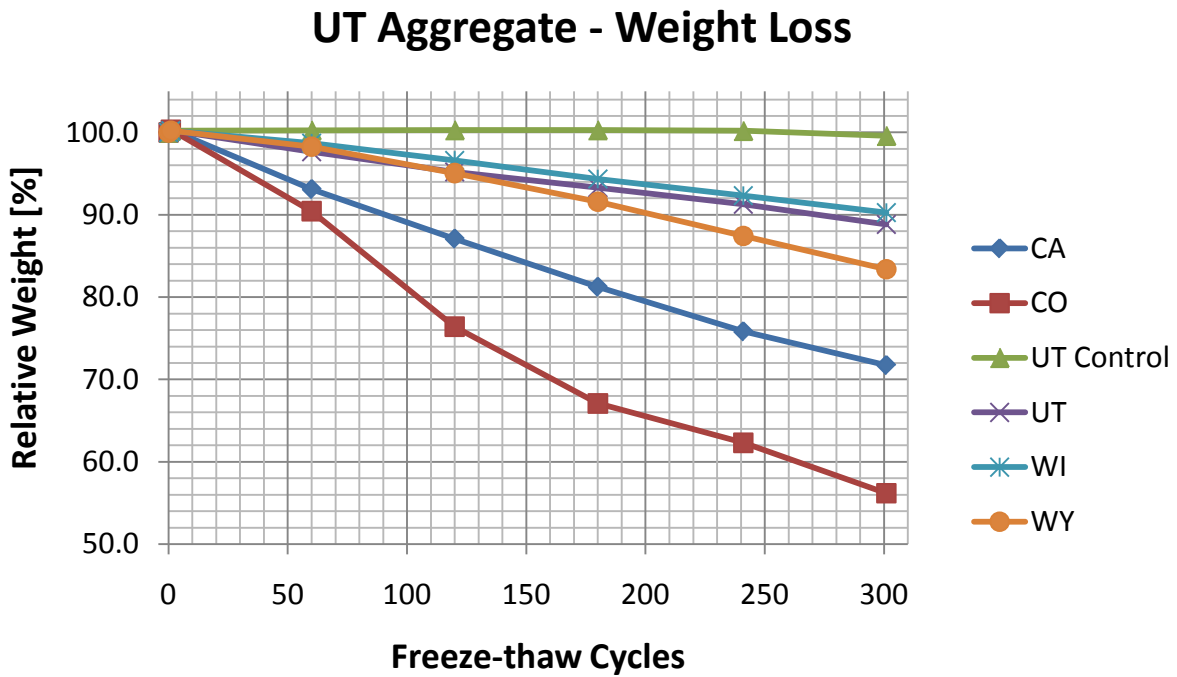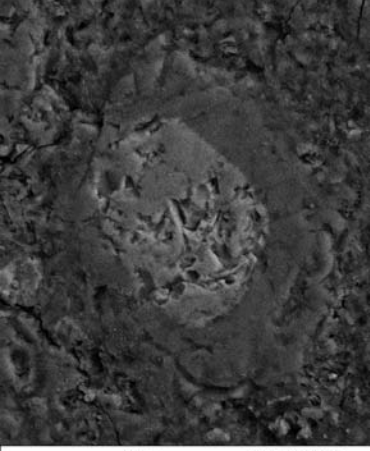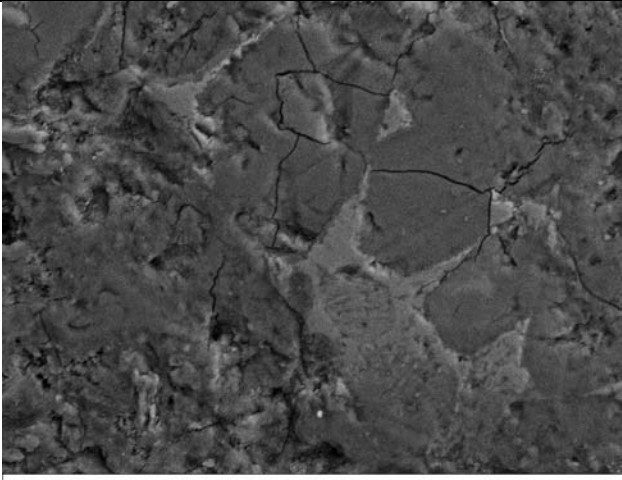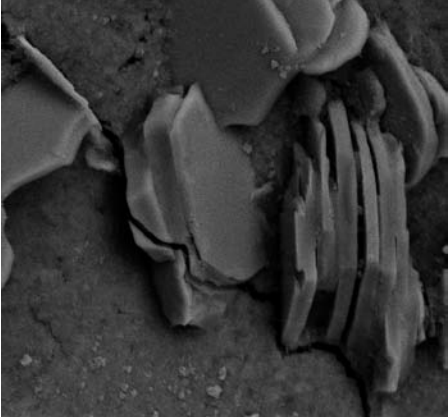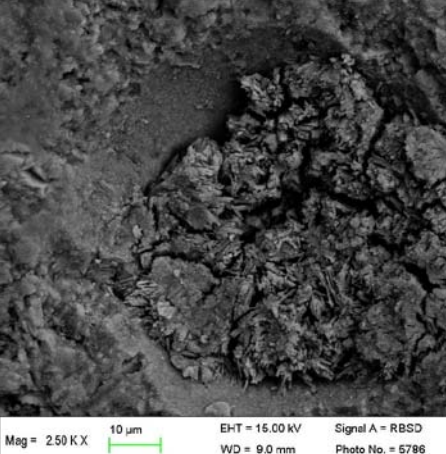
Figure 19. Relative weight loss of Utah aggregate specimens with freeze-thaw cycles

5.2.4 Task 5 – SEM Results

The SEM analysis identified normal cement components and dense ITZs in specimens from the C1293-Humid test to establish a control baseline of expected microstructure features. Table 22 shows some examples of expected concrete formations present in the specimens.

Table 22. Expected cement and hydrated cement compounds

Expected cement and hydrated cement compounds			
Compound	Formula	Image of compound	Ratio of elements
Cement particle (Alite particle) (CO on UT C1293-Humid 9mo)	$3CaO$ SiO_2		Reaction Rim: $Ca/Si = 1.7$ Unhydrated center: $Ca/Si = 2.7$
Cement Particle (Belite Particle) (CO on UT C1293-Humid 9mo)	$2CaO$ SiO_2		Reaction Rim: $Ca/Si = 1.7$ Unhydrated center: $Ca/Si = 2$
Calcium Hydroxide Crystal (WI on UT C1293-Humid 6mo)	$Ca(OH)_2$		$Ca/O = 1$

Ettringite Crystal (CO on WI C1293-Humid 3mo)	3CaO Al$_2$O$_3$ 3CaSO$_4$ 32H$_2$O		Ca/Al = 2.8 Ca/S = 3.4

Investigation of Potassium Acetate Penetration

While handling samples for SEM at 3, 6, and 9 months, it was noticed that the specimens were becoming extremely fragile even at the center of the cylinder. This led to the belief that the potassium acetate deterioration was deeper then 15mm as seen in previous work. Infrared Spectrometry (IR) was conducted to determine how far the acetate penetrated into the specimens at one year. This test was conducted on concrete samples with the following four microfine and aggregate combinations: CA on UT, CO on UT, WI on WI, and WY on WI. From each specimen, a slice was taken at three inches from the finished cylinder surface. Samples from this slice were taken in three locations using a 5/32 hammer drill bit, at incremental intervals from the surface. First the center was analyzed and then a comparison was taken from the edge to determine if acetates had reached full strength in the core of the piece. If it had not, then pulverized samples were available for analysis heading towards the edge to determine the depth of penetration.

When analyzing the IR spectra results, each spectrum was subtracted from those of the ASTM C1293-Humid specimens which had no deicer exposure, but the same composition. To normalize the intensity, both spectra were normalized with respect to the quantity of concrete seen by the IR by using a peak at 1813 cm^{-1} as it is sharp and independent on the quantity of acetate in the specimens. Subtraction of these spectra rendered a clearer signal for the absorption bands of acetate, otherwise buried under the stronger absorption bands of other species in concrete. The peak at 1578 cm^{-1}, due to the asymmetric stretching of acetate, is compared to determine if acetate penetrated.

It was determined that in all cases, the acetate had penetrated to the core of the samples. The method of examination did not allow a precise measure of the quantity of acetates that had penetrated. It was also deducted that the acetate in the system is likely complexed with calcium. This is another indication that the acetate could be altering the typical microstructure of the normal cement hydration porducts. See appendix 4. Investigation of Potassium Acetate Penetration for more information detailing the results of this test.

Formation of New Mineral phases:

Potassium acetate was included in the analysis by examining the modified C1293-Deicer specimens. It was observed that potassium acetate changed in the concrete forming various compounds as described below.

Potassium Sulfate Products: Large areas composed of potassium sulfate crystals (molecular formula K_2SO_4 abbreviated KS) were observed in the ITZ of many of the deicer treated specimens (figures 20, 21, and appendix 5 for other C1293-Decier specimens with KS). Normally in the early ages of forming the ITZ layer, ettringite forms and eventually transforms into monosulfate. CSH is continuously formed along with CH. By immersing the fresh concrete specimens (24 hours of curing) into the deicer, KAc penetration was relatively unimpeded compared to more mature concretes. To understand the formation of the KS observed in the ITZ, the source of sulfate and its transformation were needed. Typically the sulfate originates from gypsum, and potassium originates from the deicer solution (6.4MKAc) since contributions from some siliceous aggregates or clays would be relatively minor. The sulfate in gypsum usually transforms to form ettringite in very early stages of concrete hydration, which eventually transforms to monosulfate. Thus, in order to form these potassium sulfate crystals the sulfate must be pulled out from either ettringite, monosulfate, or both. This transformation is expected to prompt a change in the microstructure of the ITZ and to the adhesion of the cement paste to the aggregate. The formation of KS is not the only chemical reaction that can extract sulfates from ettringite, this also happens in the formation monosulphoaluminate. The formation of the KS also should limit the carbonation of monosulphoaluminate, which leads to the formation of secondary ettringite. In these concretes secondary ettringite was not observed to line the voids and cracks of specimens.
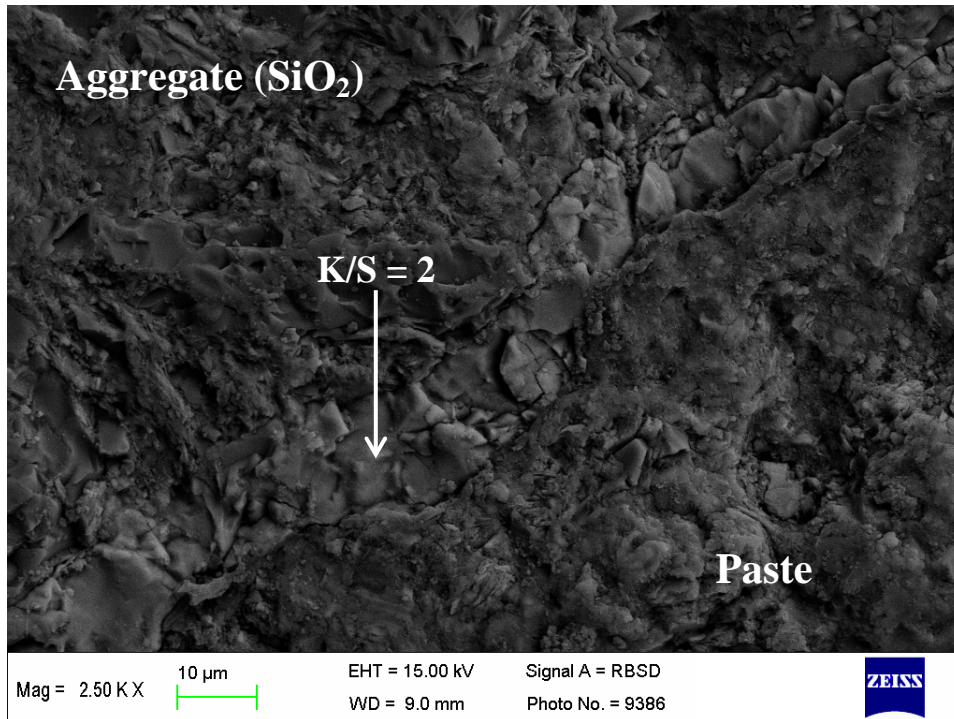
Figure 20. Potassium sulfate complex in CA on UT Deicer specimen after 6mo
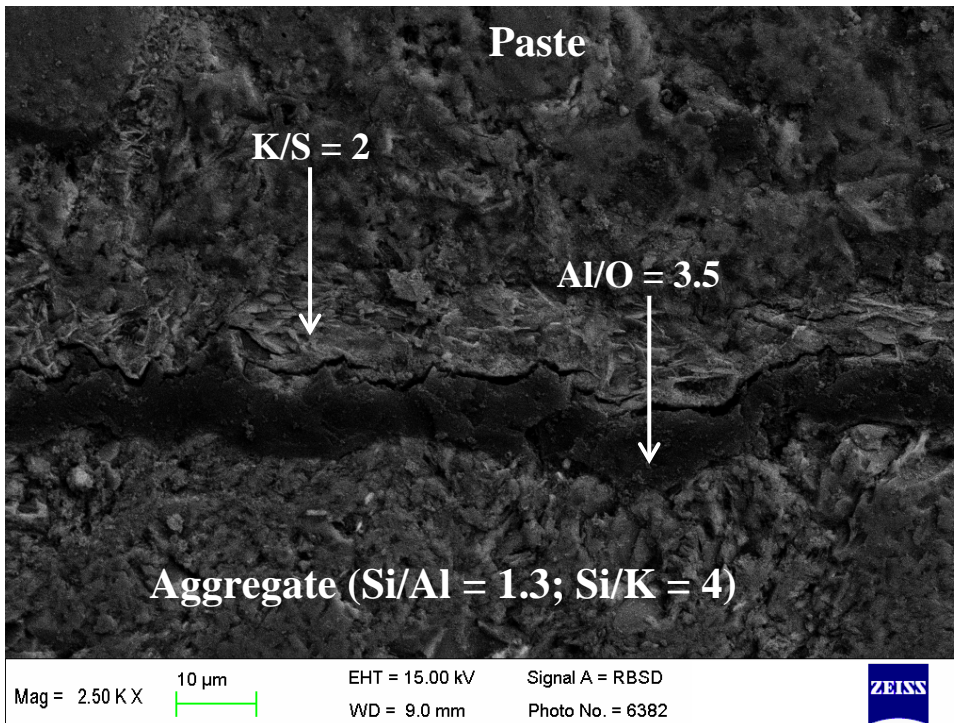
Figure 21. Potassium sulfate complex in CO on UT Deicer specimen after 9mo

Thermodynamic simulation verified that the KS complex obtained the sulfur from the ettringite and shows that KS is favored over ettringite and monosulfate. Potassium and sulfate complex formation is favored by increasing pH. (See appendix 5 to see the thermodynamic simulation for the formation of KS.) Further simulations show that if there are low amounts of potassium, the SO_4^{-2} is free, but if there are high amounts of potassium then KSO_4^- forms. It is important to point that this complex is in solution and not existing as a solid in the form of a crystal. Crystal formation only occurs upon drying. This is important for two reasons: the formation of KS shows the KAc was chemically attacking the concrete paste, and this formation was not the direct cause of the observed expansions. However, if the sulfate bearing compounds are broken down, the remaining constituents will go to form other by-products that could cause expansion.

Equilibrium diagrams in appendix 5 predict that the aluminum ions should be mainly as a calcium aluminum silicate and aluminum hydroxide $(Al(OH)_3)$ in a stable phase. The micrograph of figure 20 shows the presence of a rim of aluminum hydroxide (or oxihydroxide) particles between the K_2SO_4 crystal formation rim and the aggregate. Following the diagrams of appendix 5 calcium ions should be mainly as portlandite and calcium aluminum silicates. EDS analysis showed areas in the bulk cement paste that contained spikes of calcium and spikes of aluminum. This could be the segregation of the aluminum hydroxide from the ettringite and the calcium could go to CSH or portlandite. Areas with the composition of the aluminum calcium silicate predicted in the diagrams of appendix 5 were also observed. These new formations throughout the system lead to an overall altered paste material which likely differs in properties from normal cement paste.

Potassium in the bulk
The bulk paste was examined to determine if the potassium entered the system near the problem areas. Abundant potassium was observed in the paste. The potassium was further traced to determine if it was paired with the acetate or if it attached itself to some other compound in the bulk matrix. The potassium was observed to exist with varying amounts of carbon and oxygen indicating it may be associated with the acetate. Combinations of Ca, Si, Al, and K in the bulk were clearly observed with the possibility that free potassium ions exist in the pores of the matrix of CSH or CH or the potassium could be combining in at exchangeable sites of the CSH. It is observed that the platy crystals typical of the KS seen in the ITZ are also seen in some cracks and pores of the bulk as in figure 22.
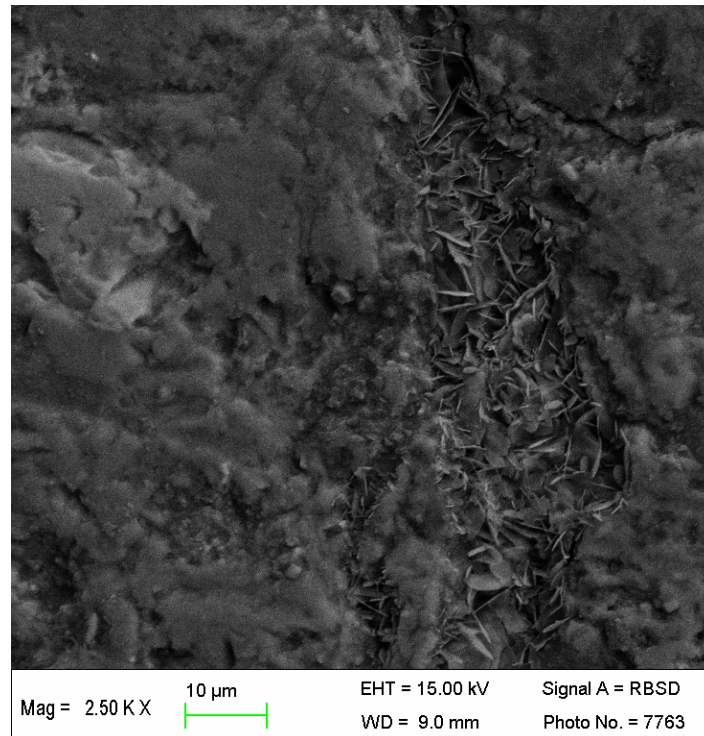
Figure 22. KS complex existing in a void in the bulk

ASR Products

One of the objectives of this research was to determine if KAc and microfines promote ASR. ASR is the combination of silica with alkali ions commonly in the form of calcium silicate with sodium and potassium ions. In concrete systems of this research, silicates are readily available from some of the aggregates and all of the microfines. There is also silica in the system from the paste although it is more difficult to liberate the Si from hydrated particles in the form of CSH. Thermodynamically, the silica from the aggregates will be soluble silicates in high concentrations at a pH of 12.5 and higher. The CSH will not be destroyed until the pH rises above 13.5 where in the silica becomes $SiO_2(OH)_2^{-2}$. The alkali ions originate from the microfines, or the pore water with counter ions as hydroxide and acetate. The conditions of the concrete exposed to the KAc in the modified C1293-Deicer tests are thus favorable to ASR. Gels containing silica, calcium, potassium, and sodium would be indicators of this reaction.

Figure 23 shows various gels seen in the potassium acetate specimens. The gel structures are composed of Ca, Si, and K. The data show there was potential for ASR and some species that resemble it. Typical deterioration would be visible as distressed aggregates and gel expanding into the paste. These indicators of distress were not observed in the research specimens. The conditions are favorable for ASR and some ASR was present, but it was not observed as a significant cause of deterioration.
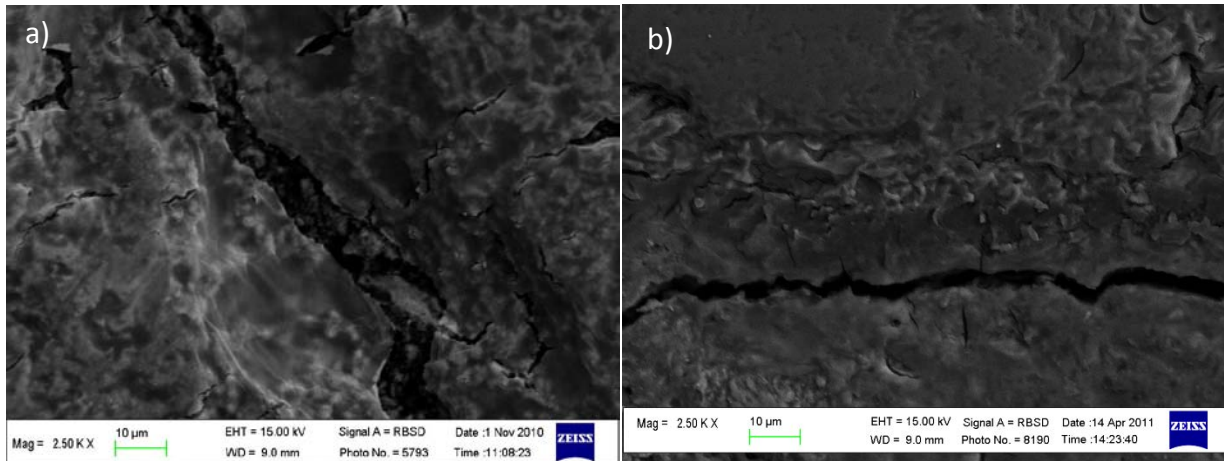
Figure 23. a) A sheety, gel material, composed primarily of calcium and silica, found in the CO on WI Deicer species after 3mo, and b) gel material, composed primarily of calcium and potassium, found in the UT control deicer species after 9mo

Expansion

This chemical degradation discussion has been centered on the formation of new mineral phases in the form of large crystals including K_2SO_4. Gels are a commonly recognized mechanism for expansion. Expansion can also occur from the precipitation of various salts when the pore water gets very concentrated upon drying. It may be that the molar volumes of the new phases are larger than that of the parents or the pore volume. With this in mind, the pore water in these specimens had a high ionic strength which alters the solubility of species normally found in the cement paste. KAc degraded the monosulfate. The alkali ion content was very large and increased the pH of the pore solution leading to attack on the paste matrix.

The data from the C1293-Deicer results indicate that specimens containing different microfines and different aggregates expand in distinguishable amounts. This leads us to believe that the microfines and aggregates react with the potassium acetate or the concrete distinctly. As stated before, the specimens that have been subjected to the KAc protocol often contain KS. Potassium is most obviously coming from the KAc. Sulfur originates from the cement as neither KAc nor sulfur is contained in any of the microfines. In addition, since KS was present even in the control specimens, the formation of KS was unrelated to the presence of microfines. Expansions from microfines without KAc did not occur in the timeframe of this research. The most likely contribution from the microfines is the introduction of highly reactive silica that created new phases. While the clays present the ability of some physical expansion from their individual behavior this was not observed in the C1293-Humidity test results and unlikely to be the large contributor to expansions that distinguish the C1293-Deicer test results.

Specimens containing Wisconsin aggregates expanded about one third less than the specimens containing Utah aggregates. The Utah aggregates had siliceous aggregates that were likely deteriorating in the high alkaline and high pH environment. Typical ASR gel was not widely

observed in the specimens, but the silica was likely deteriorating. With the destruction of the siliceous aggregates and the introduction of silica from the microfines in the presence of KAc, the system could transform into $Ca_2Al_2Si_3O$ and $CaSiO_2$ or Ca_2SiO_4 (we can see this in the WY on UT C1293-Deicer specimen.) When $Ca_2Al_2Si_3O$ is formed, the formation of $KAlSiO_3$ as a solid is also seen from thermodynamics when there are low levels of calcium present. This was present in the UT cont C1293-Deicer specimen. These new solid phases could cause expansion as the new formations likely occupy a larger volume then the aggregate. See appendix 6 for further information on the thermodynamic simulations showing these new formations are an expected formation in the concrete system.

Deterioration

Deterioration of the paste was observed as an increasing porosity in later stages of the KAc testing. Extreme deterioration of the ITZ was also observed and in most cases the bond between the aggregate and the paste was completely destroyed (see figure 24). Therefore, it appeared that normal hydration products were attacked, breaking down sulfate compounds, CSH, and CH. Many of the ions released in this attack form new associations leaving the normally solid phases broken. See appendix 7 to see more evidence of deteriorated aggregates. See appendix 8 to see how the various microfines deteriorated in the modified C1293 tests.
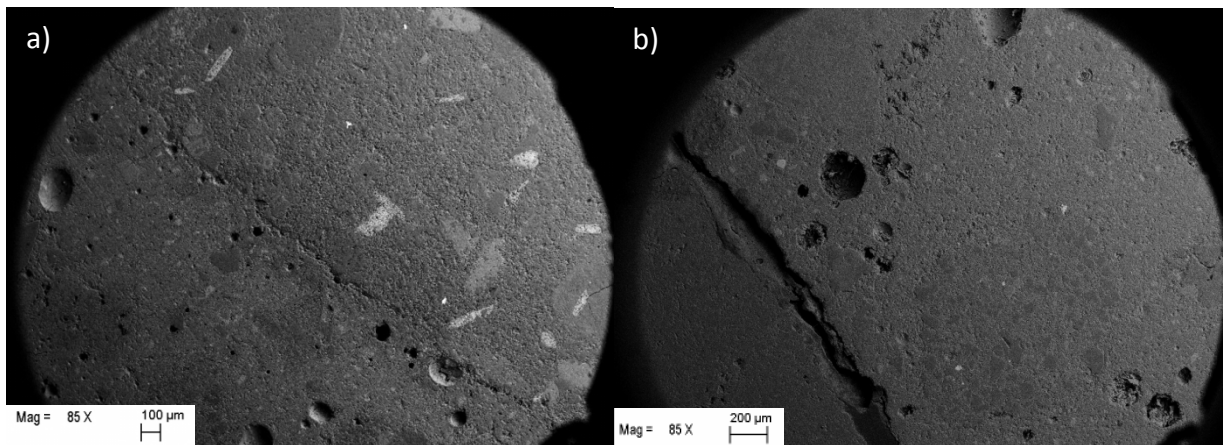
Figure 24. Images showing the deterioration over time; a) WY on UT Humid 3mo b) WY on UT Deicer 9mo

5.3 Task 6 – Identifying hydration products associated with different curing environments

Samples for this task consisted of two-inch cubes of mortar containing two coated coarse aggregate pieces. Fine aggregate and coated aggregates as in Task 5 were used to make direct comparisons. Microfines were not added to the bulk of these specimens as in Task 5 leaving the total microfine content only that which adhered to the aggregate. Mortar was mixed in the ratio of 2:1sand:cement, and 0.45 w/c with no air entraining admixture. The mortar was mixed and poured in two even layers. At each layer, one coated aggregate piece was placed into position as previously depicted in figure 2.

Specimens were demolded 24 hours after initial pouring and placed directly into their specified environments. After soaking for three days, two of each types of sample were removed, one of which was cut to make an SEM sample, and one of which was frozen for future use if needed. (After 56 days of soaking, the third cube that had been residing in each solution was tested in the same manner as that of the 3 day specimen.) SEM sample prep procedure above was followed for these specimens as well; however, these aggregate and bulk samples were cut directly from the cube since, in this case, the location of the aggregate was known.

In general, sodium hydroxide has been seen as deleterious to concrete because it is an alkaline solution and leads to conditions favorable for ASR. When the hydroxide is free and migrating in the pore solution, it willdeteriorate the aggregate or any silica sources, and the sodium and potassium ions will combine with free calcium and silica in the pore solution to form a gel.

When analyzing the specimens subjected to NaOH and KAc from Task 6 testing, a formation of a potassium silicate was observed. Some thermodynamic simulations were conducted to determine why potassium silicate was present. NaOH provided a more basic condition than in the case of the KAc. This means the aggregates and microfines were being attacked to a greater degree and freeing more silica. Thermodynamically there are three solid phases, $Si_3Al_1K_1O_8$, $K_1Al_1Si_2O_6$, and SiO_2 and these phases were observed in these samples. A similar pattern of potassium sulfates in the systems with KAc was also observed along with the silica species.

This study was designed to investigate the effects of deicer on microfines, this test sought to see if deicer causes ASR as NaOH might. The data indicates that the two solutions produce different by-products. When the cubes were subjected to the KAc, they produced similar results to the C1293-Deicer SEM analysis. When the cubes were subjected to both KAc and NaOH, the NaOH overwhelmed the system producing different results then in the C1293-Deicer.

6. RELATIONSHIP TO IPRF PROJECT 01-G-002-05-7: PERFORMANCE OF CONCRETE IN THE PRESENCE OF AIRFIELD PAVEMENT DEICERS AND IDENTIFICATION OF INDUCED DISTRESS MECHANISMS

The research reported here has a relationship to IPRF Project 01-G-002-05-7: Performance of Concrete in the Presence of Airfield Pavement Deicers and Identification of Induced Distress Mechanisms (05-7). IPRF Project 01-G-002-05-7 aimed to "understand the materials-related distresses in airfield concrete pavements that are triggered in the presence of pavement deicing chemicals." One objective was to determine the material(s) responsible for the distress in order to create a protocol to identify the culprits before they are used in future pavements. Study 05-7 examined cores from existing airfields to determine if predictions correlate with infield findings. Research completed in 05-7 suggests that distress at different airports had different causes. Damage associated with the application of KAc deicer was not consistent from airport to airport.

Cores removed from airport pavements and subject to the same modified C666 F/T protocol as conducted in this study also show rapid and severe deterioration compared control concrete subject to water F/T exposure. The 05-7 researchers also found the formation of KS in concrete exposed to KAc. In contrast to the field studies of 05-7, the laboratory experiments presented in this study were controlled and aggressive conditions focused specifically on the interaction of microfines and KAc exposure. For example, the 05-7 studies did not show the level of penetration of KAc observed in this study nor did they specifically examine the impact of microfines. The behaviors seen in this study likely would exhibit themselves in the field but under different time frames and at different levels of deterioration.

7. FINDINGS

The testing an analysis performed under this study has demonstrated that specific combinations of naturally-occurring aggregate microfines and potassium acetate deicer are deleterious to the durability of portland cement concrete systems. The degree of distress depended on the mineralogical and chemical nature of the microfines, their quantity, and the degree of penetration of the potassium acetate into the concrete material matrix. The laboratory tests conducted in this research that form these conclusions are likely worst case scenarios that may not always occur in the field. None-the-less, combinations of these materials induce chemical and physical changes that even in field concretes with less severe conditions are likely to take a toll over time. The microfines often included 1:1 and 2:1 phyllosilicates, which in some cases can have positive and negative pozzolanic attributes, and are highly reactive. In addition, it was observed that microfines containing 1:1 and 2:1 phyllosilicates are not easily removed from coarse aggregates during washing. While some microfines are more reactive than others, none examined in this study was considered inert. Microfines fall on a differential scale of likely impact on concrete systems and with some microfines inducing impacts that can be many times greater than that of other microfines present in similar concretes at similar levels.

Major findings are:
- Even in the absence of potassium acetate, the presence of microfines at levels approaching but below five percent of the total aggregate weight had significant impacts on concrete mixing.
  - Slump reductions with some microfines were significant and would prompt water additions or create placement difficulties in the field in the absence of the use of water reducers or other mitigation strategies, particularly in slip-form paving operations.
  - Specific microfines matched with specific air entraining admixtures (AEA) tended to largely neutralize the function of the AEA making it impossible to achieve freeze-thaw resistant air contents regardless of the AEA dosage level.

- Combinations of microfines at less than 5% of the total aggregate weight and potassium acetate exposure caused significant deterioration of concrete that may be mistaken for ASR cracking and expansion. However, our analyses suggest it was not ASR, at least as traditionally diagnosed through the presence of ASR gel and reaction rims around aggregates.
  - Expansions in modified ASTM C1293 produced expansions from 0.05% to 0.70% at one year depending on the type of microfine. Expansions of specimens containing microfines but not exposed to potassium acetate produced negligible expansion.
  - Expansions were larger with base aggregate known to be prone to ASR, but significant expansions (up to 0.50% at one year) also occurred in specimens with unreactive aggregates.
  - In addition, this degradation combined with the reduction in entrained air content led to dramatic loss of freeze-thaw durability. These degradations were associated with specific mineralogical profiles of microfines in the presence of potassium acetate and these profiles consistently were associated with corresponding levels of degradation.

- The KAc transformed in the concrete pore solutions to form -potassium sulfate and calcium-bearing potassium sulfate compounds.
  - Both potassium and microfines were present in all cases where distress levels were the largest.
  - During the transformation of the potassium acetate the level of hydroxide increases dramatically in the pore solution and can lead to reformation of silica species released by the microfines and the aggregates. While these reactions do not appear to be the classical alkali silica reaction, they may exhibit some similarity and create an environment where expansion internally within concrete leads to deterioration.

8. REFERENCES

1. Abou-Zeid, M., & Fakhry, M. M. (2003). Short-term impact of high-aggregate fines content on concrete incorporating water-reducing admixtures. *ACI Materials Journal, 100*(4), 280-285.
2. American Association of State Highway and Transportation Officials. Standard method of test for the qualitative detection of harmful clays of the smectite group in aggregates using methylene blue. AASHTO TP 57.
3. Bonavetti, V. L., & Irassar, E. F. (1994). Effect of stone dust content in sand. *Cement and Concrete Research, 24*(3), 580-590.
4. Balachandran, C. (2009). "Potential for Inducing and Accelerating Alkali Silica Reaction in Concretes Exposed to Potassium Acetate Deicer: Laboratory and Field Studies," Thesis – Purdue University.
5. Caliskan, S., Karihaloo, B. L., & Barr, B. I. G. (2002). Study of rock-mortar interfaces. Part I: Surface roughness of rock aggregates and micro structural characteristics of interface. *Magazine of Concrete Research, 54*(6), 449-461.
6. Caliskan, S., Karihaloo, B. L., & Barr, B. I. G. (2002). Study of rock-mortar interfaces. Part II: Strength of interface. *Magazine of Concrete Research, 54*(6), 463-472.
7. Chatterji, S. (2005). Chemistry of alkali–silica reaction and testing of aggregates. *Cement and Concrete Composites, 27*(7-8), 788-795.
8. Gullerud, K. J., & Cramer, S. M., University of Wisconsin-Madison. Deptarment of Civil and Environmental Engineering & Wisconsin Highway Research Program. (2003). Effects of aggregate coatings and films on concrete performance. Available through the National Technical Information Service.
9. Ichikawa, T. & Miura, M.. (2007). "Modified model of alkali-silica reaction," *Cement and Concrete Research*, 37(9), 1291-1297.
10. Ichikawa, T. (2009). "Alkali-silica reaction, pessimum effects and pozzolanic effect," *Cement and Concrete Research*, 39(8), 716-726.
11. Kryer, H., Lindgreen, H., Jakobsen, H. J., &Skibsted, J. (2003). Hydration of portland cement in the presence of clay minerals studied by 29Si and 27Al MAS NMR spectroscopy. *Advances in Cement Research,* 15(3), 103-112.
12. Luxán, M., Madruga, F., Saavedra, J. (1989) Rapid evaluation of pozzolanic activity of natural products by conductivity measurement. *Cement and Concrete Research*, 19(1), 63-68.
13. Moukwa, M., Lewis, B. G., Shah, S. P., &Ouyang, C. (1993). Effects of clay on fracture properties of cement-based materials. *Cement and Concrete Research, 23*(3), 711-723.
14. Muñoz, J. (2010). Effect of Microfines Associated with Aggregates on Concrete Performance and Microstructure. Thesis – University of Wisconsin-Madison.
15. Munoz, J. F., Tejedor, M. I., Anderson, M. A., & Cramer, S. M. (October 2007). Expanded Study on the Effects of Aggregate Coating and Films on Concrete Performance
16. Muñoz, J., Sanfilippo, J., Cramer, S., Tejedor, I., & Anderson, M. (2009). "The Role of Microfines in the Alkali Silica Reaction: Enemy or Ally?" ICAR Symposium, University of Texas-Austin.
17. Nassif, H., Suksawang, N., & Mohammed, M. (2003). Effect of curing methods on early-age and drying shrinkage of high-performance concrete. *Transportation Research Record,* (1834), 48-58.

18. Rangaraju, P. R., &Olek, J. (2000). Evaluation of the potential of densified silica fume to cause alkali-silica reaction in cementitious matrices using a modified ASTM C 1260 test procedure. *Cement, Concrete and Aggregates, 22*(2), 150-159.

19. State of California-Business, Transportation and Housing Agency. (1999). *Method of test for evaluating cleanness of course aggregate*, California Test No. 227

20. Tasong, W. A., Cripps, J. C., & Lynsdale, C. J. (1998). Aggregate-cement chemical interactions. *Cement and Concrete Research, 28*(7), 1037-1048.

21. Whitting, D.A., and M.A. Nagi. (1998) Manual on Control of Air Content in Concrete. Portland Cement Association and National Ready Mixed Concrete Association. Illinois.

22. Woolast, R., Mackenzi, F., & Bricker, O. P. (1968). "Experimental Precipitation and Genesis of Sepiolite at Earth-Surface Conditions," *American Mineralogist*, 53(9-10), 1645-&.

23. Zampini, D. Shah, S. P., & Jennings, H. M. (1998). Early age microstructure of the paste-aggregate interface and its evolution. *Journal of Materials Research*, *13*(7), 1888-1898.

9. ACKNOWLEDGEMENTS

Appendix 1. Thermogravimetric and X-ray Diffraction Results from Task 4

Microfines from each source were introduced into each of three solutions at 50 g/L and 76°C. Solids were extracted at 1 and 3 weeks and subject to TGA and XRD.   The three solutions were:

- Sol 1: Saturated in $Ca(OH)_2$, 0.8M NaOH; pH = 13.4
- Sol 2: Saturated in $Ca(OH)_2$, 0.8M NaOH and 5M KAc; pH = 13.6
- Sol 3: Saturated in $Ca(OH)_2$, 5M in KAc; pH = 12.6

Thermogravimetric analysis revealed that the outcomes associated with solution 1 were approximately the same as those associated with solution 2. The major differences between the TG curves of treated and untreated microfines were associated with the evolution of Ca and Mg carbonates. Carbonate content was smaller in microfines treated with solutions #1 and #2. Carbonates consisting of Mg-poor dolomite (UT and WY) transformed in the solutions much faster than highly crystallized dolomite (WI). XRD also showed the transformation of the microfines in solution 2. From these tests and analysis, given enough time, the presence of magnesium calcium double carbonate microfines in aggregates should change the mineralogy of the ITZ and therefore affect some properties of concrete.

The following TG diagrams depict the transformations of the microfines exposed to the various solutions. The upper set of lines are the DTG results and the lower set of lines are the TG results. The region near 400°C indicates the transformations associated with hydroxilated silicates. The region near 640°C and 500°C indicates the transformations of the carbonate associated with magnesium and the carbonate associated with calcium respectively.

The following XRD diagrams show the transformation of various species indicated by the 2Theta angle along the x-axis. The changes in intensity indicate the changes in the crystallography of the specimens. The XRD results are shown for solution 2 transformations.

California
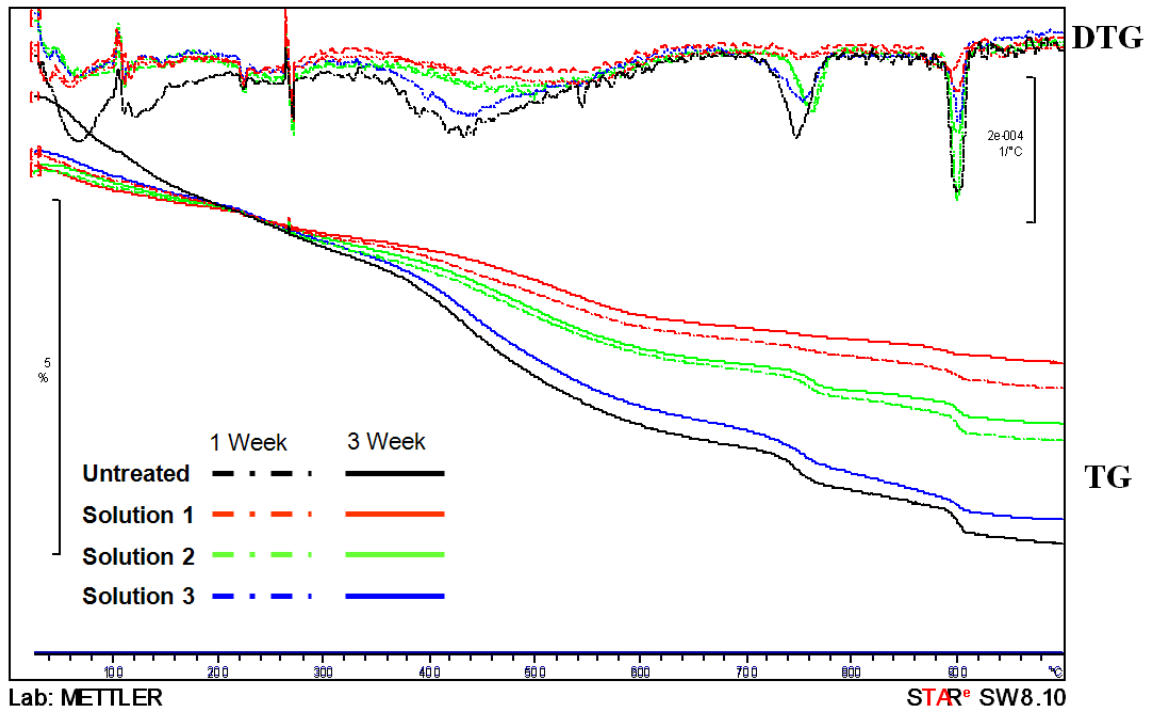
Figure A1.1. TG results from the California microfines showing solution two with carbonates and hydroxilated silicates being destroyed. Also, since the silicate is shifted possibly new silicates with hydroxide are being affected.
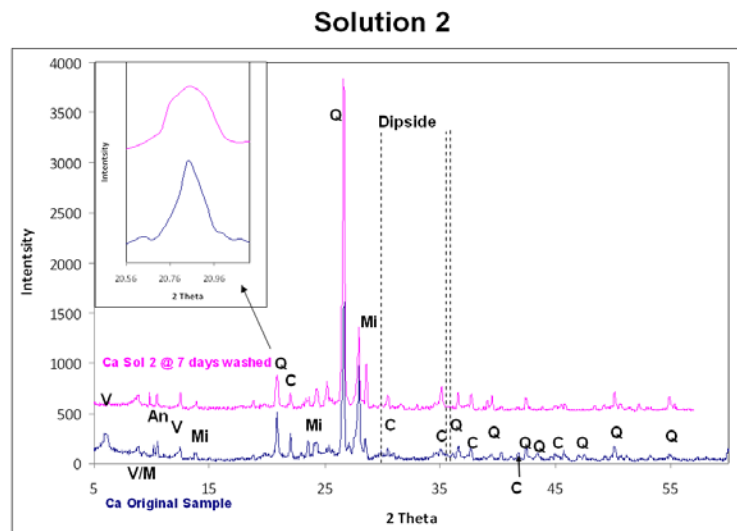
Figure A1.2. XRD results depicting silicates dissolving in the California microfines when subjected to solution 2.

Colorado
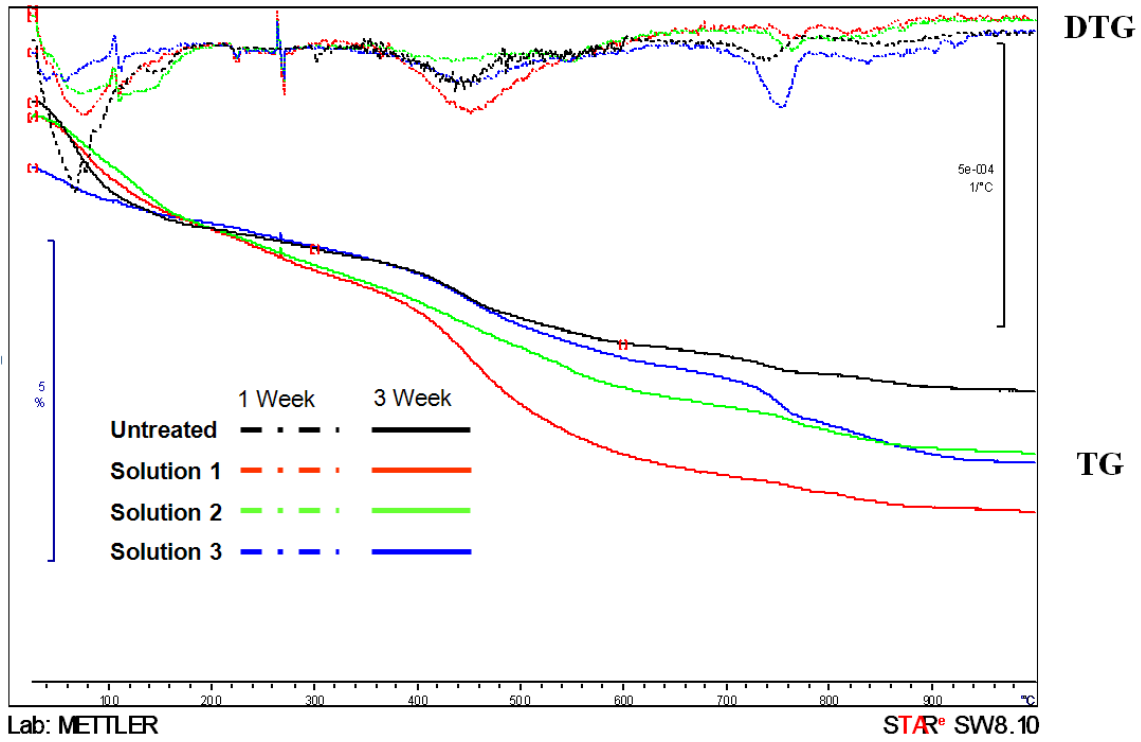
Figure A1.3. TG results for Colorado microfines indicating a decrease of species with hydroxide contents when subjected to solution 2.

Utah
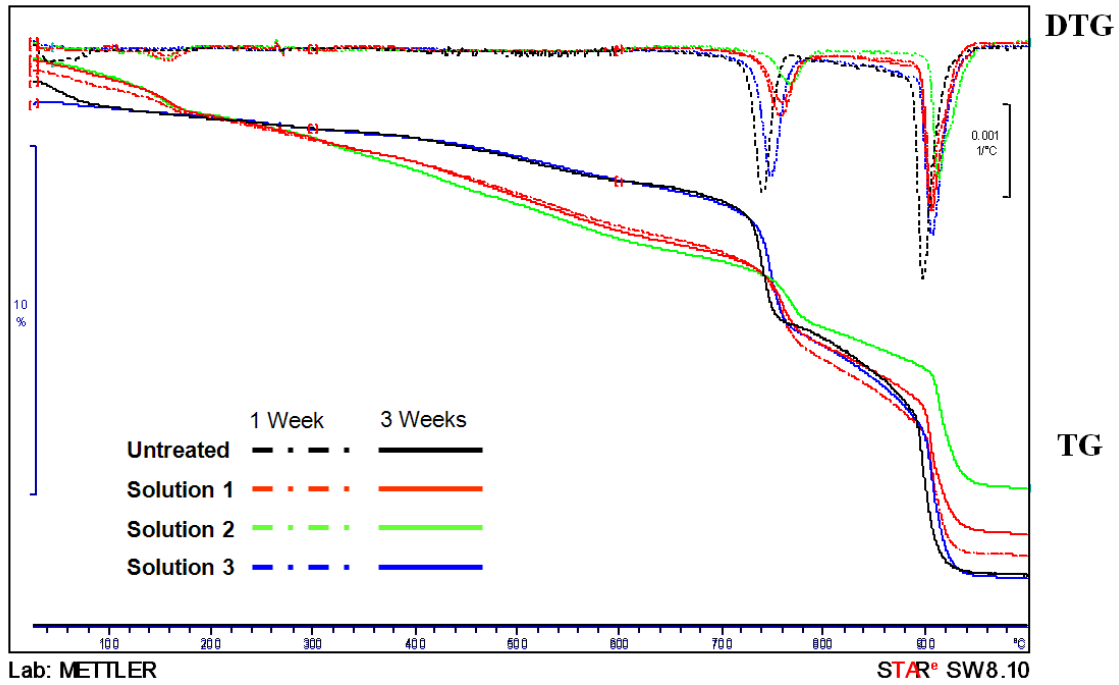
Figure A1.4. TG results for Utah microfines which depict losses in carbonate species. It is observed that the carbonate output is less defined so they react early, possibly changing to something less stable. It is also observed that magnesium is leaching because the output shows it is not as crystalline as the untreated specimen.
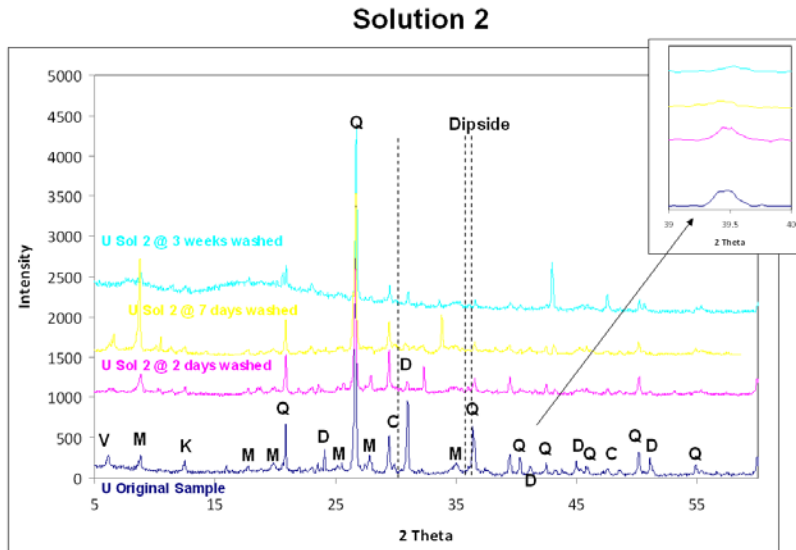
Figure A1.5. XRD results show a decrease in crystalline dolomite at 2 theta angle 32 and a reduction in crystalline silica at 2 theta angle 39.5 (shown in the exploded view).

Wisconsin
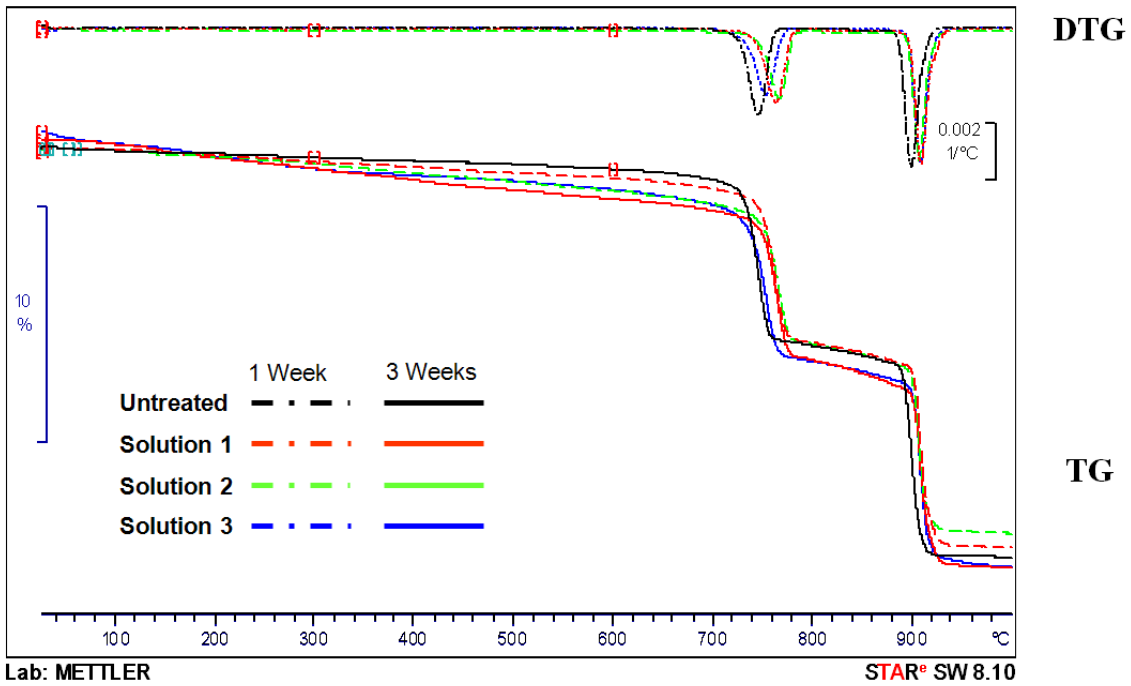
Figure A1.6. TG results show the Wisconsin microfines change the least when subjected to the various solutions and compared to the other microfines. The results indicate the microfines consist of well crystalline dolomite being barely attacked.

Wyoming
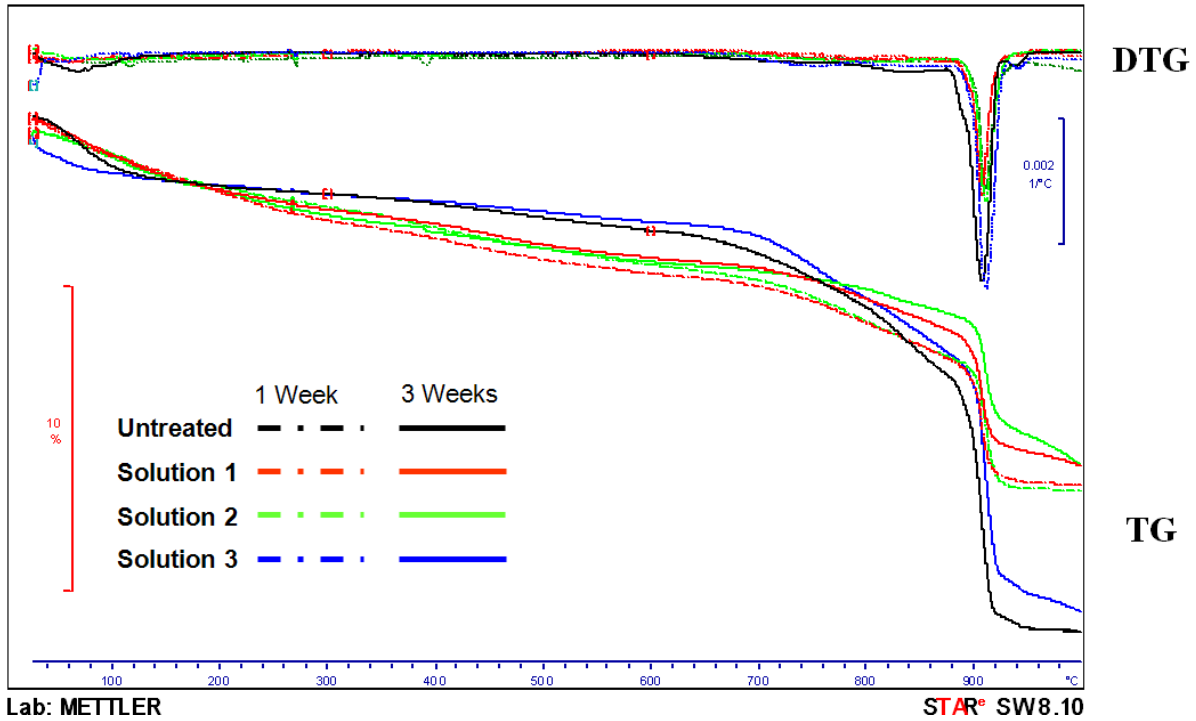
Figure A1.7. TG results indicating the Wyoming microfines consist of poorly crystallized dolomite which is more reactive. The hydroxilated silica species is minimally altered. They are not well defined in the DTG results, but losses are seen in the TG results.
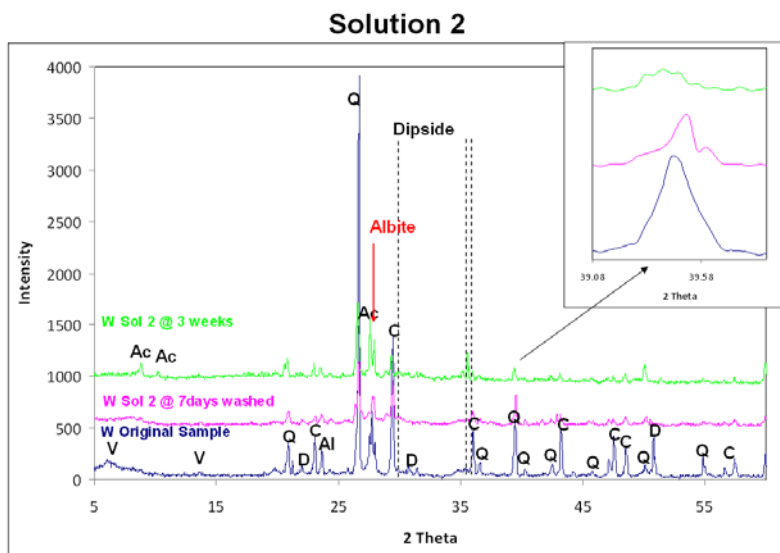
Figure A1.8. XRD result for Wyoming microfines indicate a reduction in vermiculite, quartz, and albite. In general, most species are disappearing.

Appendix 2. Air Void Analysis (Optical Microscope)

Optical microscope images were taken of the specimens used in ASTM C457 testing. The following images show a representation of the air void systems measured. Each image represents a 1.26cm wide by 0.94cm high area. WI microfines on WI aggregate specimens had the most uniform air void system.

CA on WI
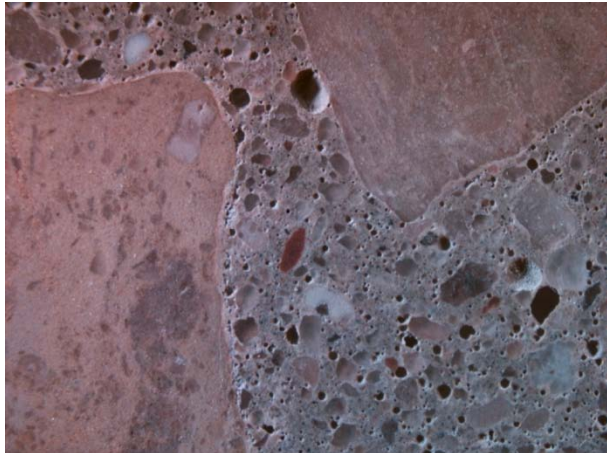
Figure A2.1
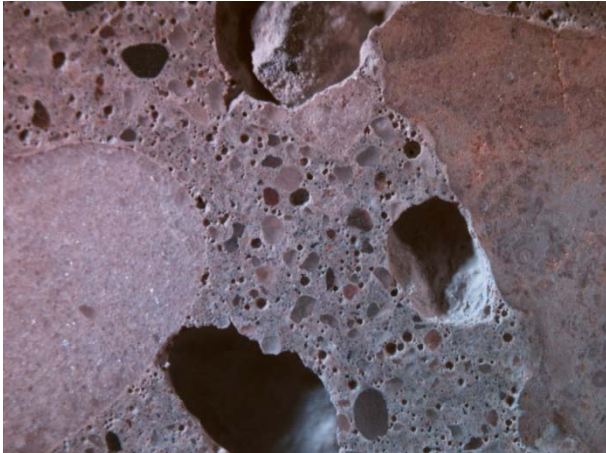
Figure A2.2

WI on WI

Figure A2.3
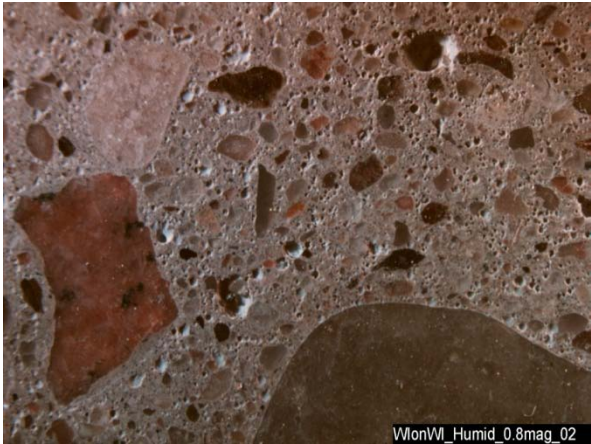
Figure A2.4

CA on UT
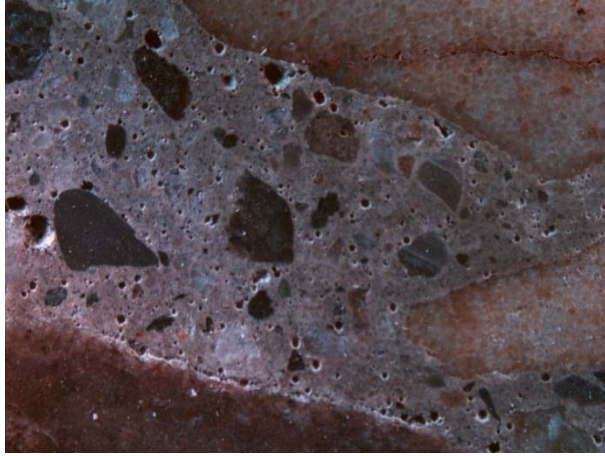
Figure A2.5
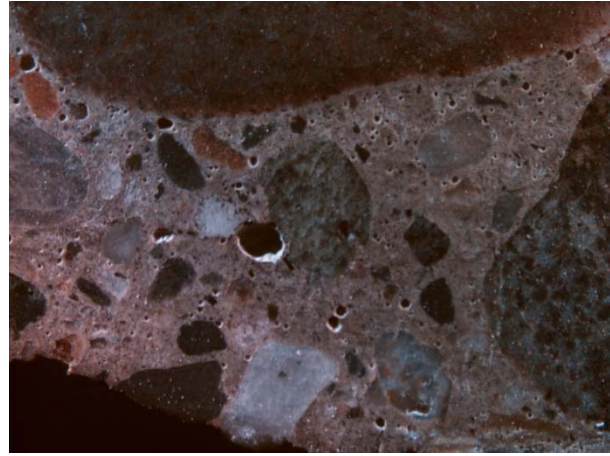
Figure A2.6

CO on UT
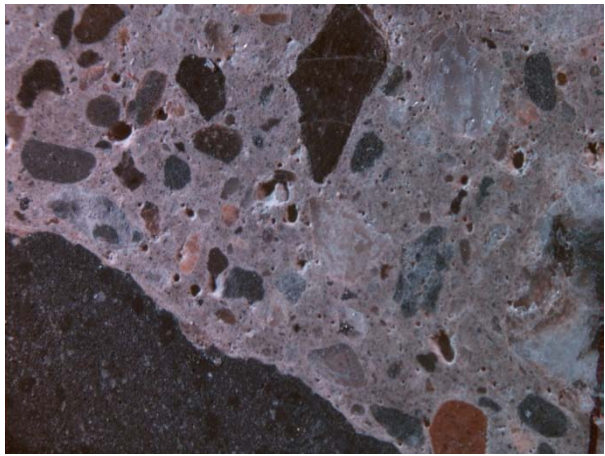
Figure A2.7
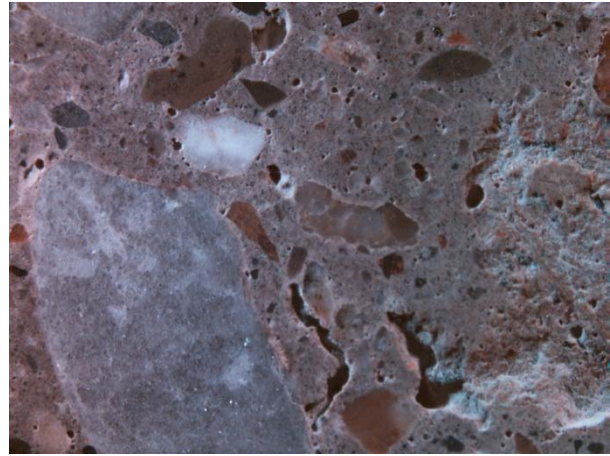
Figure A2.8

Appendix 3 - ASTM C1260 SEM Analysis

At the conclusion of the ASTM C1260 tests, specimens were cut from the center of the bar in order to conduct SEM analyses of the specimens. It was found that specimens containing the reactive Utah fine aggregate contained obvious signs of ASR. Unlike the samples from the ASTM C1293-Deicer series, a clear gel composed of Si, Na, and Ca was found despite the source of microfines. Figure A3.1 shows one example of ASR gel in the matrix from the UT microfines on UT aggregate specimens.
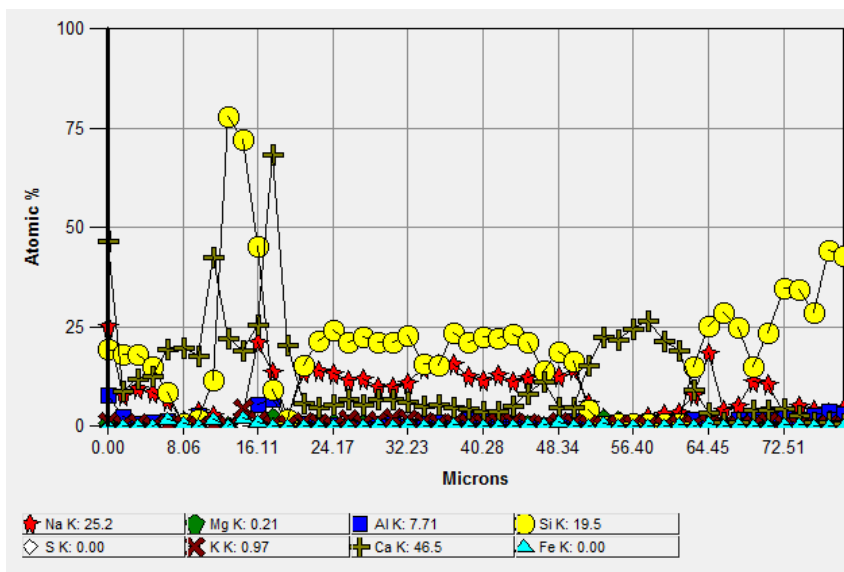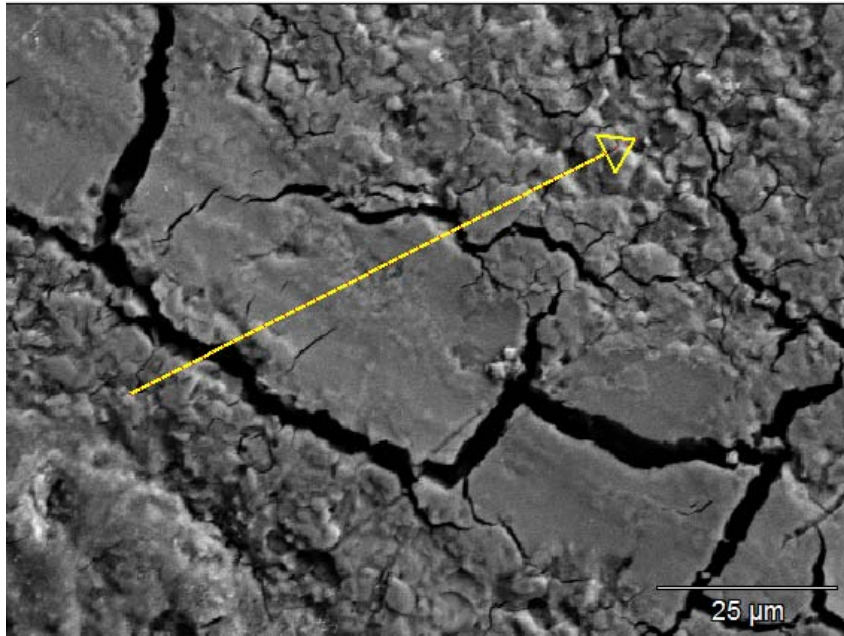
Figure A3.1. Micrograph (above) and EDS scan (below) of ASR gel in ASTM C1260 specimen (UT microfines on UT aggregate).

Appendix 4. Investigation of Potassium Acetate Penetration

While handling and examining samples for SEM at 3, 6, and 9 months, the specimens became increasingly fragile even at the center of the cylinder. This led to the belief that the potassium acetate associated deterioration was deeper then 15mm as seen in previous work. Since this concrete was immature when subjected to the potassium acetate, a test was conducted to determine how far the potassium acetate penetrated into the specimens at one year. This test used Infrared Spectrometry to determine if acetate compounds have penetrated the concrete. This test was run on concrete samples with the following four microfine-and-aggregate combinations: CA on UT, CO on UT, WI on WI, and WY on WI. These were chosen as the fresh air content varied in each and would give a better representation of ingress despite the air void system. From each specimen, a slice was taken at three inches from the finished cylinder surface. Samples from this slice were taken in three locations using a 5/32 hammer drill bit, at incremental intervals from the surface. First the center was analyzed and then a comparison was taken from the edge to determine if acetates had reached full strength in the core of the piece. If it had not, then pulverized samples could have been analyzed heading towards the edge. See Figure A4.1 for a representation of the samples taken from the cylinders. Around each numbered ring, at least 3 samples were taken from the paste regions of the specimen.
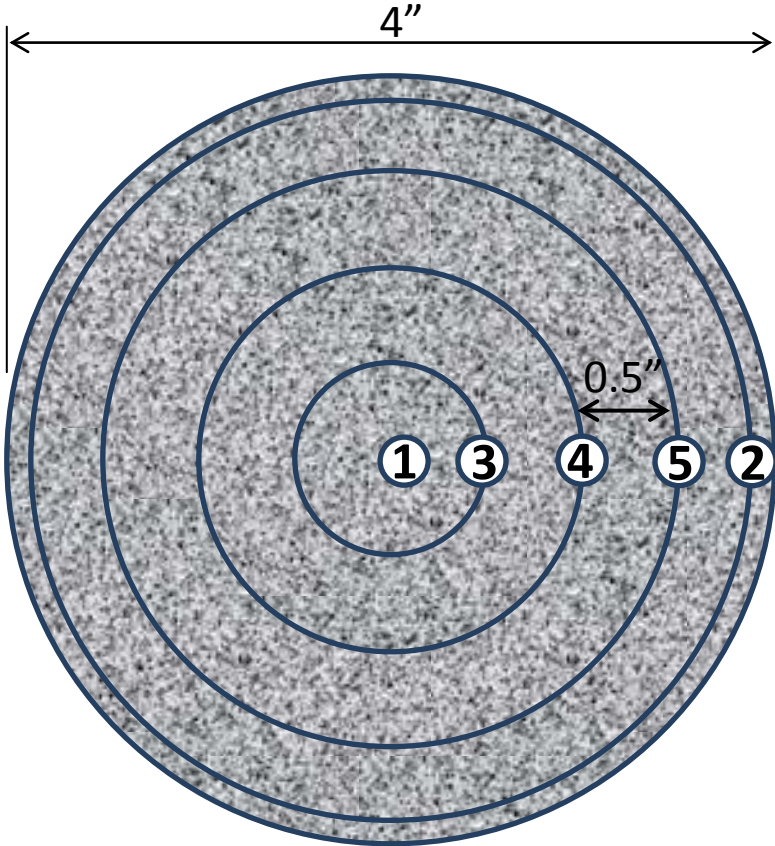
Figure A4.1. Sample sites from cylinders exposed to deicer as in C1293-Deicer tests.

The presence of acetate ions in the concrete samples should show in the IR spectra mainly through two absorption bands associated with the asymmetric and symmetric stretching of the carboxylate group. The exact position of these bands will depend on whether the acetate group is free (ionic), as it happens in KAc, or the carboxylic group is coordinated to some other metal ion present in the concrete. The asymmetric stretching is expected to appear between 1650 cm^{-1} and 1500 cm^{-1} while the symmetric stretching may show between 1450 cm^{-1} and 1350 cm^{-1}. In the spectrum of KAc these bands appear at 1560 cm^{-1} and 1420 cm^{-1}. The IR spectra of concrete are rich in absorption bands in the region of interest for the analysis of acetate ions. Consequently, the spectrum of the C1293-Humid specimens (no deicer exposure) will be subtracted from each of the spectra of the samples treated with deicer. All these concrete specimens are expected to have the same polyatomic groups (since initially they have the same mineralogy), thus, the only major difference in these spectra should be associated with presence of acetate groups.

Figure A4.2 shows the DRIFT (Diffuse Reflectance Infrared Fourier Transform) spectra of KAc, Ca(Ac)$_2$, and the spectra resulting from subtracting the spectrum of WY on WI C1293-Humid specimens from the spectrum of WY on WI treated with deicer. The subtraction spectrum of concrete shows two bands in this IR region that can be ascribed to acetate groups. The separation in frequency of these two bands is slightly larger than in the case of KAc (uncoordinated carboxylate), which leads to the conclusion that most of the acetate is weakly coordinated to some metal (probably Ca) forming a monodentate complex. The position of these bands is also different than that in the spectrum of calcium acetate. In this spectrum these two bands are even closer than in the spectra of the KAc indicating the formation of a bidentate complexes of the carboxylic group with the Ca ions. As a consequence, the acetate in concrete is not in the form of either KAc or Ca (Ac)$_2$ but it forms a not very strong, monodentate complex, most likely adsorbed on the surface of Ca(OH)$_2$ crystals. The presence of large and broad bands in this region of the concrete spectra associated with ions other than acetate (it may be due to carbonates) prohibits a more precise analysis of how much acetate is present in the concrete. The presence of acetate peaks in the spectrum of a specimen from the center of the cylinder showed that KAc penetrates all across the cylinder in this period of time.

By comparing the relative intensity of the peak at 1578 cm^{-1} (with respect to the intensity of other concrete bands) in the spectra of samples from the center and the edge of the concrete cylinder, one should be able to determine the degree of penetration of the KAc. In Fig. A4.3 we show the spectra of two samples from the WY on WI concrete cylinder, one from the center and the other from the edge. The third spectrum in Fig A4.3 belongs to a sample of concrete from WY on WI C1293-Humid specimens. We can see that even without subtraction, the asymmetric mode around 1580 cm^{-1} is very visible in the spectra of concrete treated with deicer. However, is

difficult to judge which of the two specimens have more acetates, the one from the center or the one from the edge.
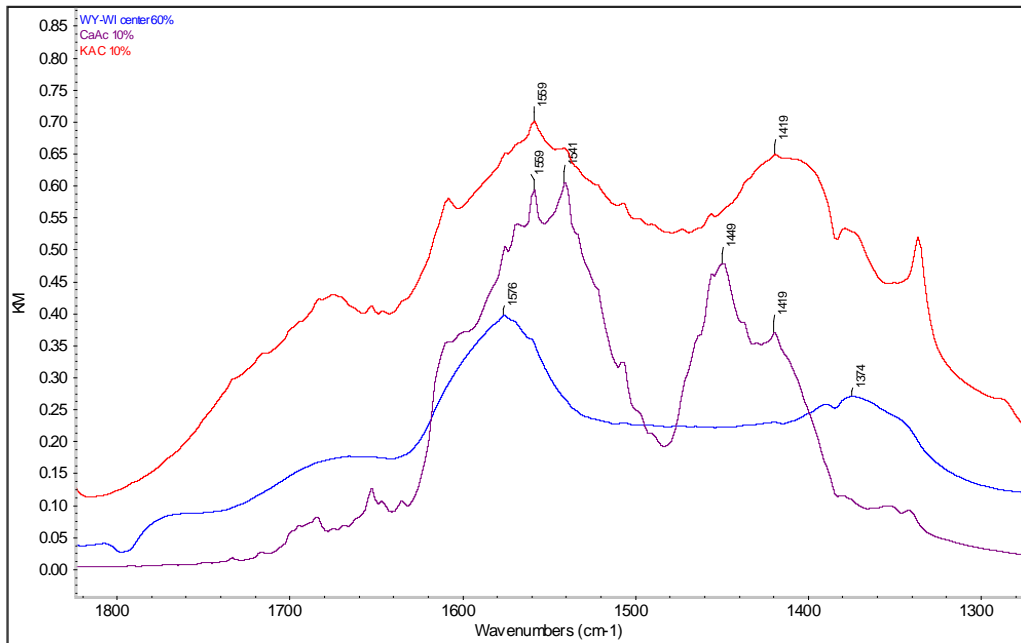
Figure A4.2. DRIFT diagram of calcium acetate, potassium acetate, and center WY on WI C1293-Deicer results. WY on WI C1293-Deicer results show most of the acetate is weakly coordinated to some metal (probably Ca) forming a monodentate complex.
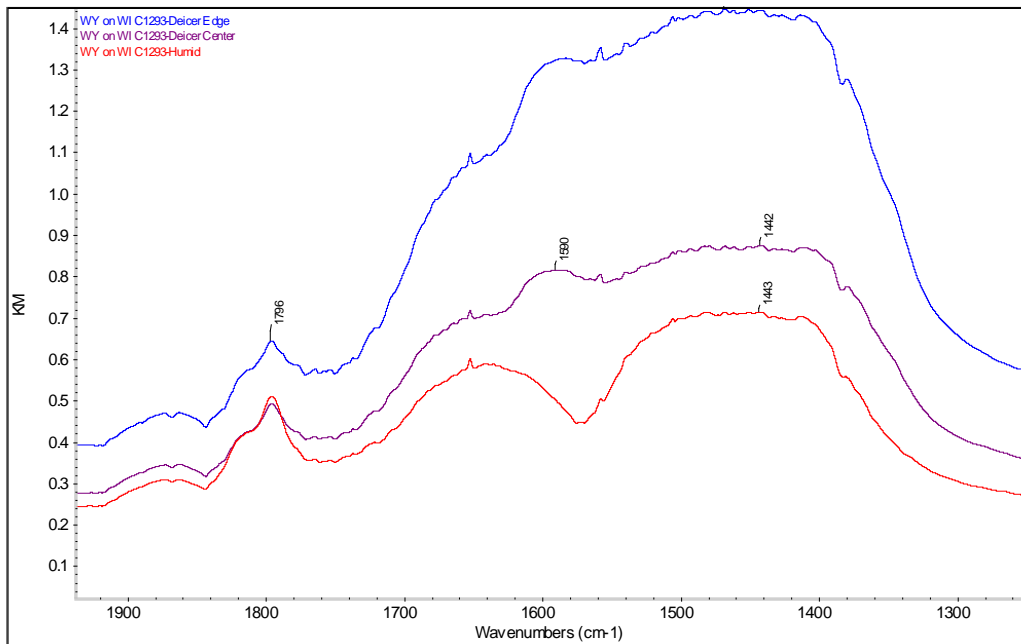
Figure A4.3. DRIFT diagram showing an acetate peak in both the WY on WI C1293-Deicer outer and center samples.

Penetration holds true for all of the specimens. From Figure A4.4 we can see that the spectra of the four humid samples do not show the absorption band, near 1590 cm^{-1} , associated with acetate. However, the spectra of the the eight concrete paste samples that could have acetate do show a band or shoulder at this wavenumber (those from the center or edge of the C1293 specimens in KAc). Although the same mass of sample and the same dilution in KBr (60%) was used to run the spectra of all specimens, the results cannot be regarded as quantitative. The reasons: band intensity using DRS not only depends on concentration but also on particle size, which has not been controlled in these experiments; also, and we believe more important, is the presence of an intense band of carbonates in the region 1500-1400 cm-1. Although the mineralogy of the specimens treated and untreated with acetate may be the same, the content in carbonate may be different. The substraction of the spectrum of humid specimens from the acetate exposed speimens may be over/under subtracting the band of carbonates when we normalize with respect to bend of silicates (1100 -900 cm-1). This over/under subtraction of carbonates should affect the intensity of the acetate bands. However, it can be said that acetates are present in both type of specimens, the ones extracted from the outer part of the cylinder as well as that extracted from the center of the cylinder. The relative intensity of this band in most of the spectra of Figure A4.4 does not show any dependency on their location in the cylinder. The exception is the WI-on-WI specimens where it seems the band in the spectrum of the outer sample is more prominent than in the spectrum of the center sample.

We can also say that the acetate is likely complexed with calcium based on the location of the peaks. The different spectra reported in Figure A4.5 shows a frequency for the asymmetric streching higher than that in the spectrum of free acetate, while the band associated with the symmetric streching appears at lower frequencies and it has structure (triplete). In our opinion a large fraction of acetate is forming monodentate complexes or asymmetric bridging with the Ca in the concrete. However, the presence of carbonate bands in this region does not allow us to be more precise on the type of acetates present in the system. So despite the varying measured fresh air content, potassium acetate can infiltrate the paste. (For CA on UT, CO on UT, WI on WI, and WY on WI the fresh air content was 3.6%, 3.2%, 7.7%, and 5.0% respectively.)
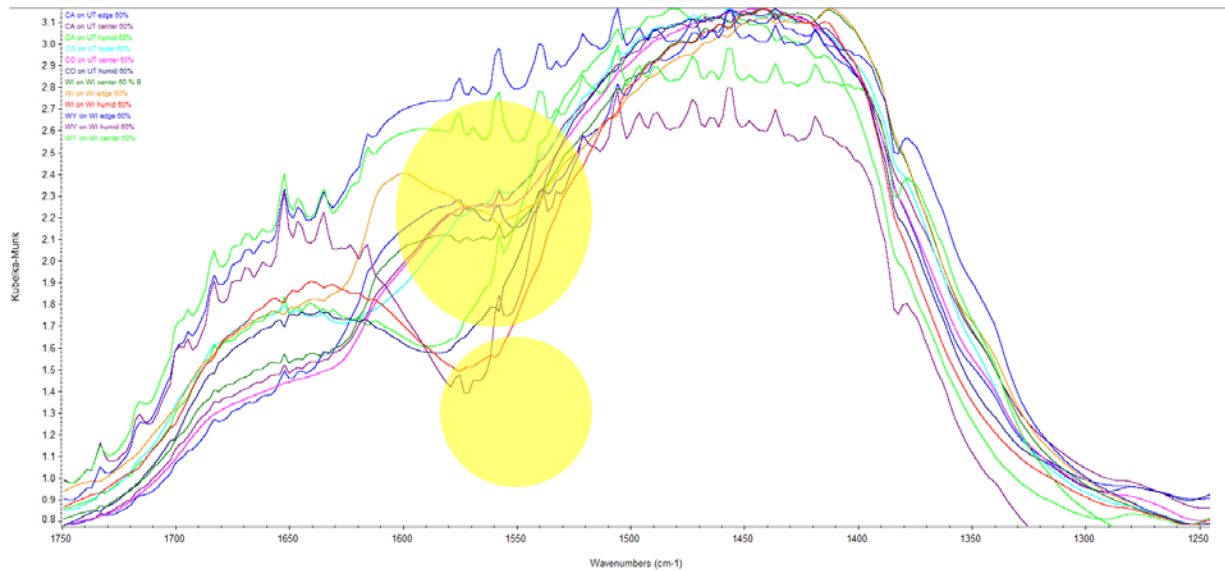
Figure A4.4. DRIFT diagram depicting acetate in all specimens exposed to deicer at both outer and center areas in the concrete and no acetate in Humid specimens.
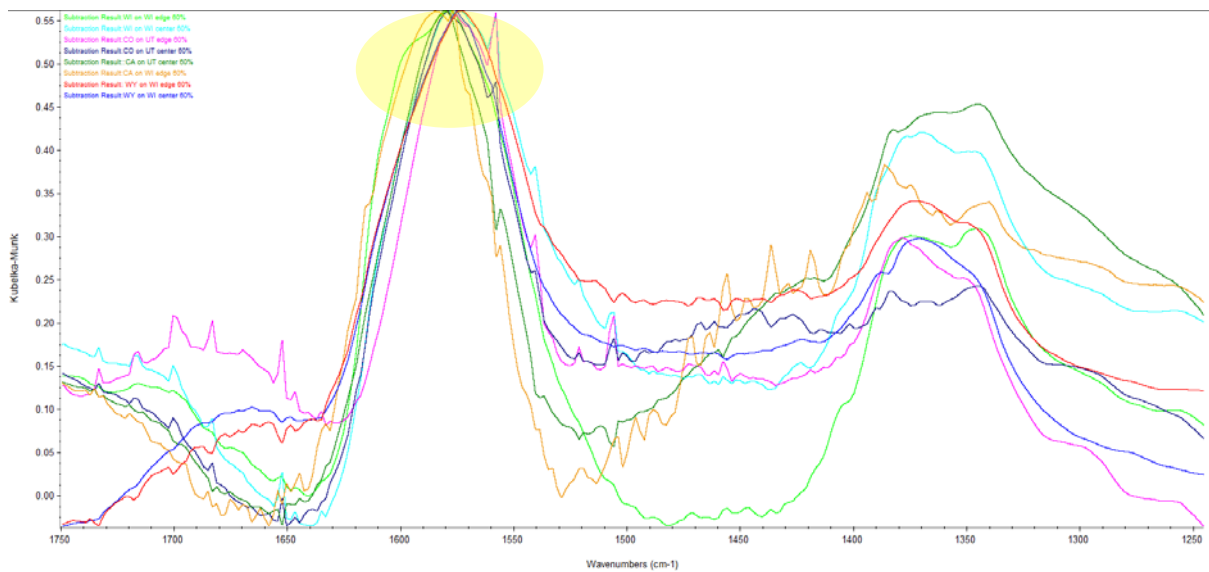
Figure A4.5. DRIFT diagram shows the peaks near 1578cm-1 are not completely overlapped indicating differing complexations of the acetate. This figure also shows the monodentate complex near 1340cm-1 appearing in the various specimens.

Appendix 5. Micrographs and Thermodynamic Simulations of Potassium Sulfate Formation in Modified C1293

The following thermodynamic simulations show possible products formed in concrete when potassium and acetate is in abundance. The figures show the simulation of an environment above a pH of 11 because this is likely the range of the pH seen in the concrete in our study. Fraction of the product is seen on the y axis while the pH range is seen on the x-axis. If the product is followed by a (c) or a (cr), the species exists as a solid otherwise the species exists in solution or as an ionic species. The information above the equilibrium diagram is the inputted concentrations of the included precursor species used in the simulation.

I= 2.000 M

$[Al^{3+}]_{TOT} =$ 500.00 mM $\qquad$ $[Si(OH)_4]_{TOT} =$ 1.00 M

$[Ca^{2+}]_{TOT} =$ 1.00 M $\qquad$ $[SO_4{}^{2-}]_{TOT} =$ 800.00 mM

$[K^+]_{TOT} =$ 5.00 M $\qquad$ $[CH_3COO^-]_{TOT} =$ 5.00 M
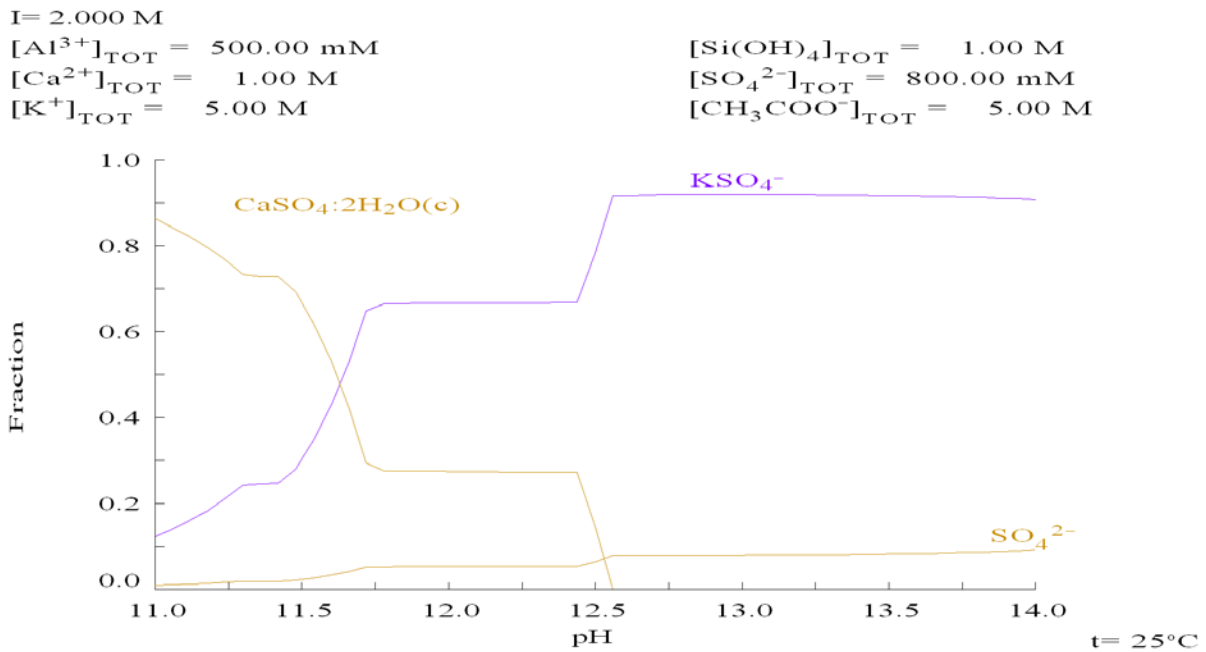
Figure A5.1. Thermodynamic simulation to show KSO$_4^-$ forms over ettringite

I= 2.000 M
$[Al^{3+}]_{TOT}$ = 500.00 mM $[Si(OH)_4]_{TOT}$ = 500.00 mM
$[Ca^{2+}]_{TOT}$ = 1.00 M $[SO_4^{2-}]_{TOT}$ = 800.00 mM
$[K^+]_{TOT}$ = 5.00 M $[CH_3COO^-]_{TOT}$ = 5.00 M
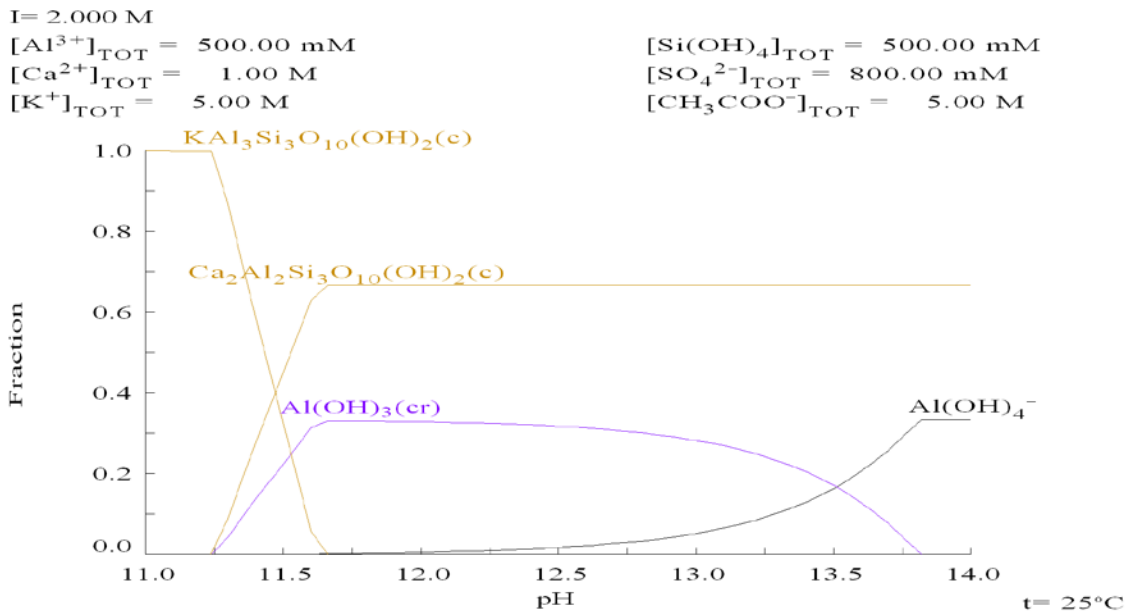
Figure A5.2. Thermodynamic simulation to show aluminum hydroxide could be seen in the system

I= 2.000 M
$[Al^{3+}]_{TOT}$ = 300.00 mM $[SO_4^{2-}]_{TOT}$ = 500.00 mM
$[Ca^{2+}]_{TOT}$ = 500.00 mM $[CH_3COO^-]_{TOT}$ = 5.00 M
$[K^+]_{TOT}$ = 5.00 M $[Si(OH)_4]_{TOT}$ = 300.00 mM
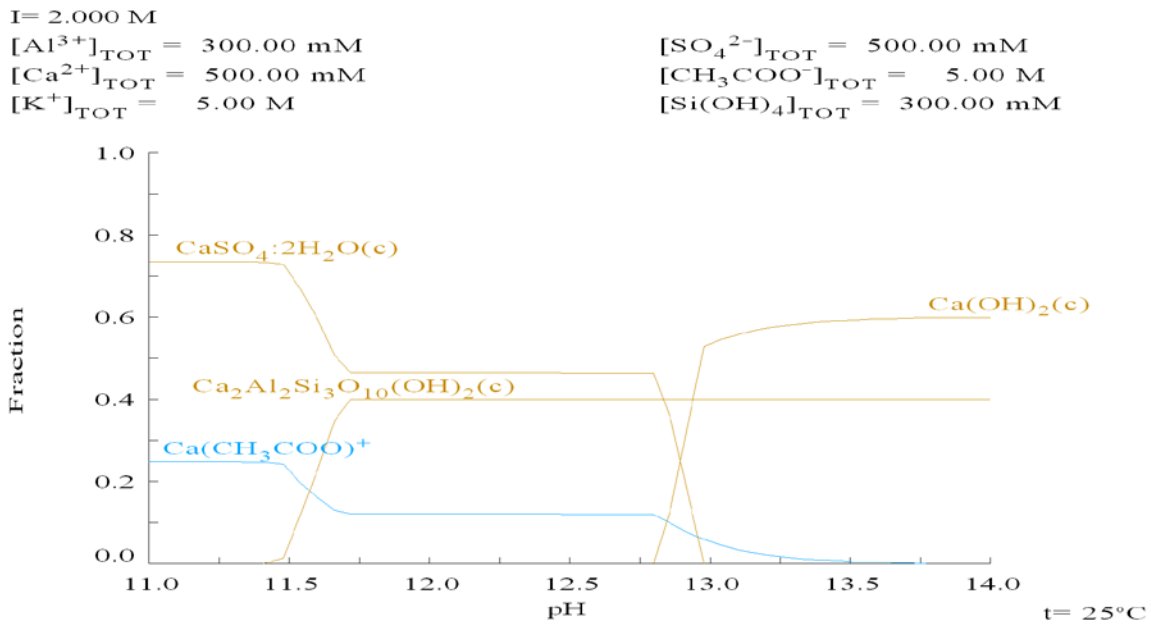
Figure A5.3 Thermodynamic simulation to show calcium hydroxide could be seen in the system

A5.2

Since potassium sulfate was shown to be a possible product in the deicer specimens, it is verified that KS was found in the specimens. Table A5.1 lists the specimens and describes the KS seen under SEM.

Table A5.1. KS descriptions for each of the C1293 Deicer specimens by microfine source.

Does KS form?	
CA	Yes. Less KS seems present in the CA on WI specimen and it is paired with Ca. In the CA on UT specimen, the KS exists as KSCaAl.
CO	Yes. In the CO on WI specimen, the KS exists with Ca. In the CO on UT specimen, it is sometimes with Ca or with Ca and Al.
Cont	Yes. The WI cont has KS in the voids, and near the ITZ. In UT cont specimen, it is seen in the bulk there is also CaAlK similar to the WI cont.
UT	Yes. KS is seen in UT on WI in a void. Yes. In the UT on UT specimens, KS is found with Ca in the ITZ.
WI	Yes. KS is found on the WI on WI specimens. No. It is not seen in the WI on UT specimens.
WY	Yes. The WY on WI contains KS with Ca. It is also seen in the WY on UT specimen, but not seen so much in ITZ.

The following micrographs show the KS in the C1293-Deicer specimens.   Next to the micrograph is the EDS scan taken along the yellow line in the micrograph. The yellow box indicates the region of KS seen in the sample. All of the scans use the following key: Sodium-red star, magnesium-green pentagon, aluminum-blue square, silica-yellow circle, sulfur-white diamond, potassium-dark red x, calcium tan t, iron-light blue triangle.

CA on WI (9mo)
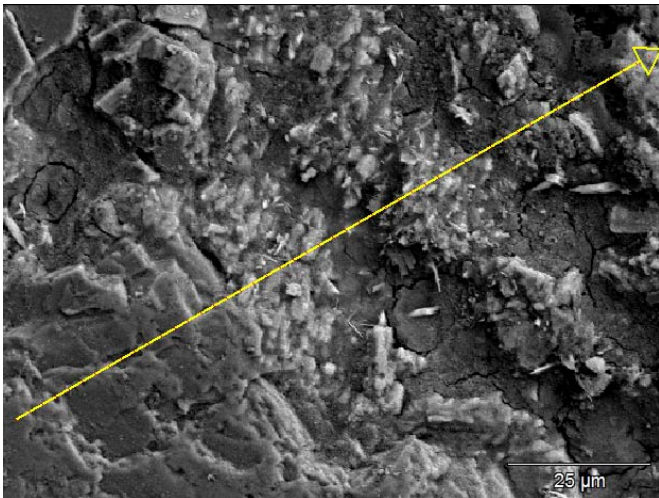
Figure A5.4
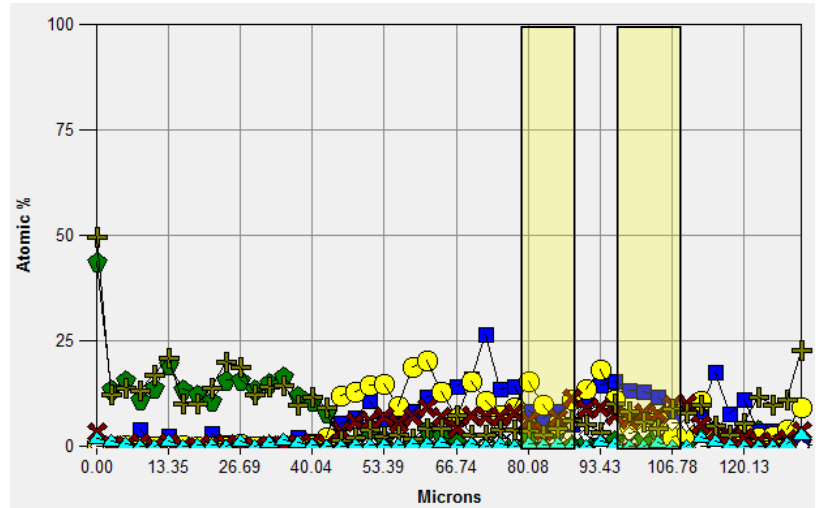
Figure A5.5

CA on UT (6mo)
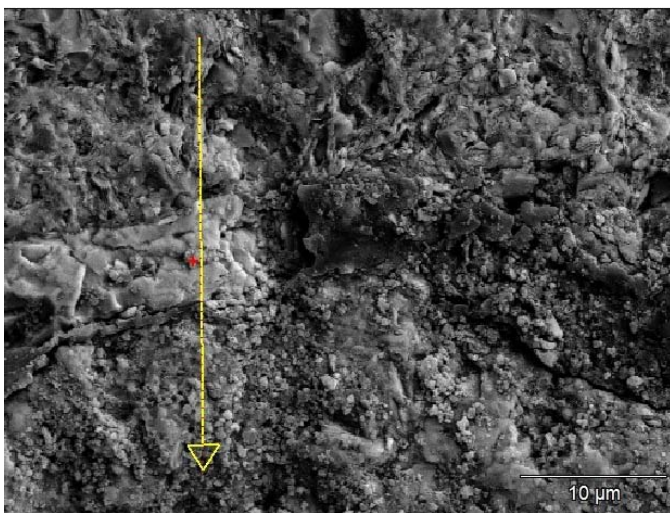
Figure A5.6
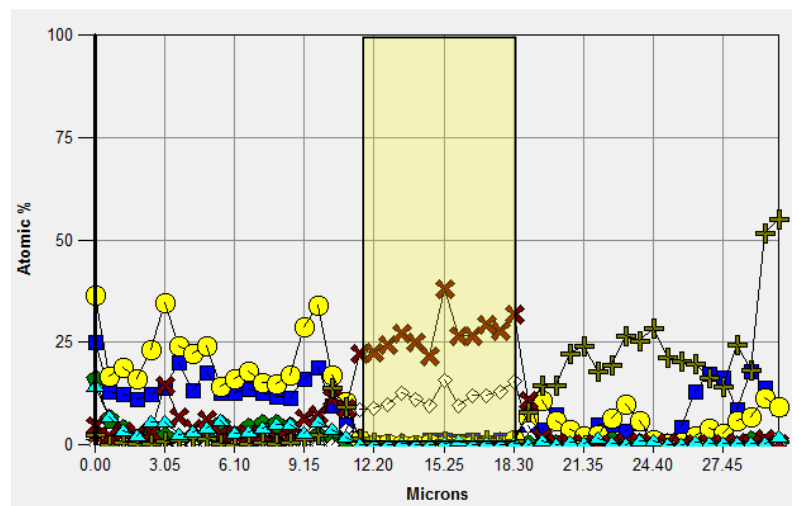
Figure A5.7

CO on WI
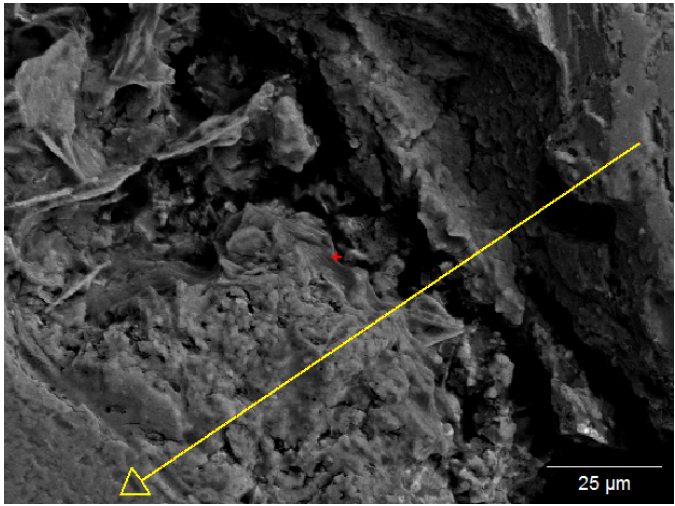
Figure A5.8
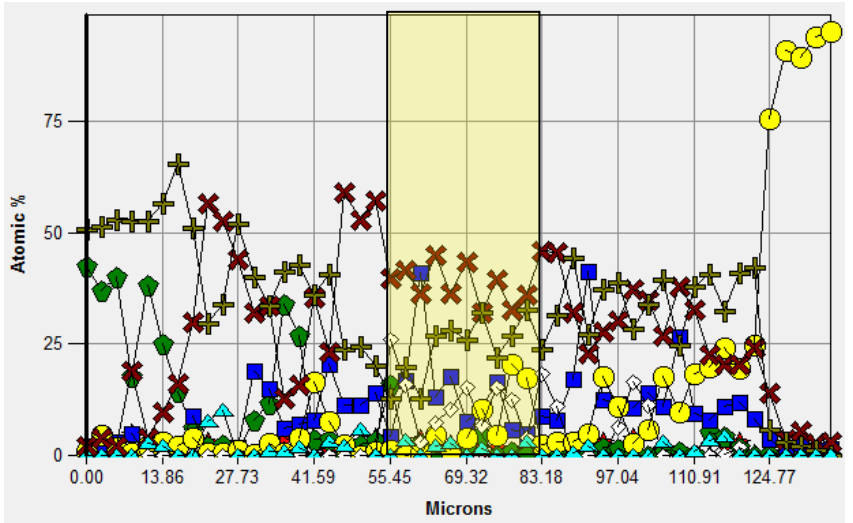
Figure A5.9

CO on UT
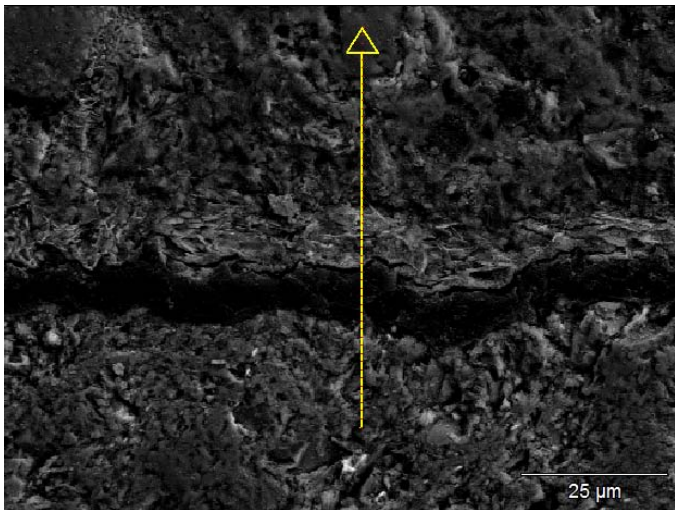
Figure A5.10
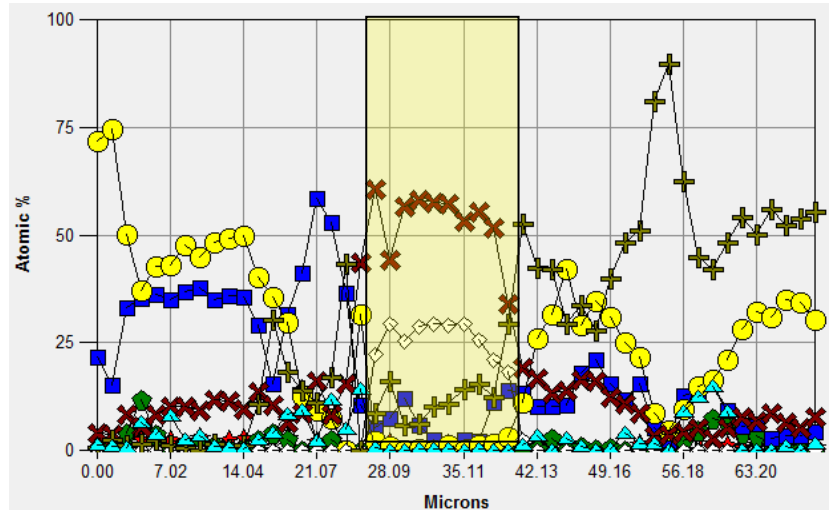
Figure A5.11

WI cont
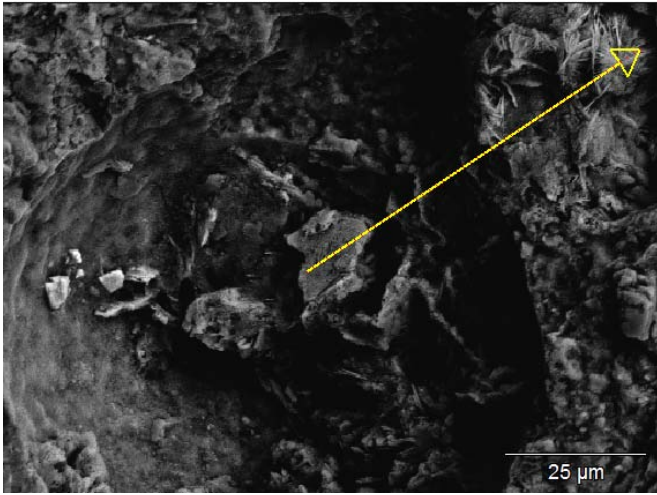
Figure A5.12
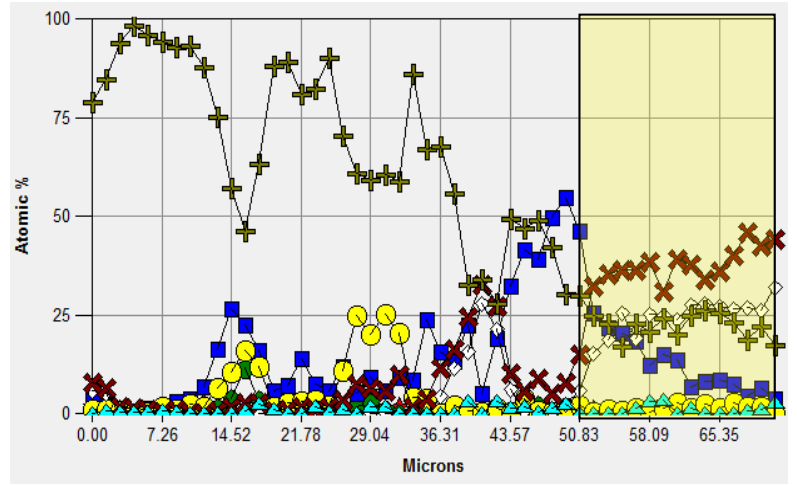
Figure A5.13

UT cont
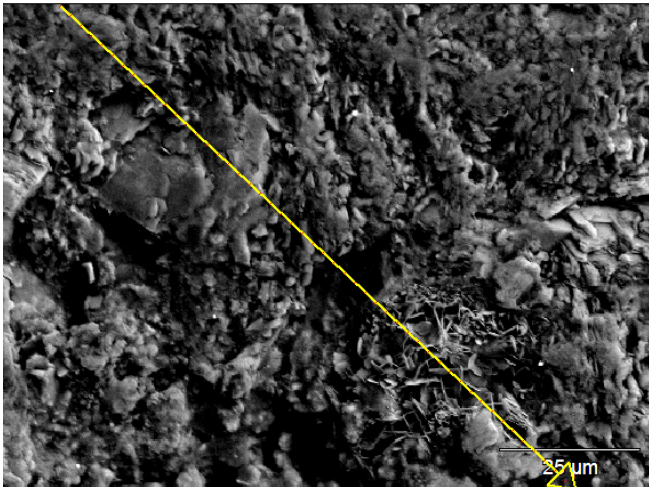
Figure A5.14
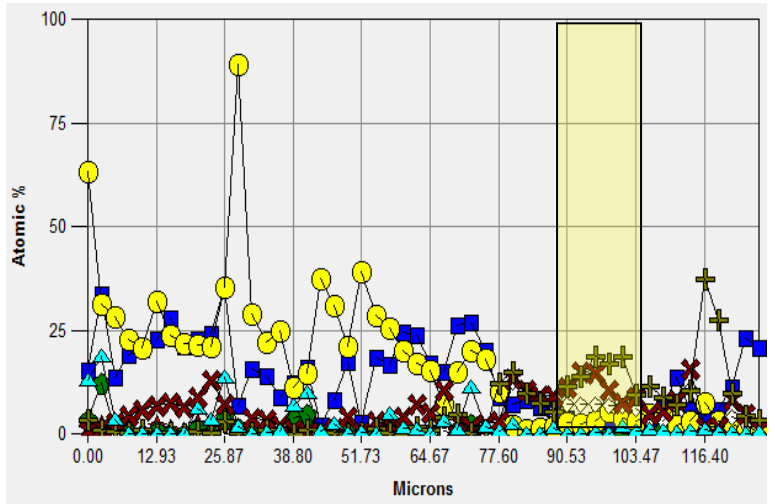
Figure A5.15

UT on WI
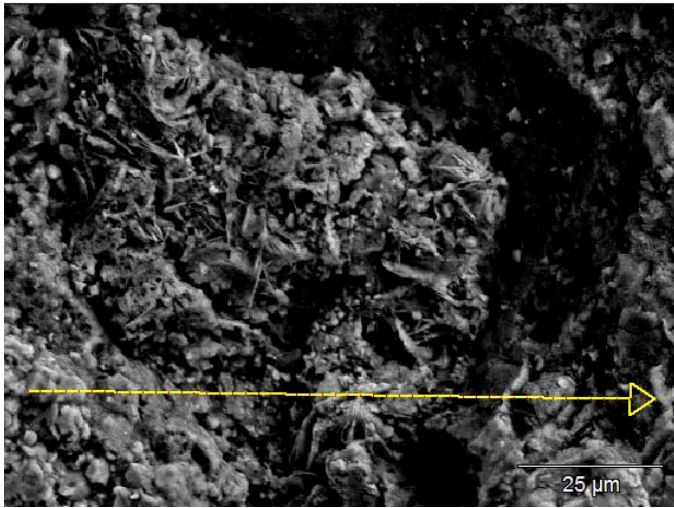
Figure A5.16
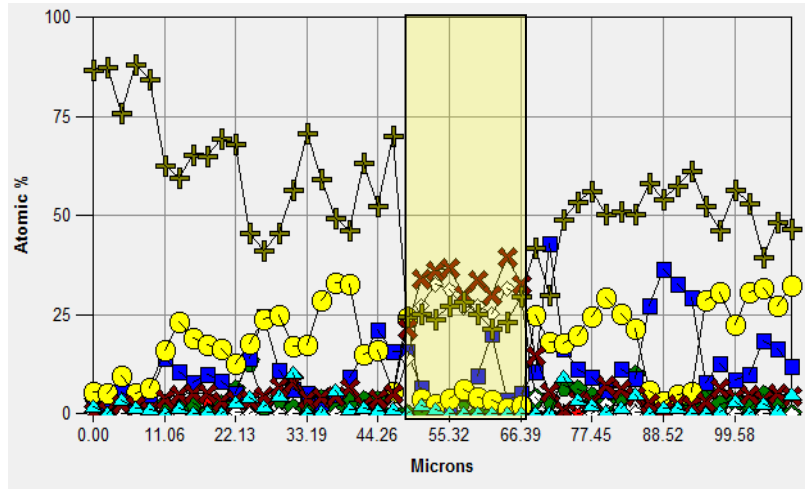
Figure A5.17

UT on UT
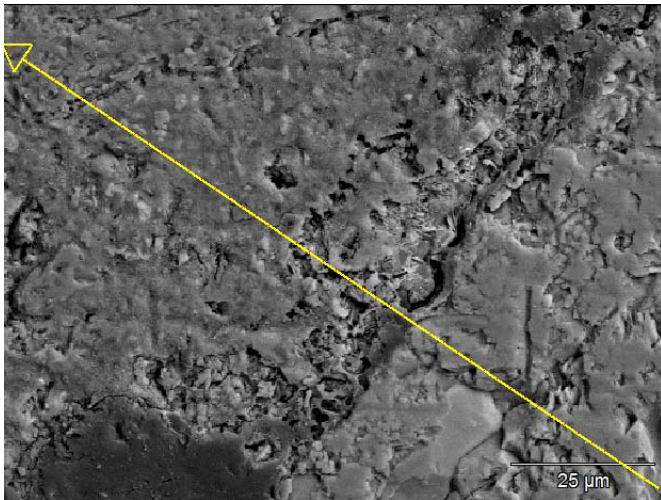
Figure A5.18
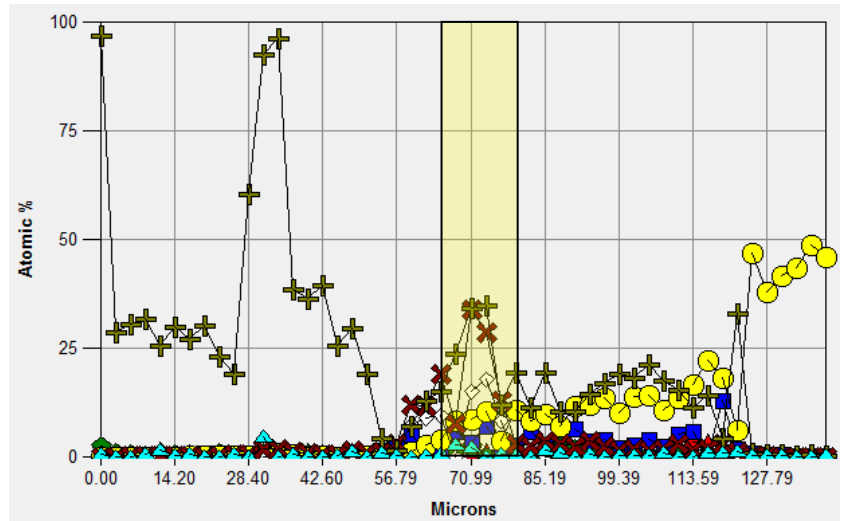
Figure A5.19

WI on WI
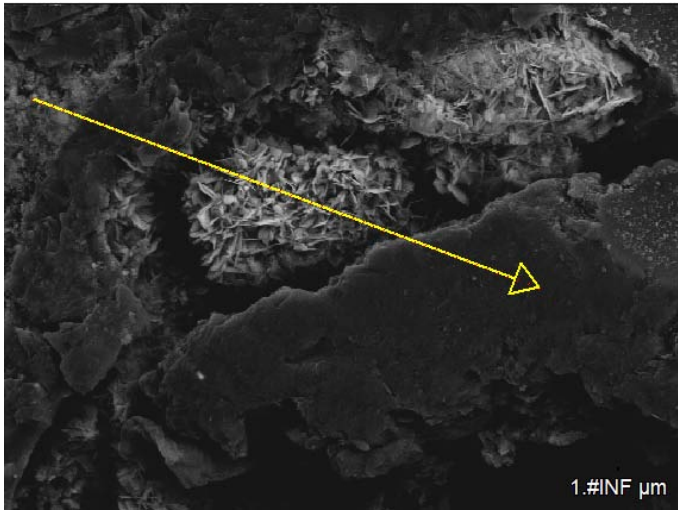
Figure A5.20
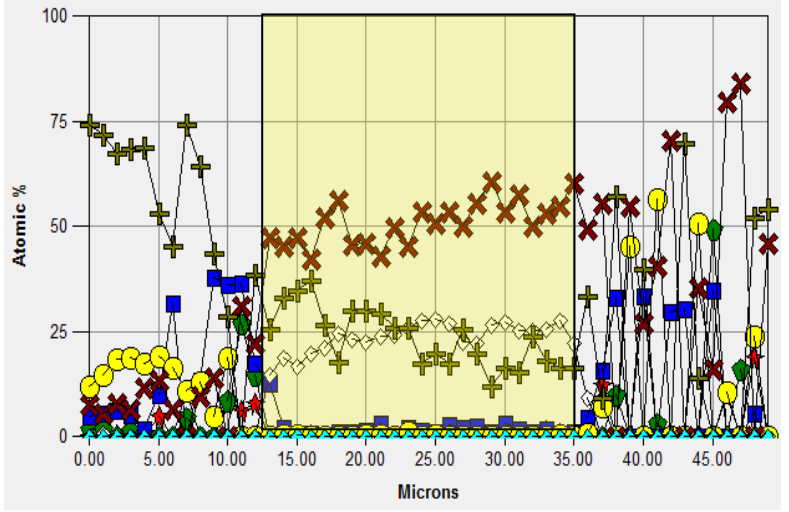
Figure A5.21

WY on WI
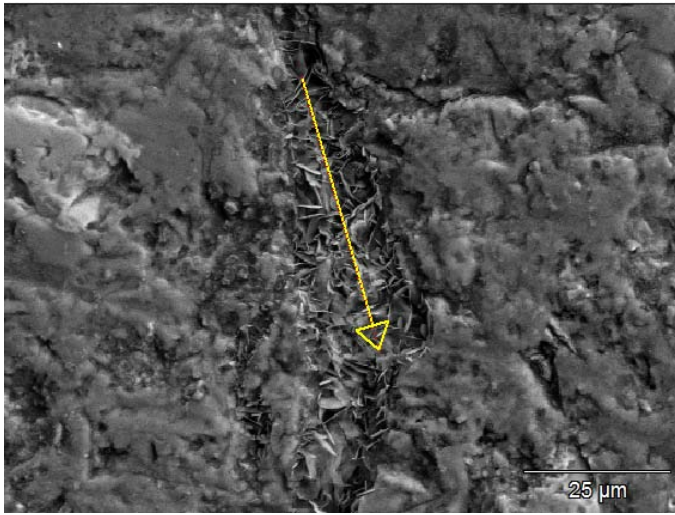
Figure A5.20
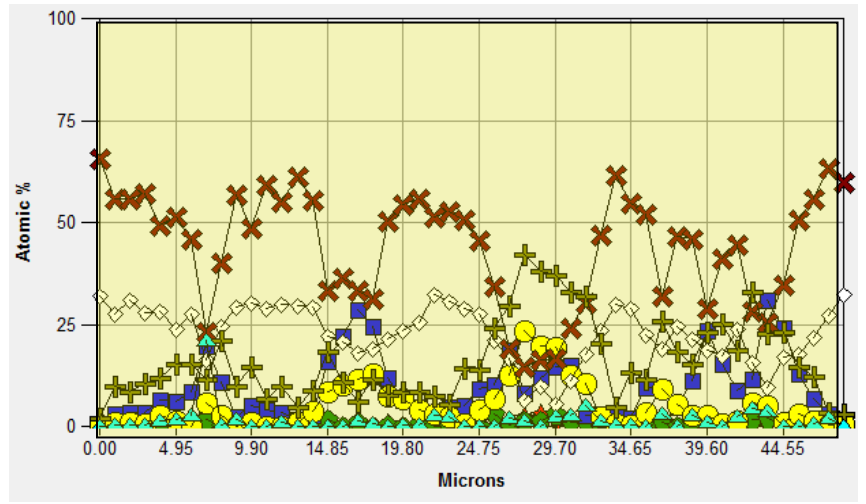
Figure A5.21

WY on UT
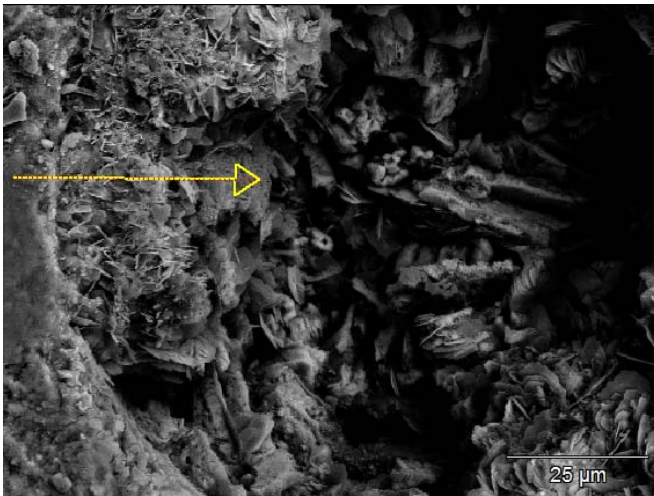
Figure A5.22
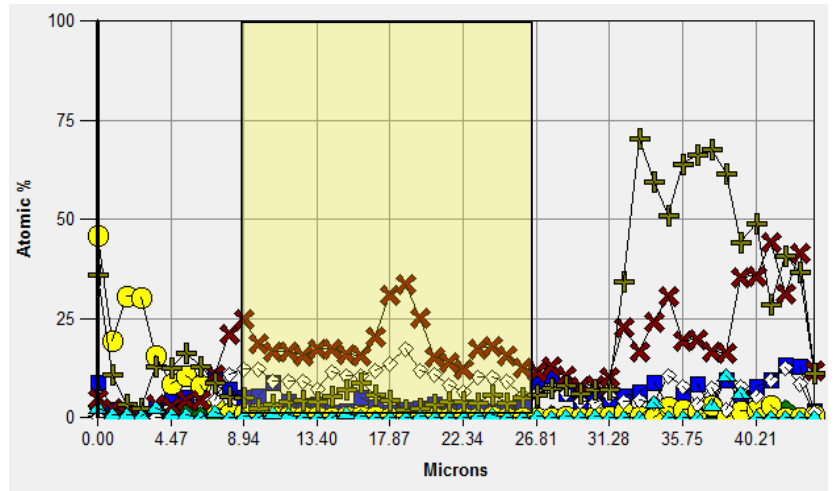
Figure A5.23

A5.9

Appendix 6. Thermodynamic Simulations for the Formation of Solid Phases in the Deicer Concrete Matrix

Expansion was present in the C1293-Deicer specimens which was due to new formation of solid phases in the bulk of the concrete matrix. With the destruction of the siliceous aggregates and the introduction of silica from the microfines in the presence of KAc, the system could transform to form $Ca_2Al_2Si_3O$ and $CaSiO_2$ or Ca_2SiO_4 (we can see this in the WY on UT Deicer specimen.) When $Ca_2Al_2Si_3O$ is formed, the formation of $KAlSiO_3$ as a solid is also seen from thermodynamics when there are low levels of calcium present. (Figure A6.1) This was present in the UT cont Deicer specimen. These new solid phases could cause expansion if the new formations occupy a larger volume then the aggregate. The following simulations show the formation of new solid phases present in the specimens.

I= 2.000 M
$[Al^{3+}]_{TOT}$ =   500.00 mM $[Si(OH)_4]_{TOT}$ =   1.00 M
$[Ca^{2+}]_{TOT}$ =   1.00 M $[SO_4^{2-}]_{TOT}$ = 800.00 mM
$[K^+]_{TOT}$ =   5.00 M $[CH_3COO^-]_{TOT}$ =   5.00 M

t= 25°C
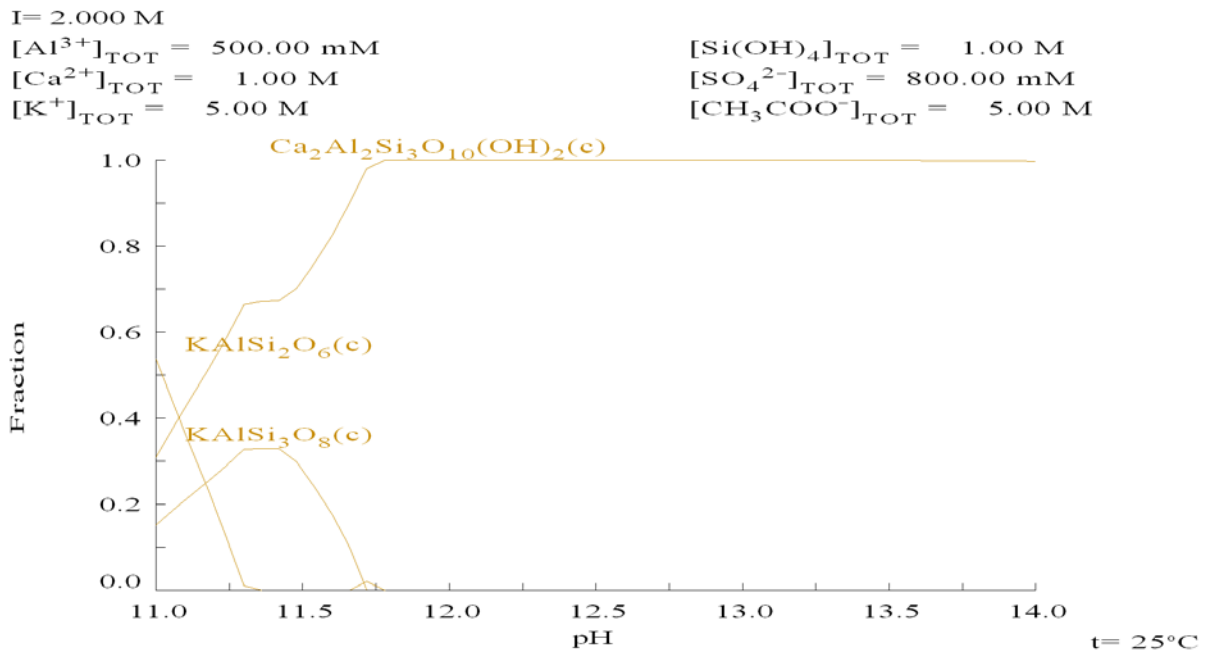
Figure A6.1. Alumino silicates (from clays) in combination with KAc can form $Ca_2Al_2Si_3O_{10}(OH)_2$ which is a new solid formation. There are other solids formed, but at elevated pH levels the calcium species will dominate. The aluminum fraction is shown.

It is possible that if the silica from the aggregate is being released into the bulk, the area near the aggregate may be rich in silica and low in calcium. If this is true, we could see the formation of new solids composed of potassium, aluminum, and silica. The Figures A6.2 and A6.3 show the silica fraction and the aluminum fraction respectively.

A6.1
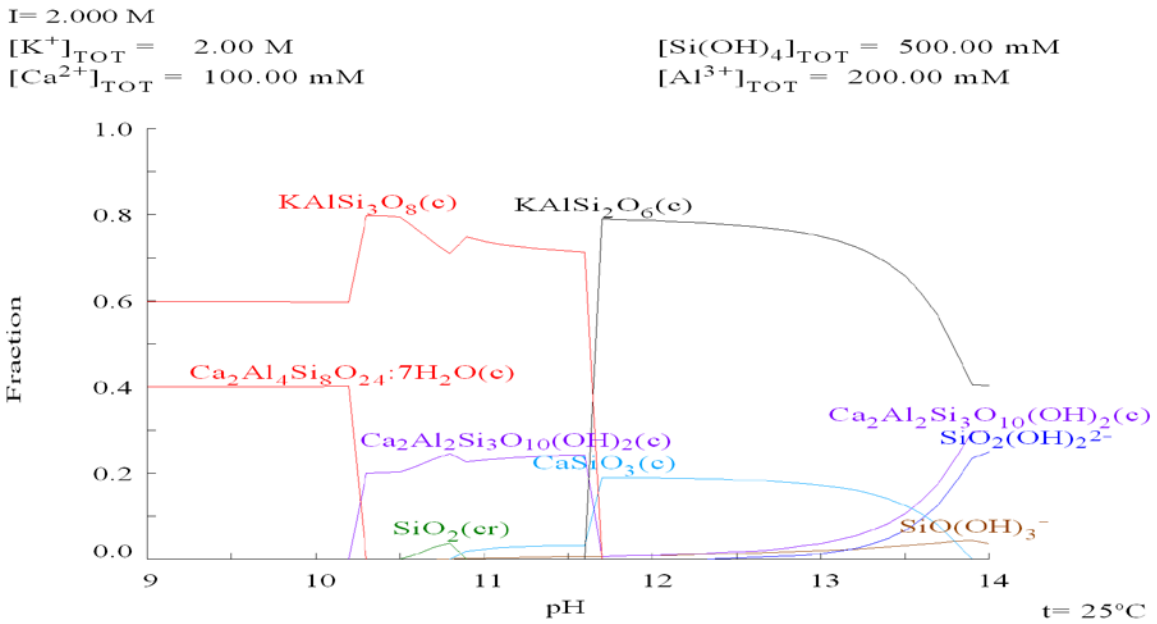
Figure A6.2. Silica fraction of a matrix with low levels of calcium and the formation of a solid species KAlSi$_2$O$_6$.
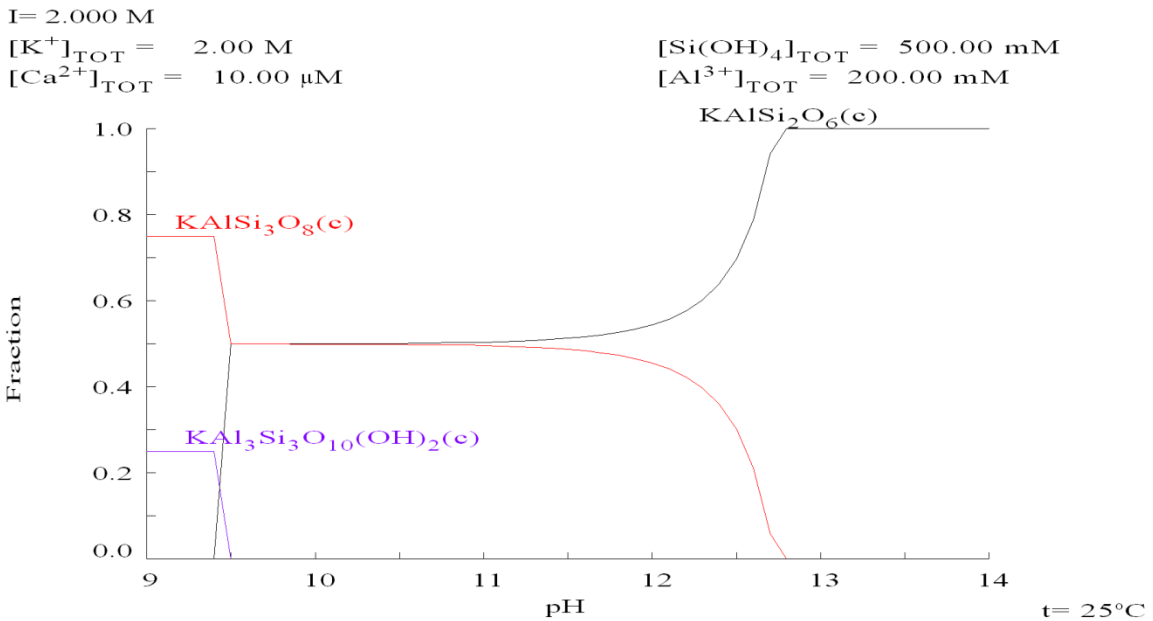
Figure A6.3. Aluminum fraction of a matrix with low levels of calcium and the formation of KAl$_3$Si$_3$(OH)$_2$ along with KAlSi$_2$O$_6$.

Appendix 7: Micrographs of ITZ Degradation in Modified C1293 Specimens

Deterioration of the ITZ was noticed in the SEM micrographs. The ITZ's are depicted here with the specimens free of KAc on the left and the specimens exposed to KAc on the right. Images were taken at a magnification of 85x and represent an area 23,500 pixels by 18,800 pixels.

CA on WI

Humid   **Deicer**
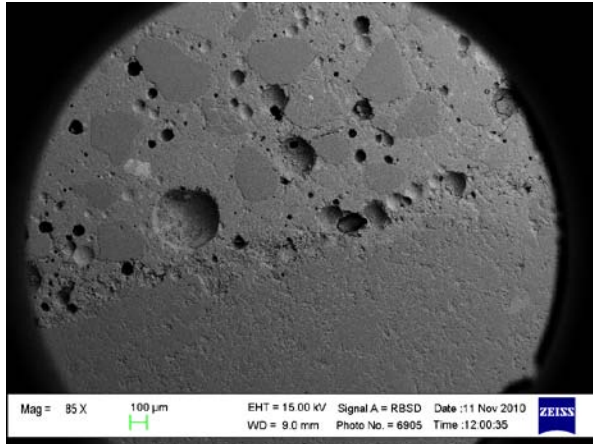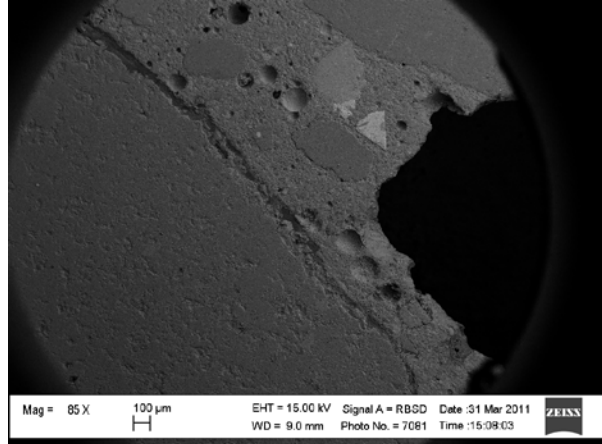
Figure A7.1

Figure A7.2

CA on UT

Humid   **Deicer**
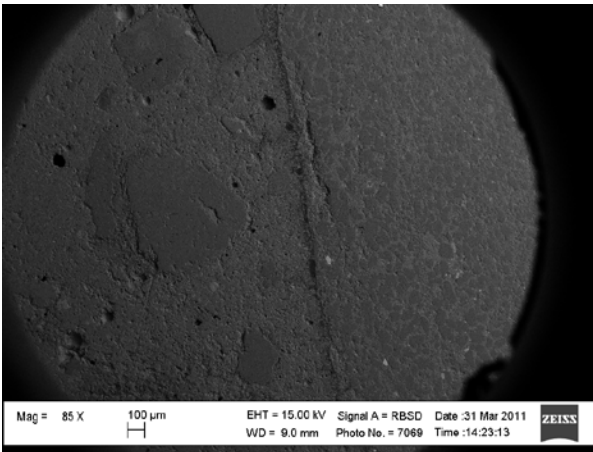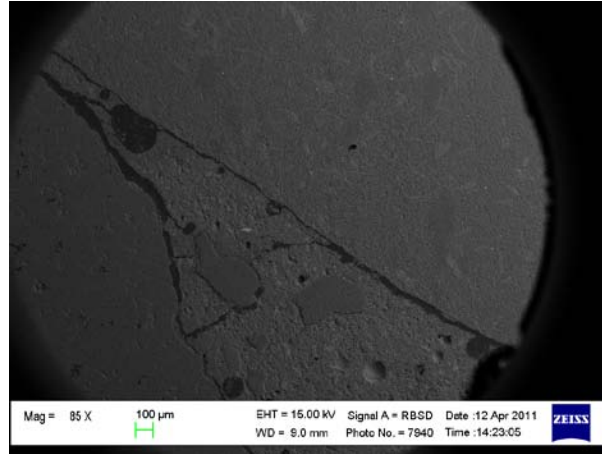
Figure A7.3

Figure A7.4

CO on WI

Humid
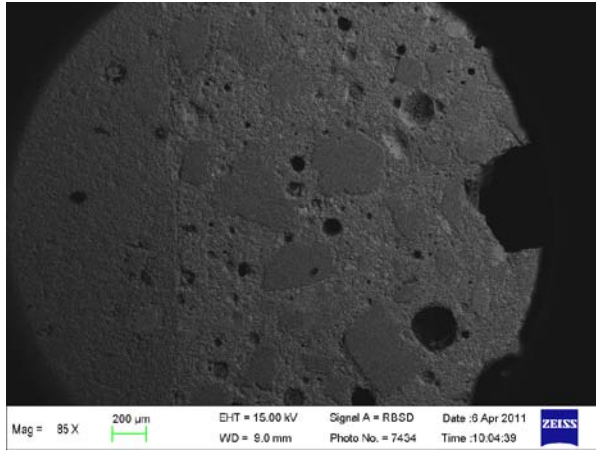
Figure A7.5

Deicer
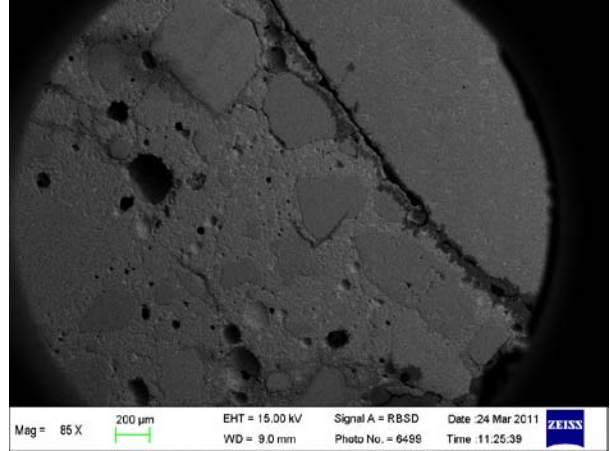
Figure A7.6

CO on UT

Humid
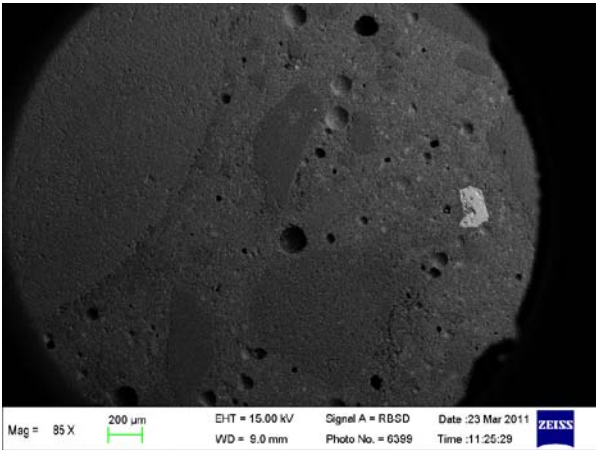
Figure A7.7

Deicer
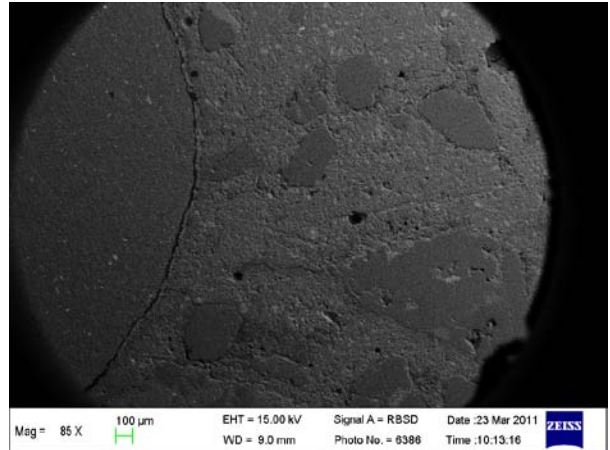
Figure A7.8

WI cont

Humid
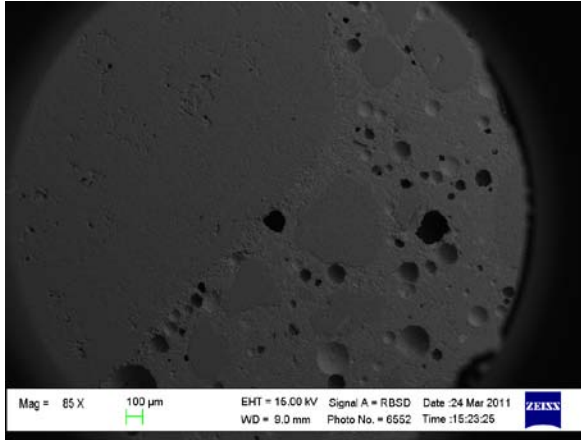
Figure A7.9

Deicer
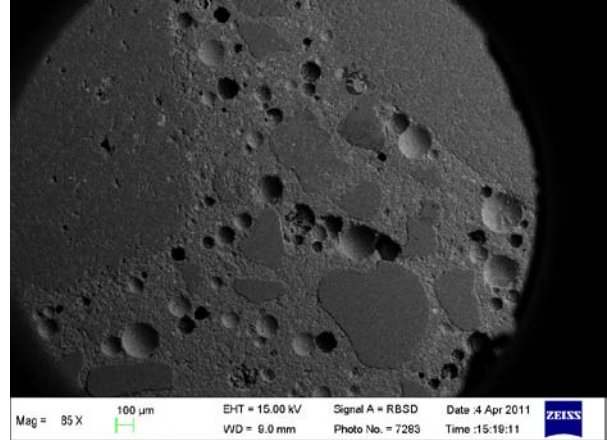
Figure A7.10

UT cont

Humid
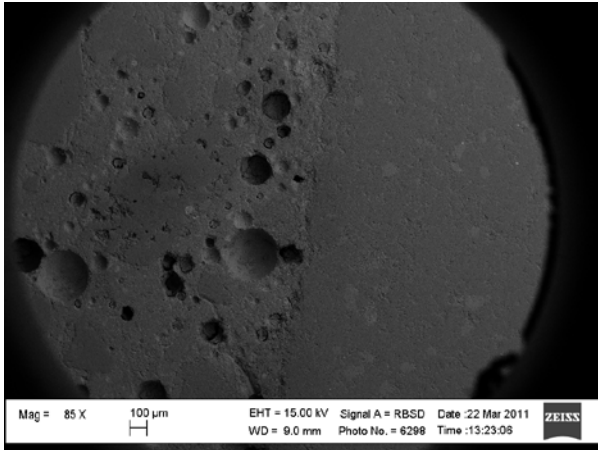
Figure A7.11

Deicer
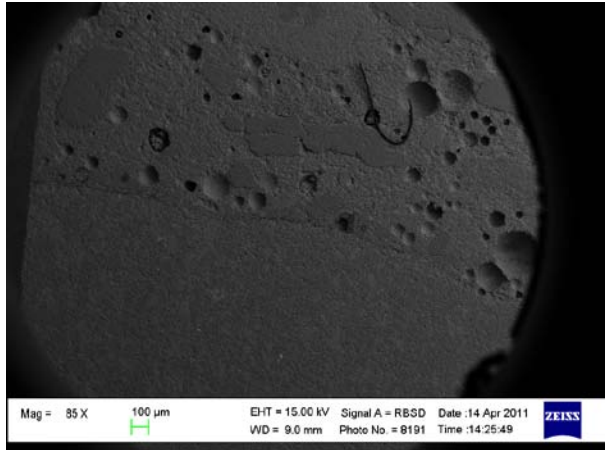
Figure A7.12

UT on WI

Humid
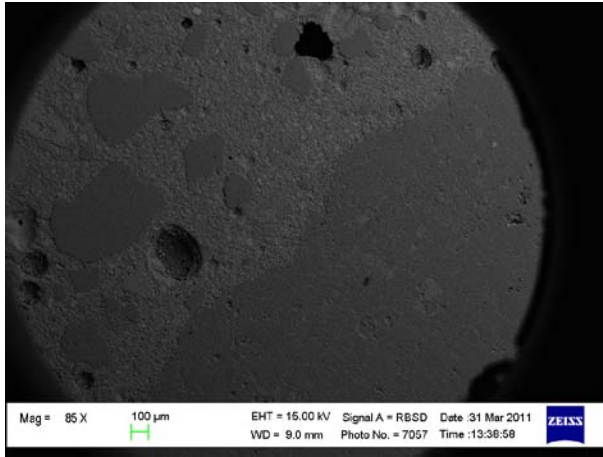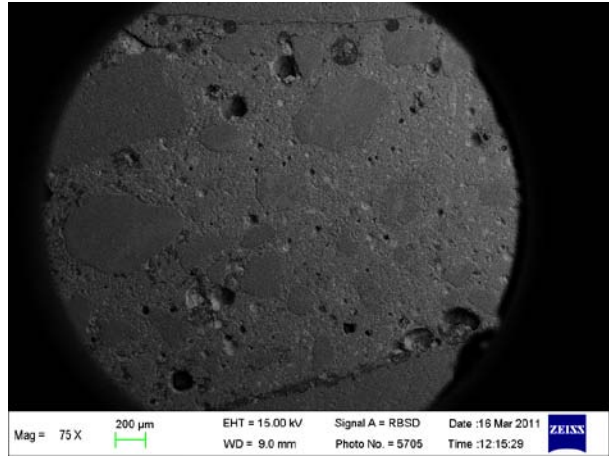
Deicer

Figure A7.13

Figure A7.14

UT on UT

Humid
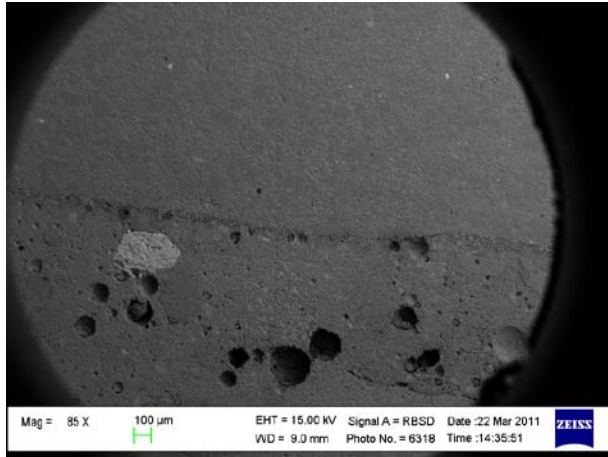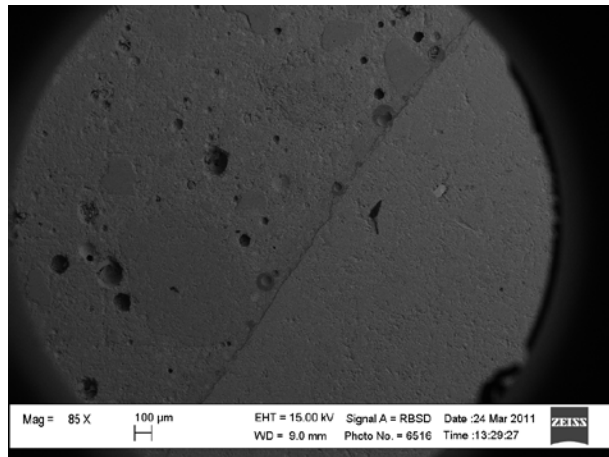
Deicer

Figure A7.15

Figure A7.16

WI on WI

Humid
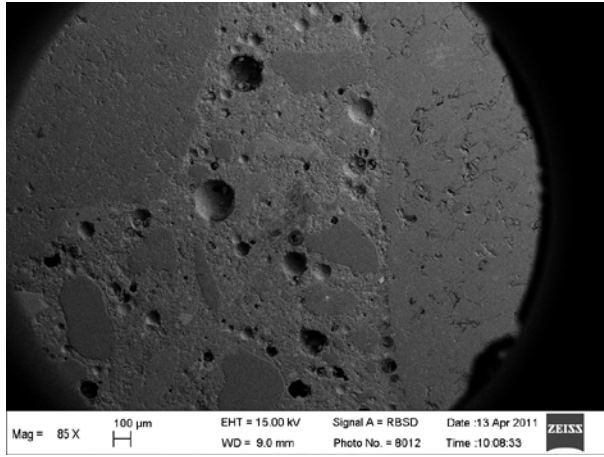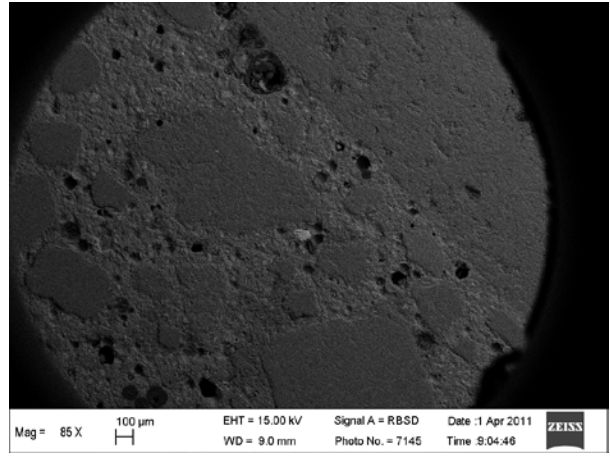
Deicer

Figure A7.17

Figure A7.18

WI on UT

Humid
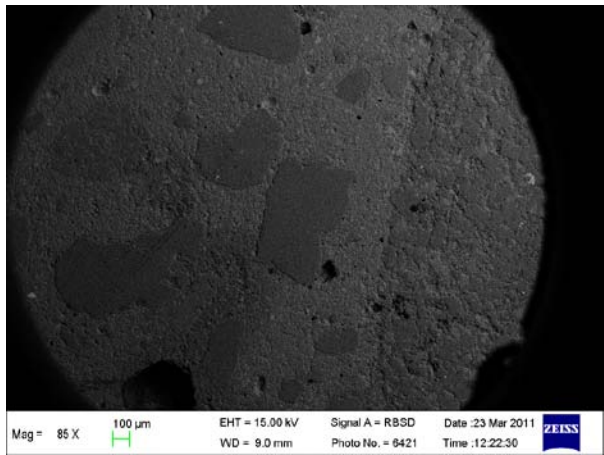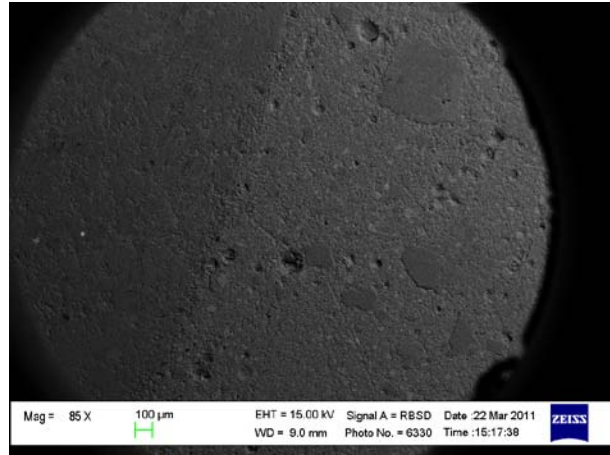
Deicer

Figure A7.19

Figure A7.20

WY on WI

Humid
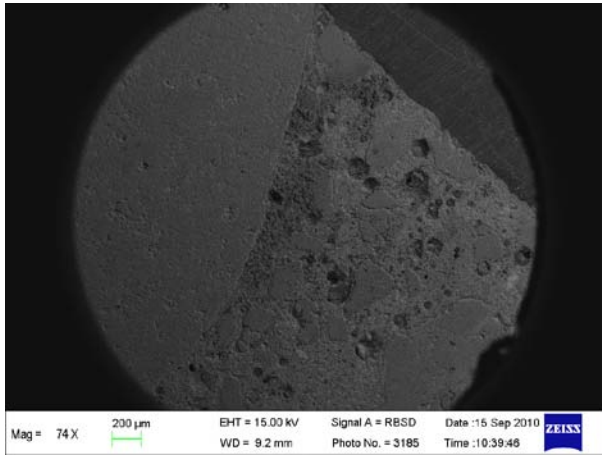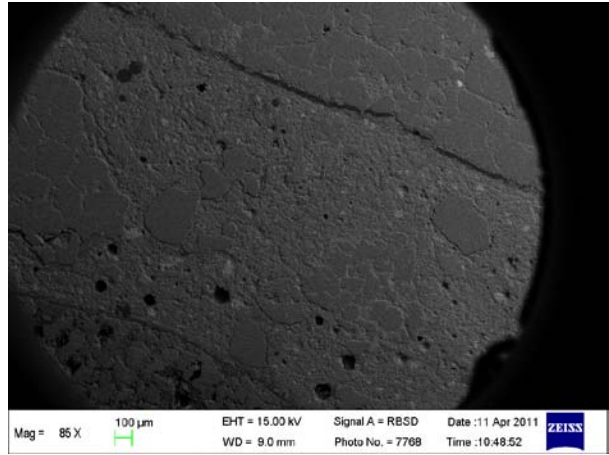
Deicer

Figure A7.21

Figure A7.22

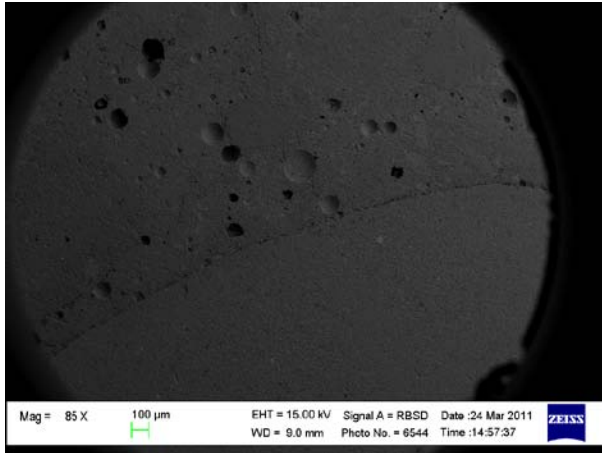**WY on UT**

Humid
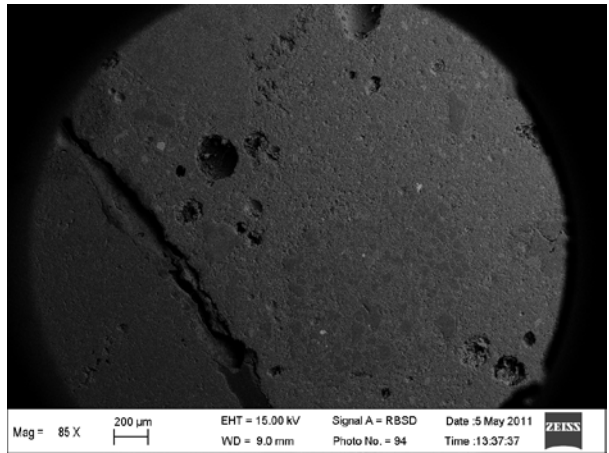

Deicer

Figure A7.23

Figure A7.24

Appendix 8. Deterioration of Microfines in Modified C1293 Specimens

Since all microfines produced different levels of expansion in the system, this appendix summarizes attempts to discern key differences. It was difficult to find unaltered microfine conglomerations in the specimens, but reported are the microfines found in various specimens. The following questions are based on the differences established in the original microfines. The images show a micrograph of 800 x 640 pixels on the left and an EDS scan on the right which follows the yellow line in the coordinating micrograph. All of the scans use the following key: Sodium-red star, magnesium-green pentagon, aluminum-blue square, silica-yellow circle, sulfur-white diamond, potassium-dark red x, calcium tan t, iron-light blue triangle.

1. In CA specimens, does montmorillonite effect the way KAc reacts in the concrete matrix?
Smectites represent the most expansive clay type of materials and they are in found in CA and CO microfines as montmorillonite. If it is calcium montmorillonite is present then the calcium could exchange with potassium to make potassium montmorillonite. This would in turn cause an overall change in the amount of free calcium which could combine to form calcium hydroxide, calcium carbonate, or some calcium acetate ionic species depending on the available carbonate and the pH. These new species could cause changes in the structure and potentially volume changes depending on how the solids form.

In some areas of the CA specimens, montmorillonite was identified. For example, in Figure A8.1. the elemental combination of Si, Al, Fe, and Mg could be identified as montmorillonite. It was also noticed that K appears in the region of the microfine and could have absorbed or exchanged in the montmorillonite layers. Note that microfine pieces were not found as large conglomerations in the CA on WI specimen.
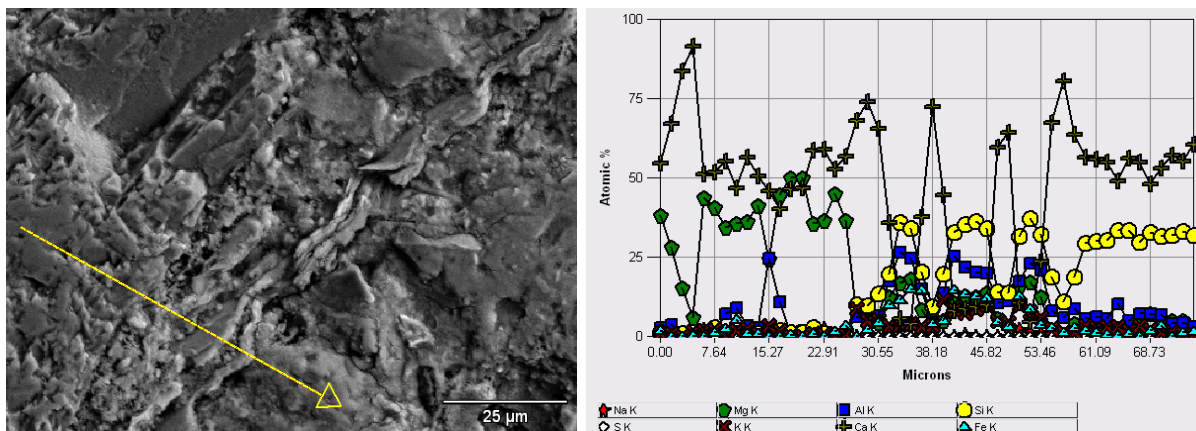

Figure A8.1. Montmorillonite in the CA on UT concrete matrix.

2. In CO specimens, does montmorillonite have an effect on the way KAc reacts in the concrete matrix?
In the CO on UT specimen there are a couple of areas with elevated Mg and Fe that could be indicators of montmorillonite (Figure A8.2.). Also notice that the differences in brightness across the BSE images which is an indicator of the density. Density of materials is an important quality because it could lead to penetration or decomposition. Areas of pure montmorillonite

were not identified which may indicate the microfines were degraded and either transformed or substitutions were made in the microfines.
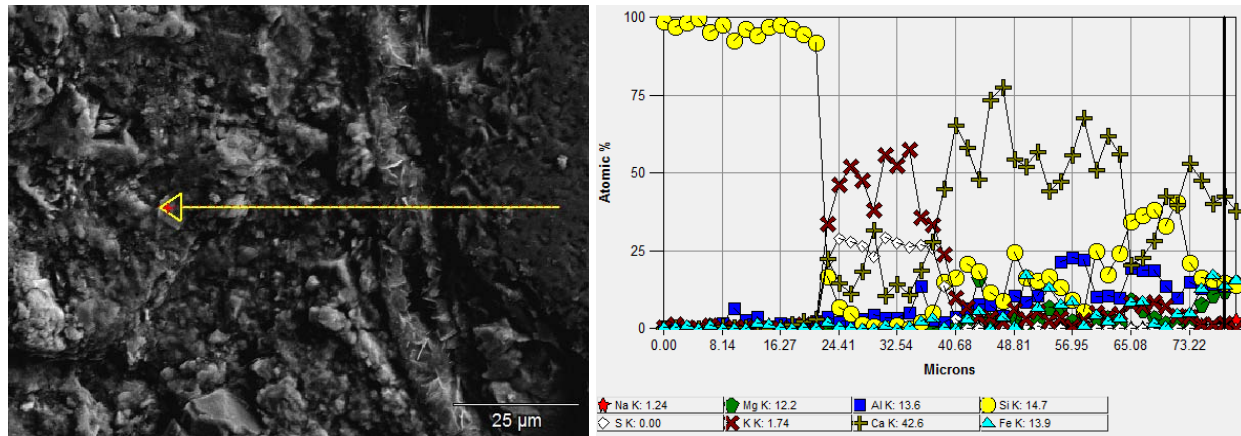

Figure A8.2. A microfine at the arrow tip with montmorillonite components.

3. In UT specimens, does vermiculite have effect on the way KAc reacts in the concrete matrix?
It is possible that the vermiculite degraded in the system because conglomerations of Si, Al, Mg, and Ca were not found in either UT on WI or UT on UT specimens.

4. In WI specimens, does talc or feldspar have an effect on the way KAc reacts in the concrete matrix?
There is a feldspar microfine which seems to be slightly depleted in Na (Figure A8.3). Following the feldspar microfine is a region of Ca which could have been stripped of its associated Si because of the Na from the feldspar. However, the region of Ca looks like it could be potentially a piece of calcite in the BSE image. Other than this possible calcite piece, no major oddities in the matrix are seen near the feldspar piece. Talc seems to have dissolved as it was not found in the specimens.
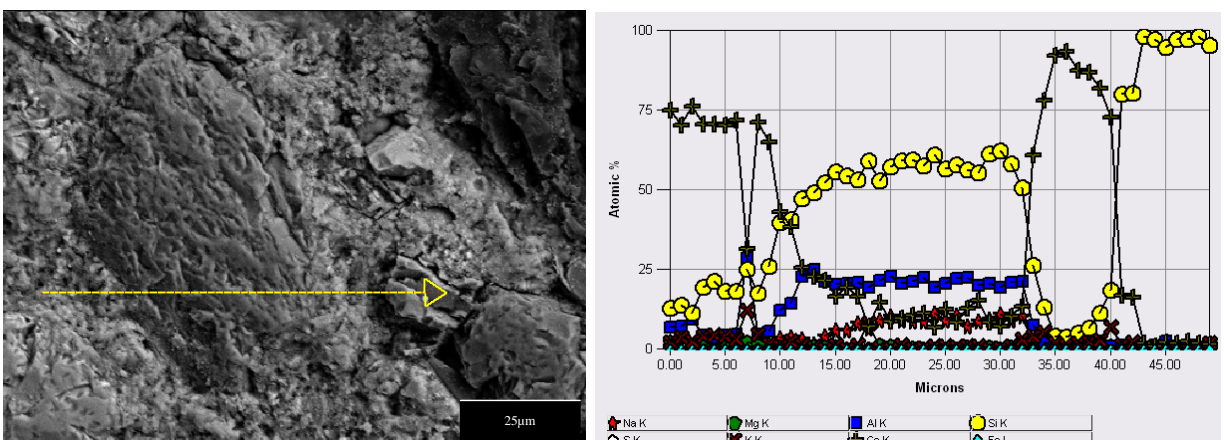

Figure A8.3. Micrograph of a WI feldspar microfine in a Deicer specimen depleted of sodium.

5. In WY specimens, does muscovite have effect on the way KAc reacts in the concrete matrix? In the WY on WI specimen, some muscovite was identified in the paste, but there doesn't seem to be deterioration due to the fines. (Figure A8.4.)
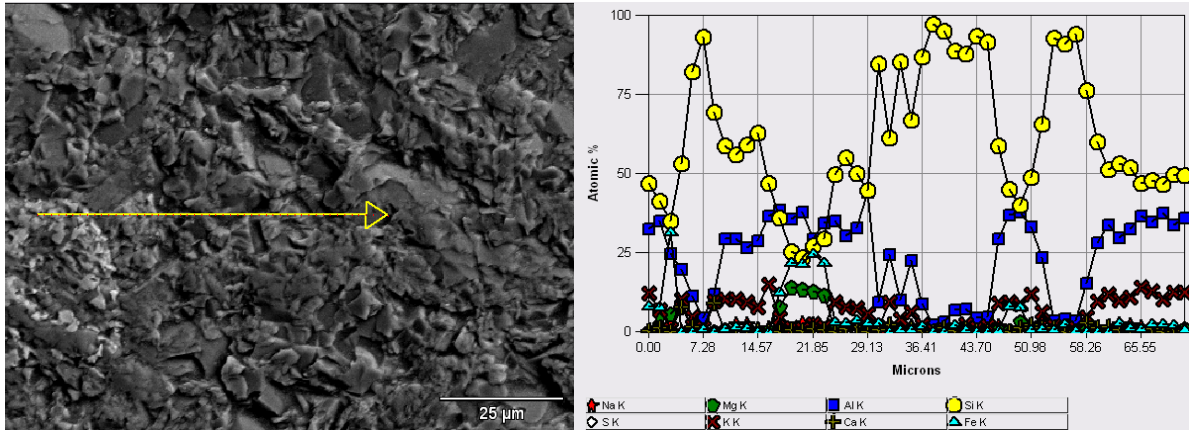

Figure A8.4. An area in the WY on WI specimen with muscovite microfines.

The WY on UT specimen has a feldspar piece that is next to a sheety deposit of CaK. (Figure A8.5.) It is difficult to say if the feldspar has caused this sheety byproduct as calcium and potassium are not in feldspar.
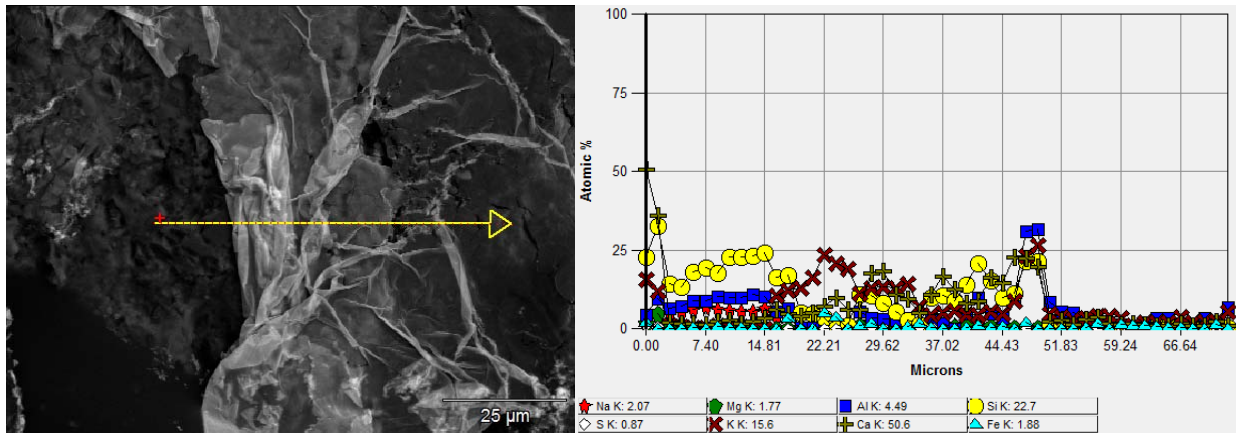

Figure A8.5. WY on UT specimen with a feldspar microfine near a secondary by-product.